ADDIS ABABA UNIVERSITY

ADDIS ABABA INSTITUTE OF TECHNOLOGY

SCHOOL OF CIVIL AND ENVIRONMENTAL ENGINEERING

AN EXPERIMENTAL INVESTIGATION ON THE EFFECT AND MECHANISM OF SIDE COVER SPALLING FOR SLENDER BEAMS SUBJECTED TO SHEAR

A Thesis in Structural Engineering

By

Kalkidan Tesfaye

May-2021

Addis Ababa, Ethiopia

A Thesis

Submitted in Partial Fulfillment of the Requirements for the Degree of Master of Science

The undersigned have examined the thesis entitled "**An Experimental Investigation on the Effect and Mechanism of Side Cover Spalling for Slender Beams Subjected to Shear**" presented by **Kalkidan Tesfaye**, a candidate for the degree of **Master of Science** and hereby certify that it is worthy of acceptance.

Dr. Esayas G/Youhannes	for	20/05/2022
Advisor	Signature	Date
Mohammed Sirage	For	20/05/2022
Co-Advisor	Signature	Date
Dr. Ing. Adil Zekaria		20/05/2022
Internal Examiner	Signature	Date
Prof. Girma Zerayohannes	for	20/05/2022
External Examiner	Signature	Date
Chair Person	Signature	Date

Mebruk Mohammed (Dr.-Ing.)
Dean, [illegible] il &
Environmental Engineering

Director of Postgraduate Program
Addis Ababa Institute of Technology
Addis Ababa University

An Experimental Investigation on The Effect and Mechanism of Side Cover Spalling for Slender Beams Subjected to Shear

UNDERTAKING

I certify that research work titled "An Experimental Investigation on the Effect and Mechanism of Side Cover Spalling for Slender Beams Subjected to Shear" is my own work. The work has not been presented elsewhere for assessment. Where material has been used from other sources it has been properly acknowledged/ referred.

Kalkidan Tesfaye

ACKNOWLEDGMENT

First and foremost, praises and glory to the almighty God and his mother St. Mary for showers of blessings, patience, perseverance and strength throughout my research work. I would also like to thank my parents for their unconditional support and encouragement throughout my years of study and during this research work.

I have had the support and guidance of several individuals, who have contributed for the success of this experimental research.

Primarily, I would like to extend my deepest and sincere gratitude to my advisor and mentor Dr.Esayas Gebreyouhannes for providing me an invaluable support and guidance. He has guided me through the difficult experimental journey with nothing but motivation and encouragement. He took time out of his busy schedule to personally monitor most of the tests. His rational and innovative thinking towards research has made it possible to obtain required results in a reliable manner. I would also like to thank him for providing me with valuable laboratory instruments, testing equipments and construction materials for the production of specimens. And also, for accommodating existing equipments within the laboratory to best suit the designed experiment. This research wouldn't have been possible without his support. His sincerity, brilliance and motivation have truly inspired me. It is an absolute honor and great privilege to be taught, advised and mentored by a humble being like him. I am extremely grateful for what he has offered me.

I would like to extend my heartfelt appreciation and gratitude to my mentor and friend Mohammed Sirage, for his unconditional assistance, for introducing me to the research area, and for helping me throughout the entire research process from idea conception to completion. He has helped me through the laborious laboratory work till the completion of this thesis by both intellectual and financial assistance.

My appreciation also goes to the technicians and staff of the Construction Material Laboratory at AAiT, Demis M., Fikru B., Biniyam and Wubet A. for their assistance and extreme patience and understanding during the long and tedious process of the experimental work. I would also like to thank technicians from the Mechanical workshop, Abiyou, Anteneh and Masresha for their technical assistance whenever their help was needed.

Lastly, I would like to thank my friends Abel S. for providing me strain gauges, Abel D. for providing me formwork, Weyneshet G. and Mahlet W. for helping me through the testing process and to the rest of my friends and family who have contributed to the successful completion of this research.

ABSTRACT

Reinforced concrete members should have an adequate safety margin against shear failure, which happens to be brittle and sudden. A lot of variables contribute to the shear resistance of beams, and to predict the resistance their influence to the shear behavior should be studied thoroughly. Past researches indicated that side cover spalling was observed for beams subjected to shear, signifying out of plane deformation had resulted from an in-plane loading. This observation however has not been explored enough to understand the mechanism and effect of side cover spalling in the overall structural resistance of reinforced concrete beams.

To investigate the effect and mechanism of side cover spalling under different variables seven full scale shear critical reinforced concrete beams were tested under one-point monotonic loading. Variables under consideration were concrete side cover thickness, stirrup cage width, and stirrup spacing. The specimens were also analyzed in a two-dimensional nonlinear finite element software, VecTor 2. Furthermore, the study assessed current code provisions and shear design theories for the design of beams subjected to shear, and checked whether or not spalling affects the ultimate resistance of a beam.

From the experimental program out of plane deformation strains were recorded for all tested specimens regardless of their side cover thickness. This deformation led to side cover spalling near peak load exemplifying that, stirrups are planes of weaknesses where spalling happens. Variable side cover thickness and stirrup spacing had observable effect on the spalling mechanism of the beams. The variation of side concrete cover thickness and spalling did not compromise the load resistance of beams as long as the core concrete confined within the stirrups was adequate enough to resist the applied loads. However, pre-peak spalling followed by premature failure happened for specimens designed with a relatively reduced stirrup cage width.

Existing international codes including Eurocode 2 (EN 1992-1-1:2004), ACI Standard (ACI 318-14), Canadian Standard (CSA A23.3-14), and Japanese Code (JSCE Standard, 1986), consider the entire beam width (bw) to be effective for shear resistance and consequently uses it as such for ultimate capacity prediction. Code prediction gave an overestimated failure load for specimens with reduced stirrup cage width, which demonstrates the inadequacy of design code provisions for beams subjected to shear with regards to the usage of the entire beam width (bw) for capacity prediction.

TABLE OF CONTENTS

LIST OF TABLES

LIST OF FIGURES

1. INTRODUCTION

1.1. Background

The versatility of reinforced concrete structures has led to its use in different types of environments, exposure conditions and various types of load resisting members. These members are designed to sustain various types and possible combinations of loads that could act on them during their lifetime. Shear critical members should have an adequate safety margin against shear failure, which happens to be brittle and sudden. A lot of variables contribute to the shear resistance of beams, and to predict the resistance their influence to the shear behavior should be studied thoroughly. Shear in beams for different variables has been studied so far, and consequently for members subjected to shear, side cover spalling was observed[1] [2] [3].

Spalling is the delamination of concrete at certain areas from the core, so far this phenomenon is explained and acknowledged for members subjected to axial compression, and torsion type of loadings. For axial compression members, spalling happens when the width of a crack along the entire length of a buckled reinforcement exceeds the critical width where confinement force of concrete cover cannot be provided.[4] Whereas for members subjected to torsion spalling occurs as a result of torsional shearing stress(τ) due to torque (T) circulating around the section and splitting generally takes place along the plane of weakness formed by stirrups.[3] [5] On the contrary, although side cover spalling has been observed in members, specifically beams, subjected to shear it has not been investigated as to why and how an in-plane loading can cause an out of plane deformation and if this loss of concrete section has an effect on the overall structural performance or shear resistance of the beam.

Side cover spalling is usually interrelated with concrete cover provisions. The need for the use of larger concrete cover in reinforced concrete structures depends on environmental condition, fire resistance requirement, required resistance to chemical attack, carbonation, proposed use and service life of structure. Concrete cover is intended to protect reinforcing steel from corrosion attacks and is so provided to structural members accordingly.

Since durability of concrete structures is a major concern, particularly in aggressive environments, a relatively larger thickness of concrete cover is required to protect steel reinforcement against threats of corrosion and fire. According to Euro Code 2[6] thickness of concrete cover to structural members is determined by taking exposure classes related to environmental conditions, durability requirements, bond requirements, fire resistance and structural class of the structure in to consideration. Therefore, larger cover sizes are to be used in certain conditions dictated by the above requirements. ACI 318-08 section 7.7[7] states cover depths up to 75mm are to be used unless greater concrete cover is required for fire protection and corrosive environments in which case it could be more.

Therefore, proper cover provision is one of the ways to ensure durability of concrete structures. However, in addition to thick cover leading to increased crack width in flexural reinforced concrete members[8] , if this provided cover delaminates and the member suffers from a loss of cross section, the cover provision will defy its whole purpose of serving for better durability and turn into the reason why the section is potentially prematurely failing. This begs the question if an increase in cover ensures durability of concrete structures.

The ways in which shear failures occur varies widely with the dimensions, loading type, and properties of a members. For this reason, there is no exclusive means to design for shear. Since shear behavior of beams is dictated by different factors a defined theory predicting their behavior is non-existent. Despite the efforts made by number of researchers, there are still gaps to be filled to understand behavior of members subjected to shear. So far theories for calculating shear strength of reinforced concrete elements, shear models and equations from design codes consider the entire web width of a beam section to be effective in resisting shear, and utilize it as such. This use lacks in considering the possible loss of concrete side cover as it could substantially reduce effective shear resisting width. It also lacks in acknowledging as to how varying the overall beam width with a constant web reinforcement cage or varying web reinforcement cage width with a constant beam width would affect the section's shear resistance behavior taking cover delamination as a variable.

One of the factors affecting shear behavior of beams is the spacing and configuration of transverse reinforcement. Studies on the effect of spacing of transverse reinforcements[9] indicate that for the same web reinforcement ratio, tighter spacing is proven to have a higher shear capacity than widely spaced stirrups if sufficient confinement is provided. On the contrary other experimental studies[2][3] state that the splitting of concrete cover from the core generally takes place along the "plane of weakness" formed by stirrups indicating that stirrup spacing could affect the spalling mechanism. Therefore, with regards to side cover spalling stirrup spacing is an outstanding variable in addition to cover thickness.

The importance of studying mechanism of spalling and it's counter effects in reference to members failing in shear is highly related to the overall resistance of the member. Even though spalling of concrete side cover is considered a serviceability condition, its effects have a lot to adversely contribute to the ultimate shear resistance of RC members. Spalling leads to a decrease in cross section which leads to the member losing its strength and stiffness. In sections subjected to shear one of the factors contributing to its resistance is width of the cross section, Therefore, knowing the effect spalling has on a shear critical beam section will help to quantify the consequence of side cover spalling on the overall beam resistance.

1.2. Problem Statement

Shear failure of reinforced concrete beam is difficult to predict accurately. Despite of many years of experimental research and the use of highly sophisticated computational tools, it is not fully understood. A lot of variables contribute to the shear resistance of beams, and to predict the resistance their influence to the shear behavior should be studied thoroughly.Experimental investigations carried out on beams for shear behavior prediction led to an observation that spalling of side concrete cover was evidently occurring. It is seen that beam members subjected to shear are experiencing side cover spalling, for an in-plane transverse loading the beams are experiencing an out of plane thrust leading to spalling, but neither the reason nor the mechanism is fully explained as to why this is happening. This observation adds side cover as one of the important variables to be investigated for shear behavior prediction.

Spalling of concrete side cover is not only an issue of serviceability, with the loss of this side cover, the effective width of the beam is reduced to the centerline of the outermost transverse reinforcement, and could potentially cause premature concrete crushing if not accounted for in design. The fact that there is limited experimental data on the spalling of concrete side cover, especially for sections subjected to shear, creates a huge gap to be filled. The phenomenon and effect of spalling need to be assessed meticulously to better predict shear behavior of beams. Side concrete cover should also be explored as a variable as it could affect the effective width of a beam resisting shear.

1.3. Objective of the Study

The main objective of this experimental research is to investigate side cover spalling for slender beams subjected to shear. The influence of concrete side cover thickness, stirrup cage width and stirrup spacing for the same web reinforcement ratio are targeted. The specific objectives are:

- To investigate side cover spalling phenomenon and its mechanism.
- To investigate how spalling affects the ultimate shear resistance and the overall performance of RC members.
- To investigate the effect of concrete side cover with reference to stirrup cage width and effective beam width.
- To investigate adequacy of current shear design provisions stipulated in building codes and shear theories.

1.4. Scope of the Study

This experimental study is limited to investigating side cover spalling for shear critical slender reinforced concrete beams subjected to force based one-point monotonic loading having concrete side cover thickness, stirrup cage width and stirrup spacing as a variable. Side cover variation is implemented in terms of thickness only, the strength, quality and density of outer cover are kept

the same as the concrete core of the beam. The specimens are only going to be subjected to an in-plane transverse loading, and any longitudinal loading to cause axial compression is avoided in the test region.

1.5. Methodology

This research follows four phases of investigative orders to meet the objectives set. The first phase includes the review of relevant literature related to shear theories, beams subjected to shear and side cover spalling in beams. The second phase of the study investigates shear provision of building codes for capacity predictions. Using the gaps observed from the reviewed literature as an input an experimental program including 7 slender reinforced concrete beams is then carried out followed by an analytical simulation using two-dimensional non-linear finite element software.

2. LITERATURE REVIEW

2.1. Shear Theories and Models

Shear failure of reinforced concrete beam is affected by various interlinked factors making its accurate prediction difficult. The prediction of the shear capacity of reinforced concrete beams is a challenging task because shear mobilizes several complex resisting mechanisms including shear resistance developed by the uncracked concrete in the compression zone (Vc), interface shear transfer by aggregate interlocking in the cracked concrete (Va), dowel action of the longitudinal reinforcement (Vd) and shear transferred by tension in the web reinforcement (Vs). Proposed theories vary from the simple 45^0 truss model[10] to the very complex non-linear fracture mechanics[11]. Yet nearly al1 the resulting design procedures are empirical or semi- empirical and are obtained by a regression fit through experimental results or through proposed models using artificial neural network. There are two key methods that have been used to predict the shear strength of reinforced concrete beams: the truss model [10] and Compression Field Theories[12].

2.1.1. Truss Model

Truss model is referred to as the best model for beams with web reinforcement.[13] For the design of linear members this model consist of longitudinal chords connected by web frames including diagonal concrete struts and reinforcement in one or more directions. The truss mechanism consists of a variable angle truss model. Ritter (1899) came up with the idea of using truss models for following the flow of internal forces in reinforced concrete structures. Based on careful remarks of the behavior of structures as well as a thorough understanding of basic principles of structural mechanics, Mörsch (1922) greatly advanced this concept and refined the classical 45° truss model.[10] The 45° truss model is based on the assumptions that the diagonal compression struts, before and after cracking of the cross section, are inclined at an angle of 45 degrees to the longitudinal axis of the reinforced concrete member; and the concrete tensile strength is negligible.[14] These procedures provide an excellent conceptual model to show the forces that are found in a cracked concrete beam.

A beam with inclined cracks develops vertical tensions in the stirrups, compressive and tensile forces, C and T, in its top and bottom flanges, and inclined compressive forces in the concrete diagonals between the inclined cracks. This highly indeterminate system of forces can be replaced by an analogous truss.[13]

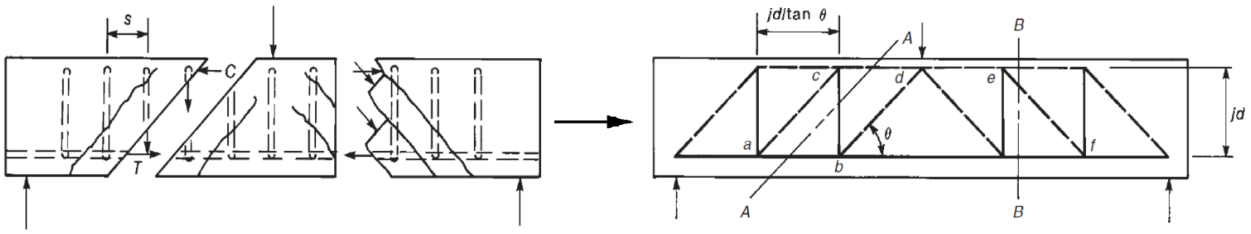

Figure 2-1: Analogous Truss Model (MacGregor et al., 2012)

In design, the ideal distribution of stirrups would be in such a way that all stirrups attain yield by the time the failure load is reached. It will be assumed, therefore, that all the stirrups have yielded and that each transmits a force of *Avfyt* across the crack, where *Av* is the area of the stirrup legs and *fyt* is the yield strength of the transverse reinforcement. When this is done, the truss becomes statically determinate depending on the stirrup's plasticity hence referred to as a plastic truss model.[13] The entire vertical component of the shear force is resisted by tension forces in the transverse reinforcement crossing this section. The average compressive stress in the diagonals is given by:

$$f_2 = \frac{V}{b_w jd \cos\Theta \sin\Theta} \tag{2.1}$$

Where *V* is the vertical force *jd* is width of web and *bw* is the thickness of the web. The web of the beam will crush if the inclined compressive stress f_2 from Eq (2.1) exceeds the strength of the concrete. But the actual inclination of the shear cracks is often less than 45°, which importantly depends on the shape of the member's cross-section. This means that Mörsch's truss analogy underestimates the shear resistance of a member.[15] Hence, the truss model predicts conservative values for the ultimate shear strength of the reinforced concrete elements since smaller inclinations can occur and concrete post-cracking tensile strength can be significant.

The other kind of truss model is called the variable angle truss model, it is a version of the 45° truss model altered by assuming flatter strut angles, $\theta \leq 45°$. In this model, the equilibrium equations can be derived in the same manner as for the 45° truss model.

2.1.2. Compression Field Theories

Using concepts from the Truss model proposed by Ritter (1899) and Mörsch (1922) a diagonal compression field theory- A rational Model for Structural Concrete in Pure Torsion was presented by D. Mitchell and M. Collins. (1974)[16]. The study presents a theoretical model for structural concrete in pure torsion by considering equilibrium conditions, geometry of deformation and stress strain characteristics of the steel and concrete.

In 1978, this method for solving the response of members in pure torsion was applied to members in pure shear in the form of the Compression Field Theory (CFT)[17]. This model is able to predict the full load-deformation response of reinforced concrete members subjected to shear using

equilibrium, compatibility, and stress-strain relationships. Since the CFT ignores the average concrete tensile stresses between cracks, it is unable to model members that contain no transverse reinforcement. Additional research performed by Collins and Vecchio in 1982, enabled the CFT to be extended to account for the tensile stresses that on average exist in cracked reinforced concrete.[16] This research resulted in the development of the Modified Compression Field Theory (MCFT).

2.1.2.1. Modified Compression Field Theory

The Modified Compression Field Theory (MCFT) was developed by Vecchio and Collins 1986 [12] by taking into account the resisting contribution of a cracked reinforced concrete member in tension. The Modified Compression Field Theory (MCFT) showed an ability to predict, with good accuracy, the shear capacity of reinforced concrete members with and without transverse reinforcement. It was developed by testing reinforced concrete elements in pure shear using the membrane element tester as shown in Figure 2-2.

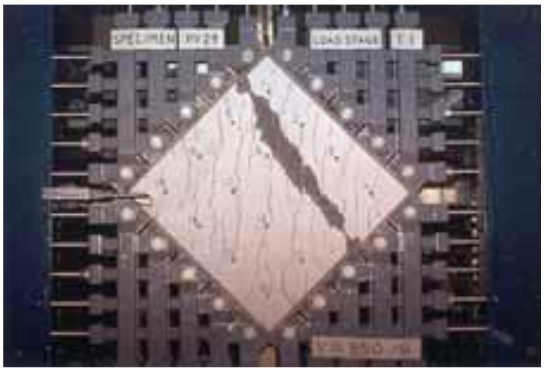

Figure 2-2: 1986, Vecchio FJ and Collins MP. Modified Compression Field Theory, Membrane Element Test

By comparing the principal compressive strain, ε_2, with the corresponding principal compressive stress in the concrete, f_2, it was found that diagonally cracked concrete was weaker and softer than the same concrete in a standard cylinder test. Furthermore, it was found that even after extensive cracking of the element, the Mohr's circle of average stress did not pass through the origin but showed a steady principal tensile stress in the concrete, f_1. Accounting for these tensile stresses in the cracked concrete changed the formerly developed compression field theory to the modified compression field theory.

Cracked concrete is treated as a new material with its own stress-strain characteristics. Equilibrium, compatibility and stress-strain relationships are formulated in terms of average stress and average strain. It focuses on the response of rectangular reinforced concrete elements subjected to in-plane shear and axial stresses. To study the relationship between the diagonal compressive stress f_2 and the diagonal compressive strain ε_2, a total of 30 reinforced concrete elements were tested under

biaxial stresses in an innovative testing machine. Unlike traditional models, the theory uses the strain conditions in the web to determine the inclination θ of the diagonal compressive stresses. It is documented that the local stresses in both the concrete and the reinforcement differ from point to point in the cracked concrete, with high reinforcement stresses but low concrete tensile stresses happening at crack locations. The compatibility conditions linking the strains in the cracked concrete to the strains in the reinforcement are expressed in terms of average strains, where the strains are measured over base lengths that are greater than the crack spacing.

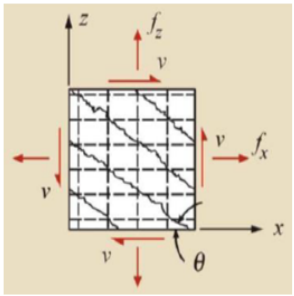

Equilibrium

Average Stresses:

1. $f_x = \rho_x f_{sx} + f_1 - \nu \cot\theta$
2. $f_z = \rho_z f_{sz} + f_1 - \nu \tan\theta$
3. $\nu = (f_1 + f_2)/(\tan\theta + \cot\theta)$

Stresses at Cracks

4. $f_{sxcr} = \frac{f_x + \nu \cot\theta + \nu_{ci} \cot\theta}{\rho_x}$
5. $f_{szcr} = (f_z + \nu \tan\theta - \nu_{ci} \tan\theta)/\rho_z$

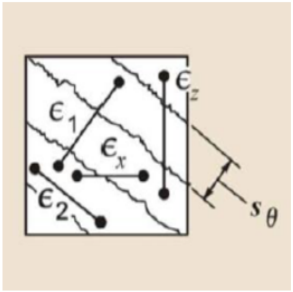

Geometric Conditions:

Average Strain:

6. $tan^2\theta = \frac{\epsilon_x + \epsilon_2}{\epsilon_z + \epsilon_2}$
7. $\epsilon_1 = \epsilon_x + \epsilon_z + \epsilon_2$
8. $\gamma_{xz} = 2(\epsilon_x + \epsilon_2)\cot\theta$

Crack Widths:

9. $w = s_\theta \epsilon_1$
10. $s_\theta = 1/(\frac{\sin\theta}{s_x} + \frac{\cos\theta}{s_z})$

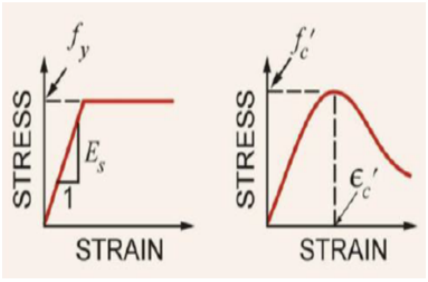

Stress- Strain Relationships:

Reinforcement:

11. $f_{sx} = E_s \epsilon_x \le f_{yx}$
12. $f_{sz} = E_s \epsilon_z \le f_{yz}$

Concrete:

13. $f_2 = \frac{f_c'}{0.8 + 170\epsilon_1}\left[2\frac{\epsilon_2}{\epsilon_c'} - \left(\frac{\epsilon_2}{\epsilon_c'}\right)^2\right]$
14. $f_1 = 0.33\sqrt{f_c'}/\left(1 + \sqrt{500\epsilon_1}\right) MPa$

Shear Stress on Crack:

15. $v_{ci} \le \frac{0.18\sqrt{f_c'}}{0.31 + \frac{24w}{ag+16}}\ MPa, mm$

Figure 2-3:1986, Vecchio FJ and Collins MP. Modified Compression Field Theory (MCFT) Equations

The equilibrium equations, the compatibility relationships, the reinforcement stress-strain relationships, and the stress-strain relationships for the cracked concrete in compression enable the average stresses, the average strains, and the angle θ to be determined for any load level up to the failure. Nevertheless, solving the equations of the MCFT requires an iterative procedure and the knowledge of a relatively high number of parameters, which introduces extra difficulties in the design perspective.

2.1.2.2. Disturbed Stress Field Model

The Disturbed Stress Field Model (DSFM) was introduced in Vecchio (2000)[18] as an alternative formulation for describing the behavior of cracked reinforced concrete elements. The theory is an extension of the Modified Compression Field Theory (MCFT), with advancements made primarily with respect to modelling of shear slip along cracks. The notion was to address the diminished accuracy seen from existing procedures under certain conditions, particularly for beams or wall elements containing no shear reinforcement. This new formulation combines aspects of rotating-crack and fixed-crack models, giving an improved representation of crack mechanism and thereby resulting in increased accuracy.

2.1.2.3. Simplified Modified Compression Field Theory

Due to its iterative nature, the MCFT is not a straightforward design methodology, and a simplified MCFT (SMCFT) approach of this method was proposed by Bentz, Vecchio and Collins (2007)[19] to overcome this aspect. This model takes into account the tensile stress installed in the cracked concrete and inclination of the diagonal compressive strut, and requires a smaller number of model parameters than MCFT. The shear strength of a section is taken as a function of two parameters: the tensile stress factor in the cracked concrete (β), and the inclination of the diagonal compressive stress in the web of the section (θ). It presents a simple equation for β and a simple equation for θ. While simple, the method provides excellent predictions of shear strength. The average ratio of experimental-to-predicted shear strength of the simplified MCFT is 1.11 with a COV of 13.0%.[19]

2.2. Building Codes Shear Design Provision

The shear resistance mechanisms of a reinforced concrete member still remain as a complex and controversial problem in spite of research efforts for the last several decades. Therefore, based on different experimental and theoretical backgrounds, different building codes have their own shear provisions. Shear failure is undesirable since it is a brittle mode of failure which occurs with little or no warning, unlike flexural failure which shows significant deflection prior to failure giving warning of impending damage. The flexural failure load is readily calculated, for this reason, all codes give comparable design provisions for flexure. This is not the case for shear failure where the semi-empirical equations typically provided in design codes give variable results. Simple experiments can be performed on reinforced concrete beams subjected to pure flexure and the clear results from such tests have been used to improve the theory but in shear, there is no agreed basis for a rational theory.

Current code-based shear design procedures are based on the assumption that shear failures occur when the shear capacity of a critical section is exceeded. Thus, the objective of these procedures is to assess the amount of transverse reinforcement required to carry that portion of the shear force in excess of the value which can be sustained by concrete alone.

According to the 2014 ACI's database for shear test[20] most code provisions for the shear capacity of structural concrete members with shear reinforcement have been, more or less, semi-empirically derived with only partial reference to a truss model and the maximum shear capacity or the strength of the inclined struts is based on tests.

2.2.1. Eurocode 2 (EN 1992-1-1: 2004)

The current European Code for the design of concrete structure (EN 1992-1-1: 2004)[21], for members with shear reinforcement, a variable angle truss model based on the lower bound theory of plasticity is incorporated. However, for the potentially more dangerous cases of members without shear reinforcement Eurocode 2 uses totally empirical procedures. Adequate shear reinforcement is provided where the design shear resistance of the member without shear reinforcement is less than the resulted shear force. Anywhere in the member shall the design shear force exceed the maximum shear force sustained by the member limited by crushing of the compression strut. An empirical formula is given for calculation of the contribution from the concrete in resisting shear.

$$V_{Rd,c} = max\begin{cases}(C_{Rd,c}\,k(100\rho_1 fck)^{\frac{1}{3}} + k_1\sigma_{cp})b_w d \\ (v_{min} + K_1\sigma_{cp})b_w d\end{cases} \tag{2.2}$$

The empirical formula for concrete contribution takes into account effective depth and beam width as cross-sectional information, the longitudinal reinforcement ratio, the compressive strength of concrete and the presence of axial force. The maximum shear force sustained by a member limited by crushing of the compression strut is defined by:

$$V_{Rd,max} = \frac{\alpha_c b_w z v fcd}{(cot\theta + tan\theta)} \tag{2.3}$$

The shear resisted by stirrups is defined by:

$$V_s = \frac{A_{sw} z f_{ywd} cot\theta}{s} \tag{2.4}$$

The calculation of shear force resistance contribution of the transverse reinforcement is based on the variable angle Truss model. Eurocode doesn't have a specific value for the diagonal crack angle θ. But it gives a recommended limit of $cot\theta$ between 1 and 2.5. The code also puts an empirical equation in place to compute the actual value of the diagonal crack angle.[21]

$$\theta = 0.5 \sin^{-1}\left(\frac{V_{Ed}}{\left(0.2fck\left(1-\frac{fck}{50}\right)\right)}\right) \quad (2.5)$$

2.2.2. ACI Standard (ACI 318-14)

The ACI and CSA design codes provide guidance on the use of sectional and strut-and-tie models for the shear design of reinforced concrete members. Sectional models are based on the assumption that plane sections remain plane, and are largely independent of how the forces are introduced to the member. Strut-and-tie models however, are primarily used for disturbed regions where there is a complex flow of internal stresses and the principles of sectional design do not apply. Strut-and-tie models are typically used for the design of deep beams.

The ACI sectional shear model in ACI 318-14[22] is an empirical extension of the 45° truss model originally proposed by Mörsch in 1902 , The shear strength formula is comprised of a concrete contribution, V_c, equal to the shear that causes diagonal cracking, and a steel component, V_s, calculated using the 45° truss equations. Code provisions for the shear capacity of structural concrete members with shear reinforcement have been, more or less, semi-empirically derived with only partial reference to a truss model. In the provisions of ACI 318-14, the truss model is used to determine the stirrup contribution to shear capacity, and then an empirically derived concrete term is added. The simplified shear strength formula is summarized as:

$$V_n = V_c + V_s \leq 0.83\sqrt{f_c'}b_w d$$
$$V_c = 0.17\lambda\sqrt{f_c'}b_w d \quad (2.6)$$
$$V_s = \frac{A_v f_y d}{s} \leq 0.66\sqrt{f_c'}b_w d$$

The shear capacity is limited to a maximum of $0.83\sqrt{fc'}bwd$. The shear area of the member is computed using the effective web width, bw, and effective depth d. This differs from the CSA code which recommends the use of the approximate flexural lever arm dv for calculating the shear area. The concrete contribution, Vc, is a simplified formula used for non-prestressed members derived from empirical test data. The concrete strength $\sqrt{fc'}$ in is not to be taken larger than 8.3MPa to account for the reduced crack capacity of high strength concrete. The steel contribution, Vs, is limited to $0.66\sqrt{fc'}bwd$ which is intended to prevent an over reinforced failure by diagonal crushing of the concrete. Since this limit is a function of $\sqrt{fc'}$ rather than fc' like the CSA code, members that utilize high strength concrete do not receive a proportional increase in this limit.[23]

2.2.3. Canadian Standards (CSA A23.3-14)

The Canadian Standard CSA A23.3-94 provides two methods for predicting the shear strength of reinforced concrete members - the Simplified Method and the General Method. The simplified method is similar to the ACI 318 method except that the effect of member size is considered. The general method is based on the modified compression field theory (MCFT) and thus has the same background as the AASHTO LRFD method. The Canadian code also recommends the use of the strut-and-tie method for the design of deep beams and other portions of members in which the variation in strain is complex (D regions).

2.2.3.1. Simplified Method

The simplified method is based on the 45° truss model. The shear resistance is also divided into two components, *Vc* and *Vs* . The concrete contribution, *Vc*, can be taken by:

$$V_c = 0.2\sqrt{f_c'}\,b_w d \ when\ A_v \geq \frac{0.06\sqrt{f_c'}\,b_w s}{f_y}\ or\ d \leq 300mm$$

$$or\ V_c = \frac{260}{1000 + d}\sqrt{f_c'}\,b_w d \geq 0.1\sqrt{f_c'}\,b_w d \ when\ A_v < \frac{0.06\sqrt{f_c'}\,b_w s}{f_y}\ or\ d > 300mm \qquad (2.7)$$

The steel contribution Vs is calculated as:

$$V_s = \frac{A_v f_v d}{s}\ where\ V_s \leq 0.8\sqrt{f_c'}\,b_w d \qquad (2.8)$$

2.2.3.2. General Method

In the general method, the nominal shear strength of a beam is given as the sum of concrete contribution, steel contribution and component in the direction of the applied shear of the effective prestressing force[24]:

$$V_{rg} = V_{cg} + V_{sg} + V_p \leq 0.25 f_c' b_w d_v + V_p$$

$$V_{cg} = \beta\sqrt{f_c'}\,b_w d_v \qquad (2.9)$$

$$V_{sg} = \frac{A_v f_y d_v(\cot\Theta + \cot\alpha)\sin\alpha}{S}$$

To utilize this approach, longitudinal strain εx is calculated and the coefficients, β and θ, are obtained from a table and used to find both steel and concrete shear contribution.

2.2.4. Japanese Code (JSCE Standard, 1986)

The JSCE code examines three limit states[25] : ultimate, serviceability and fatigue. Design for shear requires examination of the capacities V_{yd} design shear capacity, and V_{wcd} design ultimate diagonal compressive capacity of web concrete.

It assumes that, after inclined cracking, the shear force is carried by shear reinforcing steel and that the load carrying system is a truss type mechanism. Members can then lose their resistance to shear by yielding of the shear reinforcing steel that are the tension web chords of the truss or by compressive failure of the web concrete. V_{yd} is the sum of the shear components carried by the concrete, V_{cd} , the shear reinforcement, V_{sd} and the vertical component of the prestress force, V_{ped} .

Table 2-1: Design Shear Capacity Equations JSCE Standard

<table>
<tr><td colspan="2">$V_{yd} = V_{cd} + V_{sd} + V_{ped}$ (2.10)</td></tr>
<tr><td>$V_{cd} = \beta_d\, \beta_p\, \beta_n\, f_{vcd}\, b_w\, d/\, \boldsymbol{\gamma}_b$, $\boldsymbol{\gamma}_b = 1.3$
$f_{vcd} = 0.2\sqrt[3]{f_{cd}'} \le 0.72$
$\beta_d = \sqrt[4]{1000/d} \le 1.5$
$\beta_p = \sqrt[3]{100P_v} \le 1.5.\ \ P_v = As/(b_w d)$
$\beta_n = 1 + 2M_o/M_{ud} \le 2, for\ N_d \ge 0$</td><td>$V_{sd} = A_w f_{wyd}(\sin\alpha_s + \cos\alpha_s)z/S_s\boldsymbol{\gamma}_b$, $\boldsymbol{\gamma}_b = 1.1$
$z = d/1.15$

$V_{ped} = P_{ed} \sin\alpha_p\, /\boldsymbol{\gamma}_b$</td></tr>
</table>

2.3. Concrete Side Cover Spalling

Spalling failures originate when a transverse force acting near to the concrete surface exceeds the tensile resistance of the concrete cover. The actions originating spalling failures can have different sources. The literatures reviewed are based on studies relevant to load induced spalling in reinforced concrete beams.

2.3.1. Experimental Studies on Pure Torsion

Beams structurally loaded in torsion experience torsional moments acting on the cross section of the beam. This causes shearing stresses that circulates near the periphery, making concrete side cover an important parameter to investigate. Since the behavior of torsional shearing stress created by the application of twisting moment in structures can be corelated to shearing stresses formed by vertical forces, results documented in pure torsion are relevant for the study of pure shear. Side cover delamination factors observed in torsion should be investigated for shear as well.

In 1974, Mitchell and Collins' research[16] aimed at presenting a theoretical model for structural concrete in pure torsion tested two specimens, PT5 and PT6 , to investigate the effects of spalling of cover under pure torsion. The specimens had identical reinforcing cages and similar concrete strength. Specimen PT5 had a cover of only 2 mm, whereas Specimen PT6 had a 40 mm clear cover. The steel cage was similar in both specimens, but the outer dimensions of these square sections were 356 mm and 432 mm, respectively.

Specimen PT6, suffered from severe spalling at approximately the level of torque PT5 resisted and did not resist higher loading. After yielding of the transverse reinforcement, larger crack widths were observed in the specimen with larger cover. It was indicated by the experiment that relatively large concrete covers increase the potential of spalling and diagonal crack width, hence do not increase the torsional capacity.

Figure 2-4 shows the two beams at failure indicating the spalling of the concrete cover. The stirrups were visible at failure in both beams offering evidence that the concrete cover does indeed spall-off down to the hoops. The overall torsional stiffness lies between the spalled and the unspalled sectional stiffnesses. The ultimate torsional capacity of the member will be governed by the strength of the spalled section.

Figure 2-4: 1974, Mitchell and Collin Beams PT5 and PT6 at failure

In 1989, Nagataki et al.[2] tested the torsional behavior of three specimens namely C1, C2, and C3 with concrete covers to the centerline of the stirrups of 5, 30, and 55 mm respectively. Larger crack widths and severe spalling were observed in the specimen with 55 mm concrete cover (50 mm clear cover) near ultimate conditions.

ACI provisions[22], which assume that cover concrete contributes to the torsional resistance, were based on tests of beams with relatively small covers. However, later studies[16] on members in pure torsion showed that relatively large concrete covers may spall off under high torsional stresses.

Other studies on the effect of concrete cover in pure torsional resistance of reinforced concrete beam[26] also indicated that failure of beams with relatively larger cover were controlled by concrete cover spalling and that concrete cover spalling changes the behavior of transverse reinforcement.

2.3.2. Experimental Studies on Shear-Torsion Interaction

The scarcity of an experimental database involving shear-torsion interaction and the existence of structural members experiencing significant combined shear and torsion led to the need for additional researches. Important variables, including concrete side cover, affecting structural members in pure torsion are also to be put in question for combined loading scenarios.

Later in 1995, an experimental study on reinforced concrete beams to investigate the effect of increasing thickness of the concrete cover on the behavior of reinforced concrete sections subjected to combined shear and torsion, was carried out by Rahal, K. N., and Collins, M. P.[3]. At different shear to torque ratios and relatively low bending, seven large concrete beams with two different thicknesses of concrete cover were tested. The specimens were divided into two series. The first series consisted of the first three specimens (RC1-2, RC1-3, RC1-4), and the second series consisted of the four remaining specimens (RC2-1, RC2-2, RC2-3, RC2-4). The main alteration between the specimens of Series 1 and 2 was the clear concrete cover, which was 22.5mm and 42.5mm respectively. Dimensions of the steel cages remained the same in specimens of both series, but the concrete outer dimensions were altered to allow for the change in the thickness of concrete cover. The cross-sectional dimensions of the three specimens of series 1 were 300mm wide by 600mm deep and for series 2 the dimensions were 340mm wide by 640mm deep. Each specimen was loaded in stages up to failure at preselected torque to shear ratio.

Spalling was initiated by separation of the concrete cover from the concrete inside the stirrups, but this was not always accompanied by falling off of pieces of concrete. The occurrence of separation was checked by knocking on the concrete with a steel hammer, and listening to the sound. A "hollow" sound indicated occurrence of separation. This check was carried out at every load stage and once or twice between stages when higher load levels were reached. For the beams of series 1 cover spalling was not detected until after the ultimate loads had been reached, for Series 2 it was detected before the ultimate shear capacity was reached.

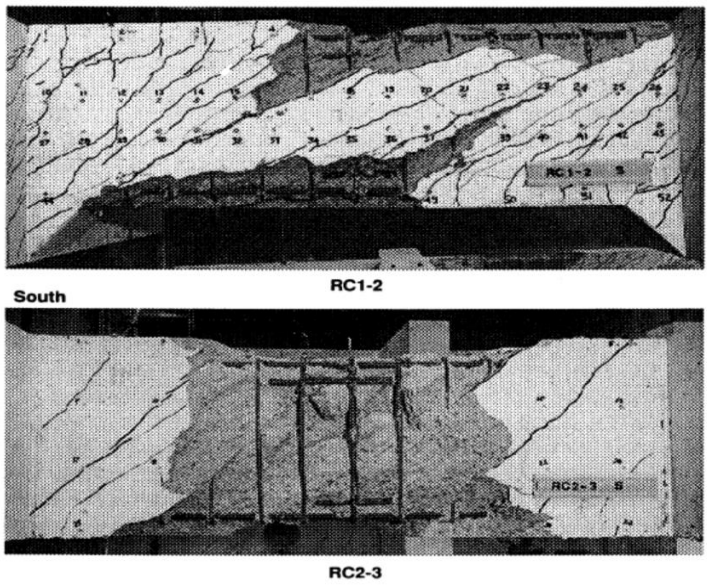

Figure 2-5: 1995, Rahal KN,Collins MP.Observed Spalling on south and north faces of Specimen RC1-2 and RC2-3

The study concluded that the cover concrete of members subjected to torsion and shear can contribute significantly to the resistance of members but that it results in an undesirable increase in crack spacing. In this study beams with a relatively small cover (22.5mm) did not spall until after the maximum load had been reached. On the other hand, beams with a relatively large cover

(42.5mm) spalled prior to the maximum load being reached. In these cases, the post spalling capacity was greatest when spalling was restricted to the side where shear and torsional stresses combine. In addition, an increase in concrete side cover also led to an increased average crack spacing. The spalling at both south and north faces of the test region of specimens RC1-2 and RC2-2 tested under "pure shear" raises a concern indicating that for larger concrete side cover, spalling occurs even for members subjected to shear alone.

2.3.3. Experimental Studies on Pure Shear

Earlier in 1974 tests were performed by Arbesman [23], at the University of Toronto for development of the Compression Field Theory (CFT) investigating cover spalling phenomenon for a beam specimen in shear. The beam had two test regions, SA3 and SA4; one with no clear cover and another with 40 mm clear cover on the vertical sides. The outer dimensions of the concrete were similar in the two test regions, and the steel cage dimensions were reduced to accommodate the change in thickness of the cover. Both specimens had a large amount of shear reinforcement with $\rho_v f_y / f_c'$ equaling 0.116. The full geometric properties of the specimens are presented in Figure 2-6 along with the observed and predicted failure shears.

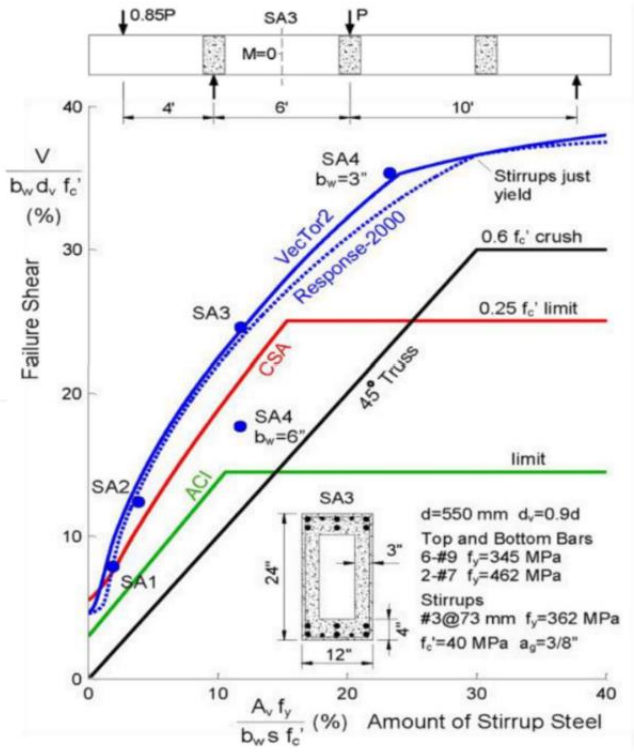

Figure 2-6: 1974, Arbesman, SA3 and SA4 Geometric Properties and Observed and Predicted Results

The test results of SA4, indicated that side cover spalling was initiated as the stirrups began to yield, reducing the effective width of the beam from 152 mm to 76 mm, which led to a capacity that was 73% of SA3. The observed failure is substantially below the predicted values (labelled

SA4, b_w=6" in Figure 2-6), if the width of the beam is assumed to remain at 152mm. The experimental value is accurately predicted if the width is assumed to be spalled (76mm labelled SA4, b_w=3" in Figure 2-6).

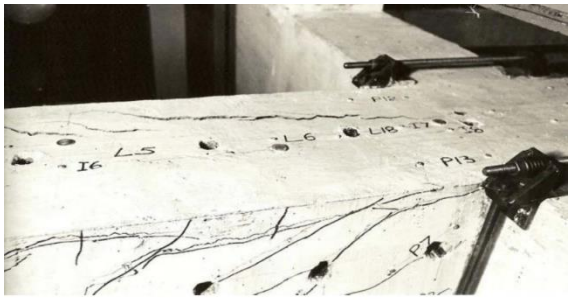

Side Cover Spalling Top View

Side Cover Spalling Bottom View

Figure 2-7: 1974, Arbesman, SA3 and SA4 Side Cover Spalling Observation from Top and Bottom Views

The region with larger cover resisted a 26% smaller load than that with zero cover due to severe spalling of side cover. It is to be noted that Test Region SA3 was tested first, and hence Test Region SA4 was pre-cracked when it was tested. This research also gives an insight on the effect a reduced stirrup cage could have on the ultimate load resistance of a beam because not only cover thickness was altered but the steel cage dimensions were reduced.

In 2006, following the shear-torsion interaction study[3], Khaldoun N. Rahal conducted a study to examine the effects of varying concrete side cover thickness on the behavior of reinforced concrete beams tested in shear.[2] Seven test results were reported. The tests were divided into two series, Series I and II, consisting of four and three test regions, respectively. Concrete side cover was varied for test regions of the same series, while the target concrete strength was varied between Series I (25MPa) and Series II (40MPa). The first specimen was cast using 25 MPa concrete and had a clear cover of approximately 5 mm on the vertical stirrups. Cast using two different concrete mixtures, the remaining three specimens had two test regions. For beams of Series I (25 MPa), the thickness of the concrete side cover varied from 5 to 75 mm and for beams of Series II (40MPa) side cover thickness varied from 25 to 75 mm. To maintain a constant value of effective depth *d*, the top and bottom cover was fixed to 40 mm in all the specimens. All the beam specimens were 400 mm deep and 3 m long, and were tested at a shear span-to depth ratio a/d =3.

It was stated that spalling is typically initiated by the separation of the concrete cover from the concrete confined within the closed stirrups. Similar to the shear torsion study, initial spalling is not always accompanied by pieces of concrete falling off. Hence, the separation was checked by

knocking on the concrete surface with a steel hammer and listening to the sound. A hollow sound indicated that separation had taken place.

The specimens with 75 mm side cover developed a sharp increase in diagonal crack width upon cracking and showed a less favorable behavior. At estimated service stresses, however, all specimens either remained uncracked or developed crack widths smaller than a suggested 0.3 mm limit.

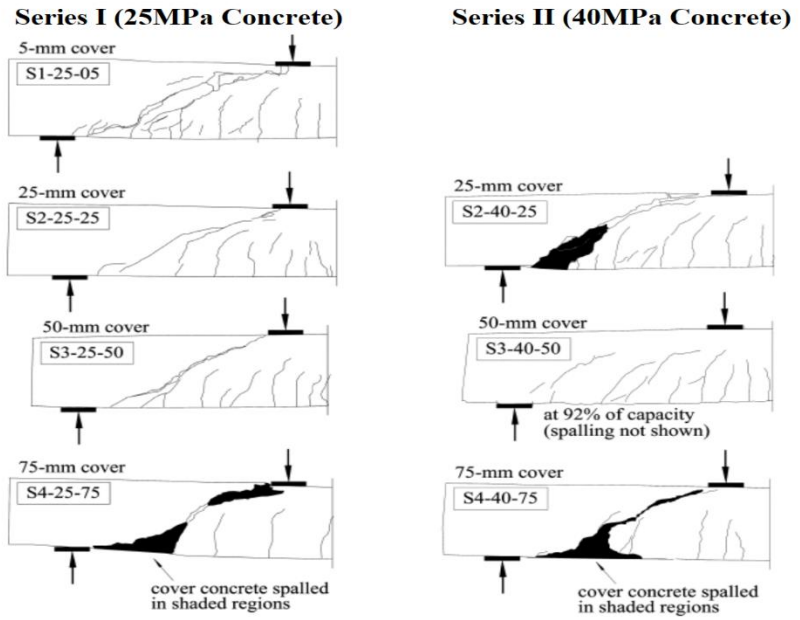

Figure 2-8: 2006, Rahal KN. Series I and Series II Specimens at Ultimate Load

The testing indicated that all beams failed in shear, and strain gauges attached to the reinforcement showed yielding in the transverse steel only. Spalling was observed near the ultimate conditions of specimens with larger concrete cover. Leaving the central and upper parts largely unaffected, the spalling in members subjected to shear (and flexure) is concentrated near the corners of the cross section. A similar trend was observed in the crack pattern of the shear test reported by Rahal and Collins[3] in spite of the difference in the test setup. The spalling observed in Arbesman's specimen,[2] SA4, was also more severe near the corners. This is unlike the case of torsion, where it has been observed that sections subjected to pure torsion or predominant torsion suffer from spalling in the cover around the whole section and not only near the corners.

The study concluded that increasing the cover (and the concrete cross section) increased the ultimate strength of the 25 MPa concrete beams significantly, but did not have a similar effect in the 40 MPa concrete beams. This suggests that spalling in the larger concrete cover had a more significant effect on the beams with the higher strength; It also concludes that the ACI shear method and the general method, based on the original unspalled section, provided conservative estimates of the strength. At loads corresponding to code-calculated ultimate loads, spalling is not

expected to take place and, hence, is not expected to reduce the shear capacity below code calculated values and that calculating the ultimate shear strength based on spalled dimensions as customary for sections subjected to torsion is not necessary.[2]
This study in particular had rather contradicting conclusion as to the effect of loss of cover on the sectional resistance of a beam. As the before mentioned studies on pure torsion[16], pure shear (Arbesman 1974) or shear-torsion interaction[3] indicated, the loss of side cover led to loss of cross section which leads to lower sectional resistance both in shear and torsion and if not lead to unfavorable conditions near ultimate load due to severe spalling.

The 2017's ACI journal paper by, Fisher A W., Bentz E C. and Collins M P.[1], further shading a light on side concrete cover spalling on beams subjected to shear, carried out an experimental investigation on four heavily reinforced coupling beam specimens with varying concrete strengths, reinforcement ratios, and side cover thicknesses. The specimens were tested to failure to understand the strength and stiffness of coupling beams for lateral performance in high rise concrete buildings and the influence of load-induced side cover spalling on shear strength. The specimens were designed for shear exceeding the ACI code limit.

Due to the design requirements that the longitudinal reinforcement of coupling beams be anchored inside the layers of shear wall reinforcement, coupling beams tend to have significant side cover thicknesses. The four coupling beam specimens, CBF1 to CBF4, had a dimension of 1600 mm length and 600 mm depth constructed monolithically with 400 mm wide shear wall end blocks. Specimen CBF1 had a coupling beam width of 316 mm with 3 mm of side cover while CBF2, CBF3, and CBF4 had a beam width of 400 mm with 45 mm side cover. A constant stirrup spacing of 60 mm was used for CBF1, CBF2, and CBF3, resulting in an amount of shear reinforcement that exceeded the upper limit on shear capacity imposed by the ACI Code. CBF4 had a stirrup spacing of 120 mm, resulting in an amount of shear reinforcement that met the ACI Code. All specimens failed in shear, characterized by yielding of the stirrups followed by slip on the crack, and then diagonal concrete crushing.

Side cover spalling was observed for all four coupling beam specimens. Based on the LVDT and LED measurements, side cover spalling began at the flexural compression corners of the coupling beam as the stirrups began to yield, progressing towards midspan at the peak load, and showing visible spalling by the end of the test. This side cover spalling causes localized changes in surface strains as the cover becomes delaminated from the core.

Figure 2-9: 2017, Fisher AW, Bentz EC, Collins MP. Coupling Beam Specimens at Ultimate Load

The study concluded that side cover spalling had minimal impact on the observed shear strengths for the four coupling beam specimens of this project due to the unexpectedly high strengths of the concrete used but it can be a problem for heavily reinforced members with design strengths that approach the diagonal concrete crushing limit. The reduction in cross-sectional area can result in a premature concrete crushing failure. It is also observed that the cover of tightly spaced stirrups (CBF1, CBF2, CBF3) has delaminated more as compared to the beam with wider stirrup spacing (CBF4). Results of this research also indicate that concrete side cover spalling does occur for heavily reinforced, high-strength coupling beams, and therefore should be accounted for in the design process and that Side cover spalling will significantly reduce the shear strength only if the loss of cover causes the remaining concrete core to crush in diagonal compression prior to yielding of the stirrups, or prior to the expected reduction in the angle of inclination of the diagonal compressive stresses in the concrete.

Although not accompanied by side cover spalling, in 2009, M. Zakaria, T. Ueda, et al.[8] carried out an experiment aimed at investigating the shear cracking behavior of reinforced concrete beams. This study chose beam size, span to depth ratio, shear reinforcement characteristics (stirrup spacing and configuration, side concrete cover to stirrup) and longitudinal reinforcement ratio as a variable. The investigated beams were divided into three series, the second series had three beams with variable concrete side cover, stirrup spacing and configuration tested at an a/d ratio of 2. The side cover for the three specimens used was 40mm, 60mm and 80mm. For the two specimens with larger covers (60mm and 80mm) it was observed that diagonal crack spacing was greater as compared to the specimen with smaller cover (40mm). Concluding that increasing the side concrete cover to stirrup leads to larger diagonal crack spacings and therefore increased crack width as well. This implies that varying side cover not only affects a beam's structural performance through cover spalling phenomenon but also causes variation in the shear cracking behavior (shear crack width and spacing).

2.3.4. Spalling Explained

As reported in the above reviewed researches, spalling has occurred for beams under different loading conditions and combination of variables. Some of these studies have made an attempt to explain the possible cause.

The 1974 Diagonal Compression field Theory[16] describes spalling for a beam in torsion by examining the equilibrium of a corner element. It explains that compression in the concrete tends to push-off the corner while the tension in the hoops holds it on. It states that at higher loads cover will spall off since it will not be possible for the hoops to hold on the concrete cover without generating large tensile stresses in the concrete.

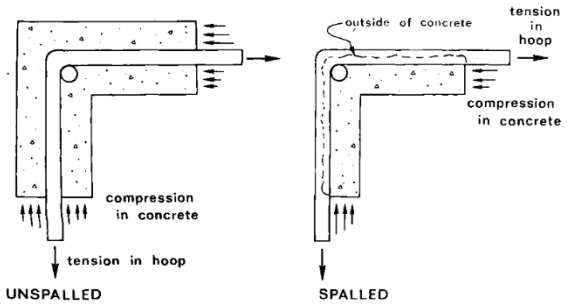

Figure 2-10: 1974, B. Mitchell, M. Collins, Spalling of concrete cover

In a similar manner the Shear-Torsion interaction study, 1995 [3] explains that shear and torsion cause shearing stress across a section. Shearing stresses v due to vertical shear force V are in the same direction as V, while torsional shearing stresses τ due to torque T circulate around the section. Due to the high intensity of shearing stresses, there is an increase in stress in the concrete and reinforcement. There is also the potential of the concrete cover outside the stirrup spalling off.

To satisfy equilibrium, the concrete compressive stresses resisting shear and torsion after cracking have to change direction near the corners of the beam which creates tensile stresses perpendicular to the directions of these trajectories. These tensile stresses will exceed the tensile resistance of the concrete if the shearing stresses and concrete cover are large enough, which causes delamination of the concrete cover away from the concrete confined within the stirrups. Furthermore, it stated that splitting generally takes place along the plane of weakness formed by the stirrups and is most critical when shearing stress due to vertical shear force and torsional shearing stress have an additive effect as shown in Figure 2-11.

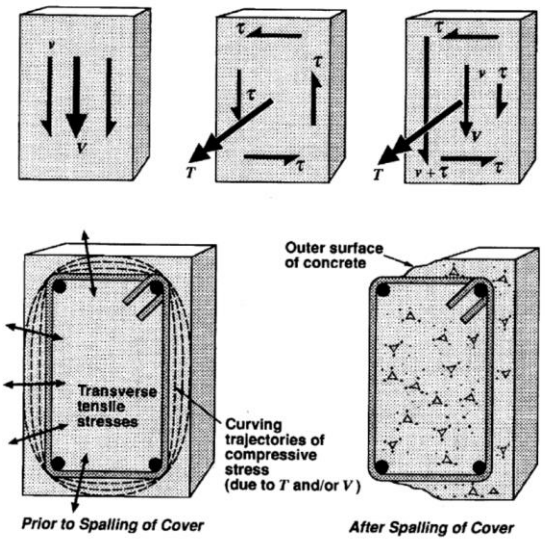

Figure 2-11: 1995, K. Rahal, M. Collins, Stresses in sections subjected to combined Shear and Torsion

Likewise, for a beam subjected to a shearing force K. Rahal 2006 [2] and A.Fisher 2017[1] explain spalling in a comparable manner, as the force resisted by diagonal compressive stresses changes direction near the corners creating tensile stresses in the direction perpendicular to the direction of the compressive stress as shown in the corner of the section in Figure 2-12.

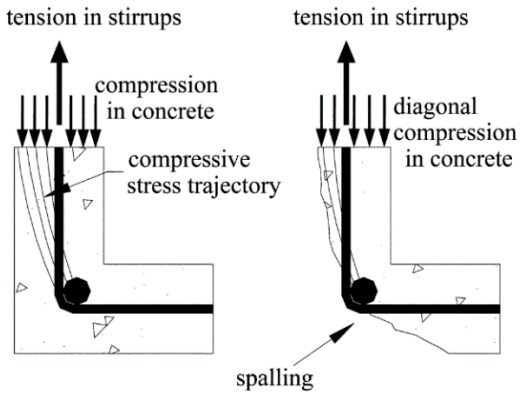

Figure 2-12: 2006, K. Rahal, Spalling of concrete cover in beams subjected to shear.

At larger cover, in addition to spalling, an increase in shear crack width[16] and crack spacing[3] was also observed. The effect side cover to stirrup has on shear cracking behavior is explained by M. Zakaria, T. Ueda, et al 2009[8] study after reporting an increase in shear crack spacing for larger covers. It was indicated that for larger concrete covers, stirrups would have a reduced ability to control crack spacing at the surface of RC members. Bond stresses are induced by the slip of stirrup through the concrete transferring force from the stirrup to the concrete between cracks.

To form a crack within an effective concrete area around the stirrup, the force which has to be introduced to concrete by bond at the end of the transfer length should exceed the cracking strength of concrete. Therefore, increasing the side concrete cover to stirrup increases both the effective

concrete area and the force introduced into the surrounding concrete by bond to cause cracking on the surface. This requires larger transfer length (crack spacing).

In the most recent experimental investigation by M. Aurelio, M. Francesco, and F. Miguel, 2021[27] spalling of concrete cover induced by reinforcement is explored. This study examined the phenomenon of cover spalling in reinforced concrete induced by bond or by the action of an inner pressure. With reference to the action of a radial transverse pressure due to bond stress and volumetric expansion of corroded reinforcement a design approach is proposed based on a simple mechanical model. One of the series addressed the effect of the concrete cover on the spalling resistance under various conditions.

2.3.5. Research Gaps and Unresolved Variables

Inconclusively different behaviors are so far reported for beams subjected to shear with variable thickness of concrete side cover indicating that side concrete cover is clearly an outstanding issue for beams subjected to shear.

The SA test series conducted in 1974 by Arbesman [1] showed that concrete side cover spalling can occur in beams with higher cover and lead to reduced ultimate load resistance. However, the specimens used had unique box beam geometry not typical to conventional beams used in the industry. To create a more relatable experimental database and to study spalling thoroughly, full scale beams with typical industry design need to be tested. In addition, stirrup cage width was reduced in the specimen with larger cover leading to the section resisting 26% lesser load. This load reduction can be attributed to the increased side cover, the reduced stirrup cage or the effect of both variables. Therefore, both parameters should be well investigated for the effect they could have on a beam's ultimate load resistance and general structural performance. Lastly it is to be noted that the two specimens are actually casted as a single beam with two different test regions, test region SA3 was tested first, and hence test region SA4 was pre-cracked when it was tested which could have compromised the reported results. Spalling was observed near the corner of the beams.

The 1995 Shear -Torsion interaction study[3] reported that beams with small cover spalled after the maximum load had been reached while beams with a relatively larger cover spalled prior to the maximum load was reached. However, since spalling was not always accompanied by falling off of concrete pieces, the occurrence of separation was checked by knocking on the concrete with steel hammer. A hollow sound indicated occurrence of separation. This is less reliable, subjective and qualitative way of reporting that puts the entire spalling conclusion in question. A scientific way capable of quantifying spalling must be devised to properly asses the issue and make plausible conclusions.

K.N. Rahal's study in 2006[2] observed spalling near the corner at ultimate conditions in specimens with larger concrete cover but reported that no load reduction was experienced. This contradicts with Arbesman's conclusion for larger concrete cover signifying inconsistent conclusions made on effect of cover.

In the experiment carried on heavily reinforced coupling beams[1], side cover spalling was clearly observed for all four specimens tested. It is to be noticed that unlike the other studies reported, spalling was not only limited to the corners but has spread to the central and upper parts as well. This observation makes the spalling "explanations" given on previous researches[3][2][16] inadequate as they state that spalling is caused by the high tensile stresses at the corner due to compressive stresses changing direction at that point. This concept however cannot be applied for spalled sections away from the corner creating a need for a better explanation for side cover spalling.

The coupling beam specimens although designed for shear by exceeding the ACI code limit all specimens failed by the yielding of the transverse reinforcement indicating that the code presents a very conservative limit. In addition, the study compares ACI and CSA's ultimate load resistance prediction based on both spalled and unspalled dimension on the coupling beams. Another important variable investigated in this research was stirrup spacing. Considering stirrups as a plane of weakness where splitting of cover takes place, it was observed that beams with tightly spaced stirrups had a more severe spalling than those with widely spaced stirrups. However, all these important parameters are experimented on lateral load resisting, stiff, highly stressed coupling beams experiencing different types of loading from adjacent shear walls and results may not apply for typical load resisting beams. Therefore, an experimental program for typical beams should be designed accordingly.

Shear design provisions according to four different design codes were reviewed and noted that all four of them use the entire beam width "bw" for shear resistance determination. However, their adequacy should be assessed for beam sections suffering from spalling as the effective shear resisting section is reduced.

3. EXPERIMENTAL PROGRAM

The experimental program is aimed to investigate the mechanism of side cover spalling, and the effect of side cover spalling for beams subjected to shear. Nine shear critical slender reinforced concrete beams were casted and seven of them (one trial beam and six main beams) were tested under monotonic one-point loading at Addis Ababa Institute of Technology's Material Laboratory. Two of the specimens could not be tested due to load resistance and stability problems that arose on the reaction frame of the test setup.
The beams were constructed with variable concrete side cover thickness, stirrup cage width, and stirrup spacing. Shear failure was ensured by providing a theoretical flexure to shear over strength factor. Prior to the experimental program, sectional analysis was carried out using RESPONSE 2000, a program based on the Modified Compression Field Theory, developed at the University of Toronto by Evan C. Bentz and Michael P. Collins. In addition, a two-dimensional non-linear finite element analysis was carried out by VECTOR 2, a software developed at University of Toronto. Prior to casting of the main specimen beams one trial beam was casted and tested to ensure the instrumentation methods designed gave the required results.

This section will elaborate on the design and construction of the specimens, test assembly and instrumentation. Properties of the materials used in the production of specimen will also be presented.

3.1. Specimen Configuration

Test specimens are configured in such a way that concrete side cover, stirrup spacing and cage sizes are varied either within or between different sets. Excluding the trial beam, the eight main specimens are divided into three sets or groups. The first two sets each have three specimens while the third set has two. Specimens in the same set have the same stirrup cage width. All main specimens have the same bottom and top cover thickness of 15mm (to maintain similar effective depth), concrete quality and strength, an overall depth of 350mm, total beam length of 2m, and length subjected to shear. An a/d ratio greater than 2.5 is maintained for all specimens.

For the first two sets, concrete side cover is varied with the same stirrup spacing. The second set is a replica of the first set, only differing in spacing and diameter of the stirrups with corresponding specimens having similar web reinforcement ratio. The final third set with two specimens is designed with a varied stirrup cage width than the other two sets. Each specimen is given a particular name based on the set in which it is in, web reinforcement diameter and concrete side cover thickness it has. For instance, in specimen designation SII10-50, the first letter "S" stands for Set while the roman number next to it signifies that the specimen is from the second set with a web reinforcement diameter of 10mm and concrete side cover thickness of 50mm.

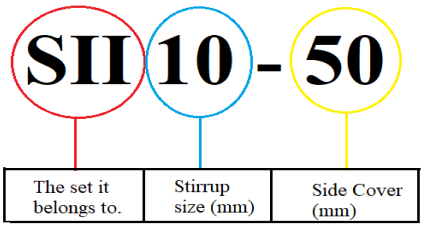

Figure 3-1: Specimen Naming and Designation

As presented in Table 3-1 below all specimens are designed with a 20mm diameter longitudinal reinforcement for both top and bottom faces of the cross section while 8mm and 10mm diameter ribbed reinforcing bars are used for transverse reinforcements.

Table 3-1: Configuration and Cross-Sectional Details of Test Specimens

Specimen Naming and Designation			Beam Dimension and Cover Thicknesses						Longitudinal Reinforcement		Transverse Reinforcement
	No of Specimen	Specimen Naming	Depth (mm)	Width (mm)	Cage Width (mm)	Total Beam Length (m)	Side Cover (mm)	Bottom and Top Cover (mm)	Bottom Steel	Top Steel	
Set I	3	SI8-25	350	200	150	2	25	15	5ϕ20	5ϕ20	ϕ8 c/c 70mm
		SI8-50		250	150		50		6ϕ20	5ϕ20	ϕ8 c/c 70mm
		SI8-75		300	150		75		6ϕ20	6ϕ20	ϕ8 c/c 70mm
Set II	3	SII10-25		200	150		25		5ϕ20	5ϕ20	ϕ10 c/c 110mm
		SII10-50		250	150		50		6ϕ20	5ϕ20	ϕ10 c/c 110mm
		SII10-75		300	150		75		6ϕ20	6ϕ20	ϕ10 c/c 110mm
Set III	2	SIII8-75		250	100		75		6ϕ20	6ϕ20	ϕ8 c/c 70mm
		SIII10-75		250	100		75		6ϕ20	6ϕ20	ϕ10 c/c 110mm
TRIAL BEAM	1	TR8-50/75		210	85	2.2	50,75		7ϕ20	7ϕ20	ϕ8 c/c 60mm
		TR10-50/75					50,75				ϕ10 c/c 100mm

The specimens have a web reinforcement ratio from the range of 0.48% to 0.72%. And an average 2.33% longitudinal reinforcement ratio with a coefficient of variation of 8.3%, was used.

These full scale highly reinforced beam sections are sought to be replicas of mostly used practical beam members in stressed regions, having a slender shear span with a span to depth ratio of 2.5 and higher. As defined by MacGregor[13] slender shear spans are those having an a/d ratios starting from 2.5 to 6 and their behavior is dictated by beam action.

An average flexure to shear over strength factor of 1.2 was provided for main specimens to ensure shear failure prior to flexural failure. This was done by over reinforcing top and bottom flexural zones of the beam specimens. The detailing of both longitudinal and transverse reinforcements were done as per Section 8 of ES-EN 1992-1-1:2004[21]. The cross-sectional details of all eight specimen are presented below in Figure 3-2, Figure 3-3 and Figure 3-4.

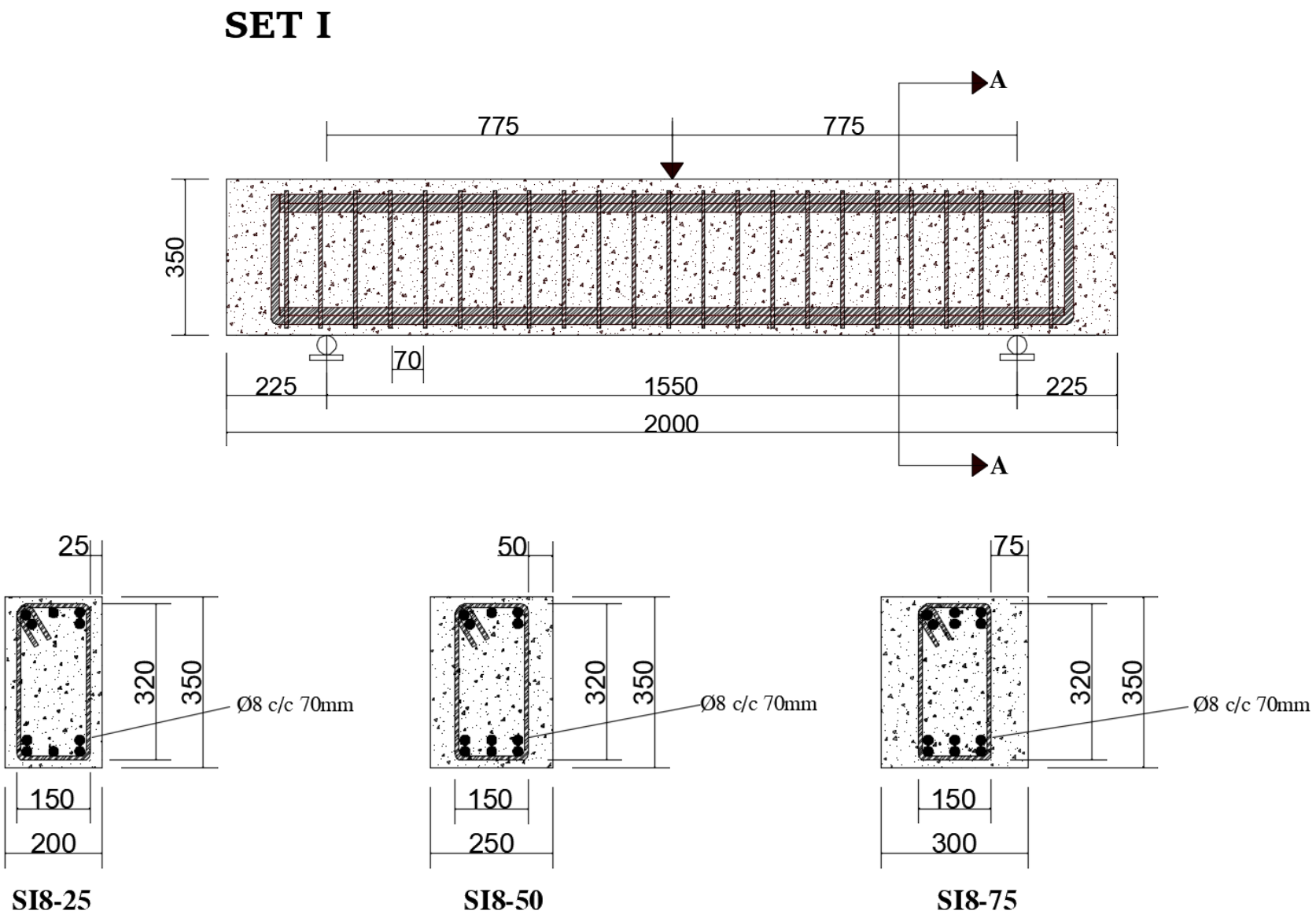

Figure 3-2: Cross Sectional Detail of Main Specimens SET I (All Dimension are in mm)

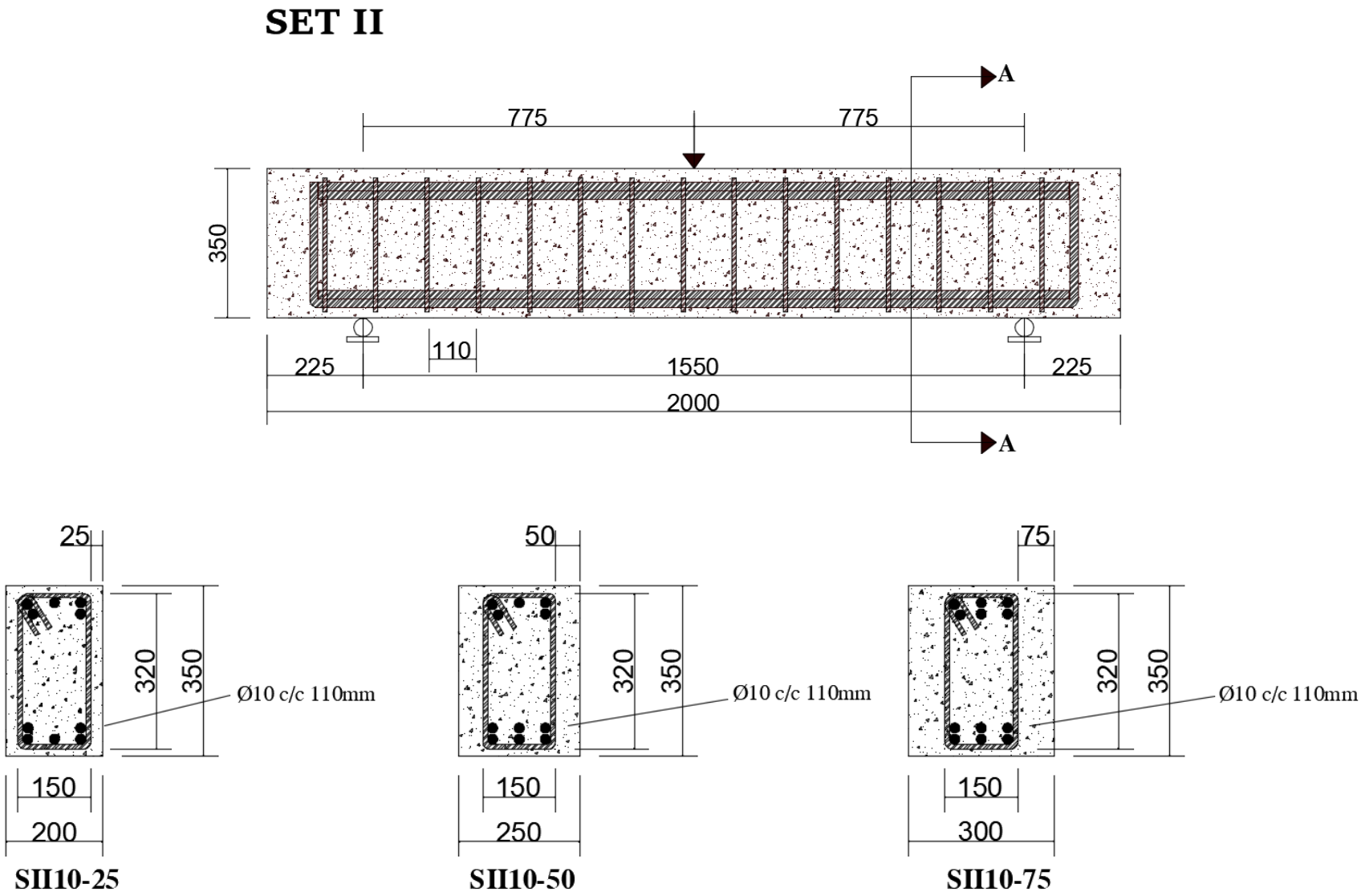

Figure 3-3: Cross Sectional Detail of Main Specimens SET II (All Dimension are in mm)

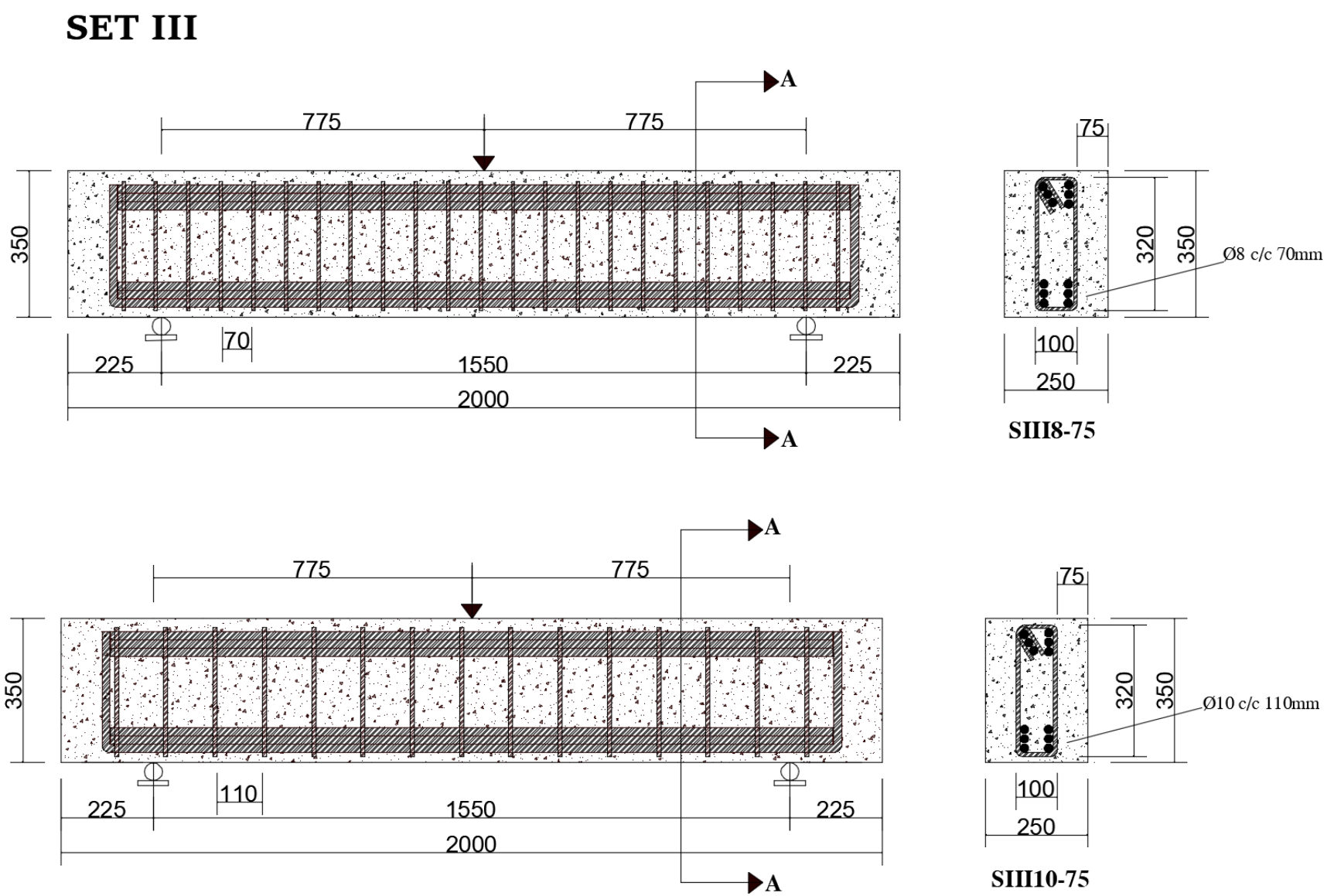

Figure 3-4: Cross Sectional Detail of Main Specimens SET III (All Dimension are in mm)

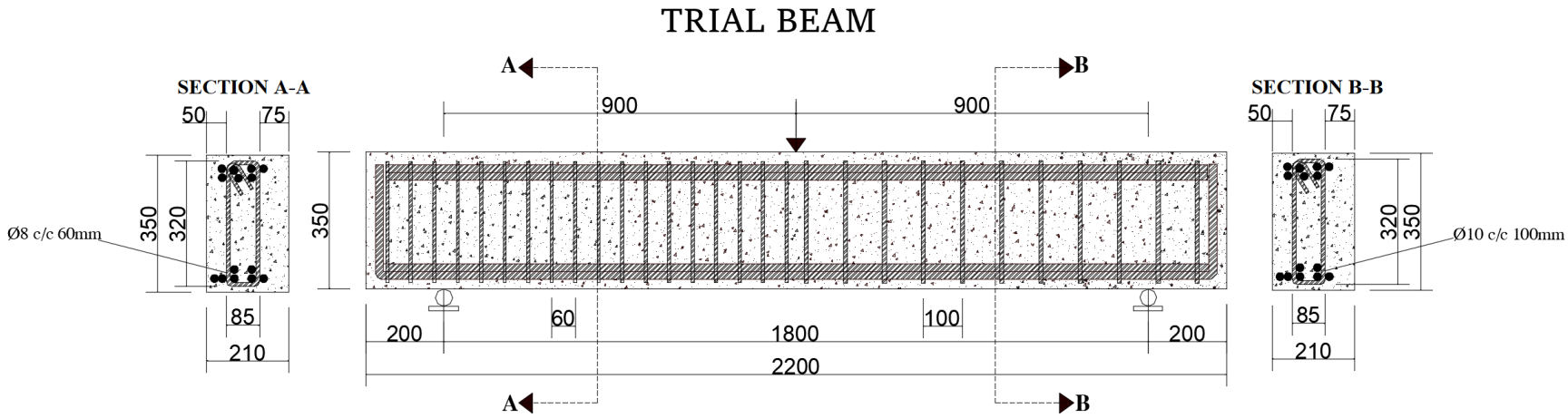

Figure 3-5: Cross Sectional Detail of Trial Beam (All Dimensions are in mm)

The trial beam was designed in such a way that it incorporates almost all research variables into one specimen. Concrete side cover was varied on the two alternate sides while for the same web reinforcement ratio, stirrup spacing was varied on the left and right side of the beam. Its main purpose was to observe possible outcomes of each defined variable and to see if the designed instrumentation method served its purpose of generating the required data.

3.2. Material Properties

3.2.1. Concrete

All eight specimens and the trial beam were made using cast in situ concrete prepared at AAiT. A mix proportion for a target compressive cubic strength of 25MPa was selected according to ACI Mix design. The concrete was specified to the use of a coarse aggregate with maximum size of 25mm, Ordinary Portland cement, and slump of 75mm to 100mm. The production of concrete was done by extreme caution in order to achieve and maintain consistence among all test specimens.

Table 3-2: Concrete Mix Design

Mix Design Specifications	
Slump	75 to 100mm
Target Cubic Compressive Strength	25MPa
Nominal Maximum Aggregate Size	25mm
Cement Type	Ordinary Portland Cement
Amount Required for $1m^3$ of Concrete Volume	
Cement	336.1 Kg/m^3
Fine Aggregate	863.1 Kg/m^3
Coarse Aggregate	1024.9 Kg/m^3
Mixing Water	142.8 Kg/m^3

A thorough material characterization and preparation was conducted before mixing of ingredients.

3.1.1.1. Coarse Aggregate

In order to follow the reinforcement detailing proposed, the coarse aggregate size had to be limited to 25mm. Therefore, the first step in preparing the coarse aggregate was to sieve and bag 25mm sieve mesh passing material in to a plastic bag to keep a consistent moisture content.

Different physical tests were done as per the Construction Material Laboratory Manual by Prof. Abebe Dinku June 2002[28] for the purpose of characterization.

Table 3-3: Material Properties of Course Aggregate Used

Coarse Aggregate Material Properties	
Maximum Aggregate Size	25mm
Gradation	Well Graded
Moisture Content	2%
Absorption	1.54%
Unit Weight	1571 Kg/m^3
Fineness Modulus	2.8

3.1.1.2. Fine Aggregate

In the preparation of fine aggregate, the silt content was first checked and was found to be 14% and needed to be washed to reduce the silt amount. The fine aggregate was therefore washed with water and placed into plastic bag after it was sun dried to maintain a constant moisture content.

Figure 3-6: Silt Content Test for Fine Aggregate

Summary of physical tests done as per the manual[28] is presented below in Table 3-4.

Table 3-4: Material Properties of Fine Aggregate Used

Fine Aggregate Material Properties	
Silt Content	1%
Moisture Content	8%
Absorption	0.8%
Finess Modulus	3.7

Prior to casting of specimens, the proposed mix deign was checked by casting trial cube samples. The samples' 7th day compressive strength was 17.3 MPa, which was more than 65% of the expected 28-day strength (25MPa), therefore the proposed mix design was adequate to yield expected concrete strength and was used in the casting of specimens. While casting the main specimens nine cube samples (150mm*150mm*150mm) and nine cylinder samples (150mm diameter and 300mm height) were prepared to check compressive and tensile strength of concrete respectively. Samples were cured in the same environmental condition as the specimens. Consequently, a consistent concrete strength was achieved for all specimens.

Figure 3-7: Concrete Compressive Test on Cube

Table 3-5: Cubic Compressive Strength of Specimens

Cubic Compressive Strength							
Beam Specimen	Cube Designation	Weight (gm)	Age at Testing (Days)	Failure Load (kN)	Compressive Strength (MPa)	Average Cubic Strength (Mpa)	Coefficient of Variation (%)
SI8-25, SII10-25	200bw-1	7750	136	938.1	41.69	36.82	9.35
	200bw-2	7686	136	776.8	34.53		
	200bw-3	7787	136	770.7	34.25		
SI8-50, SII10-50, SIII8-75, SIII10-75	250bw-1	7689	142	732	32.53	35.1	6
	250bw-2	7778	142	789	35.07		
	250bw-3	7812	142	848	37.69		
SI8-75, SII10-75	300bw-1	7789	148	746	33.16	34.59	6.03
	300bw-2	7648	148	844.7	37.54		
	300bw-3	7853	148	744.2	33.07		
TRIAL BEAM	210bw-1	8019	79	585	26	26.15	0.49
	210bw-2	8064	79	592	26.31		
	210bw-3	8055	79	588	26.13		
TRIAL MIX (7^{th} day)	1	8070	7	385.6	17.14	17.27	1.08
	2	8098	7	385.4	17.13		
	3	8108	7	394.4	17.53		

Figure 3-8: Split Cylinder Test for Tensile Strength

Table 3-6: Tensile strength of Specimens

Splitting Tensile Strength of Cylinders							
Beam Specimen	Cylinder Designation	Weight (gm)	Age at Testing (Days)	Failure Load (kN)	Tensile Strength (Mpa)	Average Tensile Strength (Mpa)	Coefficient of Variation (%)
SI8-25, SII10-25	200bw-1	12394	136	212.2	4.71	4.21	8.35
	200bw-2	12234	136	179.5	3.98		
	200bw-3	12227	136	177.6	3.95		
SI8-50, SII10-50, SIII8-75, SIII10-75	250bw-1	12285	142	176.4	3.92	4.1	3.59
	250bw-2	12312	142	184.8	4.11		
	250bw-3	12358	142	192.6	4.28		
SI8-75, SII10-75	300bw-1	12268	148	175.6	3.9	3.99	7.75
	300bw-2	12284	148	165.3	3.67		
	300bw-3	12316	148	198.3	4.41		

3.2.2. Reinforcement Steel

In all specimens a 20mm diameter deformed reinforcement was used as longitudinal bar while deformed 8mm and 10mm diameters were used as transverse reinforcements. Uniaxial tensile tests were performed on rebar samples from the different diameters used.

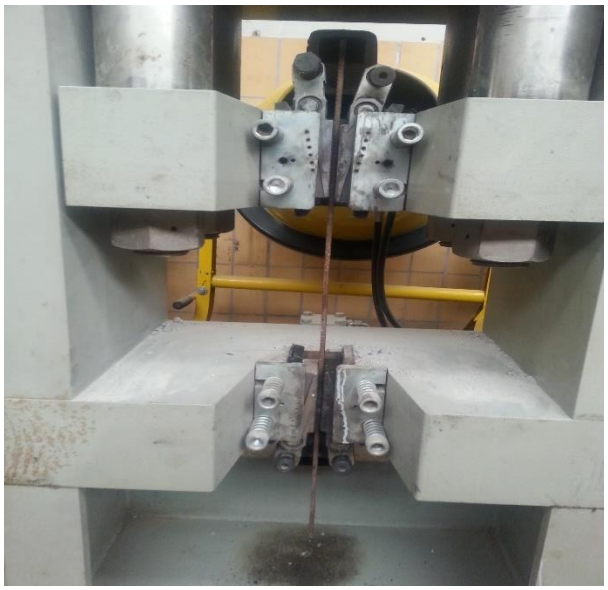

Figure 3-9: Uniaxial Tensile Test on Reinforcement

Results from the uniaxial test are reported below.

Table 3-7: Mechanical Properties of Reinforcements (Main Specimen)

Specimen	Average Diameter (mm)	Average Yield Strength (MPa)	Average Ultimate Strength (MPa)	Elongation (%)	Yield Strain ($\mu\epsilon$)
ϕ8	8.05	520.1	641.8	23.4	2600
ϕ10	10.06	544.5	676	23.5	2722
ϕ20	20.13	591.6	681.4	23	2958

Table 3-8: Mechanical Properties of Reinforcement (Trial Beam)

Specimen	Average Diameter (mm)	Average Yield Strength (MPa)	Average Ultimate Strength (MPa)	Elongation (%)	Yield Strain ($\mu\epsilon$)
ϕ8	8.06	515.82	656.24	22.4	2579
ϕ10	10.1	534.77	691.31	22.7	2674
ϕ20	20.16	586.69	649.69	22.7	2933

3.3. Specimen Production/Fabrication

The fabrication of specimens follows three main steps, the first is preparation and assembly of formworks, followed by reinforcement cage production and placement of rebar cage inside the formworks after the placement of necessary accessories. The specimen preparation is then finalized by casting the concrete inside the prepared setup.

3.3.1. Formwork

Plywood formwork, with 14mm thickness, cut in appropriate pieces for each specimen dimension was used in the making of the required mould. The plywood was purchased from a local market and was assembled at the Construction Material Laboratory's construction yard.

Figure 3-10: Plywood used for Formwork Construction

As part of the proposed instrumentation method, the plywood pieces to be placed along the beam's longitudinal sides were drilled to create 16mm holes at required coordinates. Formwork was set up in such a way that beams would be casted adjacent to each other sharing one plywood formwork on the side.

Figure 3-11: Formwork Assembly for Main Specimens

All gaps between plywood surfaces were sealed using a local sealer, "Stuko", to avoid any leakage during casting. In addition, diagonal braces were provided for exterior formworks to avoid bulging of specimens during casting. Prior to the final placement of the reinforcing cages, the plywood surfaces were coated in oil to make it easier to detach the formwork from the hardened concrete.

3.3.2. Reinforcing Cages

The reinforcing cages for the test assembly were also constructed at the construction yard of AAiT's Construction Material Laboratory. The reinforcing bars were cut to a required length using an electric grinder and bent to the designed shape according to the proposed detailing. The bars were tied together manually using rebar ties.

Figure 3-12: Reinforcement Cage for Trial Beam

Figure 3-13: Reinforcement Cage for Main Specimens (A) SII10-25 (B) SIII8-75

Before the placement of rebar cage into the prepared formwork, strain gauges were attached on one of the transverse reinforcements of each specimen to measure local reinforcement strain during testing. Strain gauges were placed on the stirrup found in the middle along the expected 45^0 shear crack spanning from the loading point to the support.

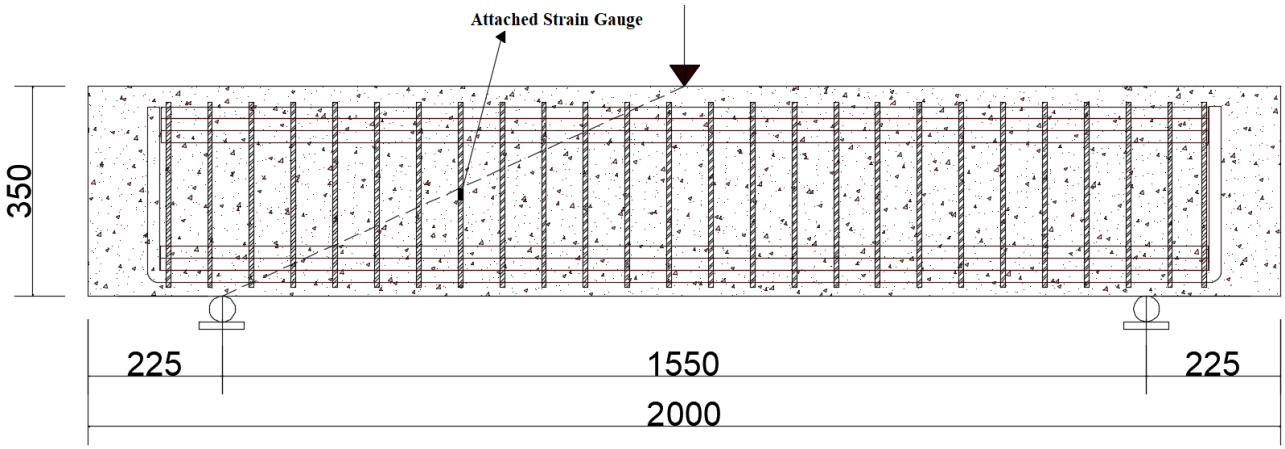

Figure 3-14: Location of Attached Strain Gauge

Figure 3-15: Strain Gauge Placement on Stirrup

In order to maintain cover provisions between the cage and the formwork, a mortar spacer produced at the casting site were tied on to both the bottom and side layer of reinforcing bars.

A PVC conduit with an outer diameter of 16mm was placed through the beam width with holes created on the formwork for instrumentation purpose after the rebar cage was placed inside the formwork.

Figure 3-16: Reinforcement Cage Placed in Formwork (Trial Beam)

Figure 3-17: Reinforcement Cage Placed in Formwork (Main Specimens)

3.3.3. Concrete Casting

For the trial beam concrete mixing was done using a small mixer found at the lab. However Concrete casting for the main specimens took place outside of the laboratory using a Tilting drum mixer which had a greater volume capacity per mix than the mixer found inside the lab. All eight specimens were cast in the same day. It took three mixes of the Tilting drum mixer to cast all specimens along with their respective cube and cylinder samples. The concrete constituents proportioned in Table 3-2 were mixed in an orderly manner and slump was checked for every mix to check consistency.

Figure 3-18: Tilting Drum Mixer used for Concrete Casting

One electric vibrator with 50mm diameter was used during casting to consolidate the concrete in both the specimens and test samples (Cylinders and Cubes).

Figure 3-19: Concrete Casting of Main Specimens

After casting, the formwork was removed after 48 hours and concrete was moist cured for 15 days by using a wet cotton cloth.

Figure 3-20: Formwork Removal of Main Specimens

Figure 3-21: Main Specimen Curing

3.3.4. Specimen Preparation

After the curing process the specimens were prepared to be tested. This preparation included cleaning the beam surfaces, cleaning the holes created and painting the specimens white for better visibility of cracks during testing.

Figure 3-22: Specimens Prepared for Testing

3.4. Test Setup and Instrumentation

The experimental program involved the testing of seven shear critical slender reinforced concrete beams in a one-point monotonic loading system. The beams were simply supported on two steel roller supports on each side. After few modifications, the existing reaction frame at the Construction Material Laboratory was used to test the beams to failure. Since the specimens were designed at a relatively larger web reinforcement ratio, their respective expected failure loads were higher than 500kN. The reaction frame at the laboratory however was not deigned to resist such a load and hence required the installation of additional stiffeners to resist the load reactions during testing. Hollow threaded clamps were used to support the main load carrying I-Section of the reaction frame. In addition, steel plates and reinforcing bars were welded both to the flange and web of the resisting I-Section.

A concentrated point load was applied at mid-span of each beam by using a manual operated hydraulic jack with maximum loading capacity of 1000kN pressed against the bottom of the resistance-enhanced reaction frame.

Figure 3-23: Original Reaction Frame

Figure 3-24: Reaction Frame After Stiffening Modification

Figure 3-25: Hydraulic Jack

Since the hydraulic jack was operated manually a fixed rate of loading couldn't be maintained but the loading rate was kept within a constant range by limiting the number of strokes pushed per minute.

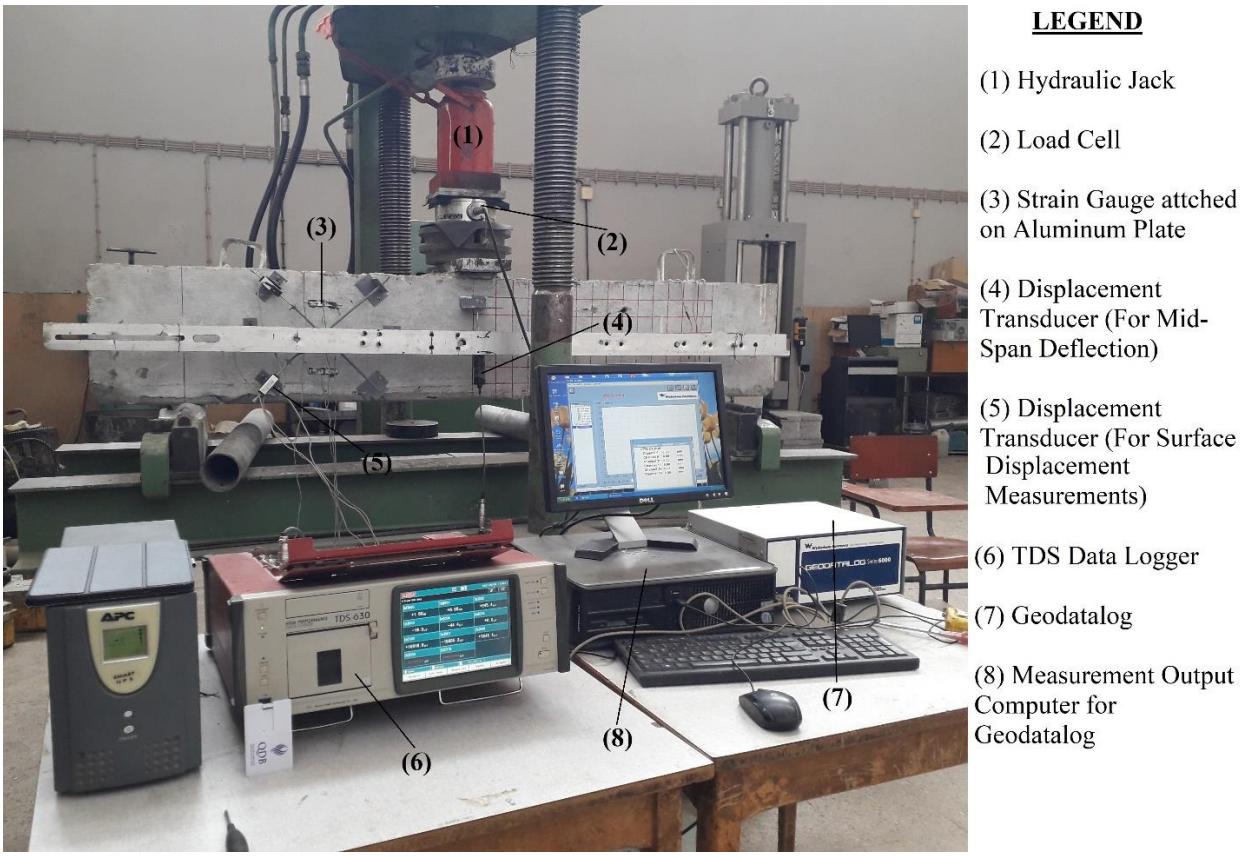

Figure 3-26: General Test Setup for All Specimens

Instrumentation for the experimental program was designed to help meet the research's objective by obtaining relevant response data from the experiment. Measurements obtained during testing were, applied load in kN from load cell, mid span deflection in mm from displacement measuring transducer, surface displacement measurements from surface mounted transducers and out of plane strain measurement from strain gauges attached on aluminum strips. The general test setup is shown in Figure 3-26.

The TDS-630 datalogger was used to monitor and record data. Load reading from the load cell, midspan deflection reading from the transducer and out of plane strain measurements from strain gauges were recorded in 1 second interval and extracted in an excel format using the TDS datalogger.

Figure 3-27: Load Cell

Figure 3-28: Displacement Transducer (For Mid-Span Deflection)

Figure 3-29: TDS-630 Datalogger

In addition, a digital caliper was used to measure crack widths and spacing with better precision and a rebound/ Schmidt hammer was used to test the compressive strength of beams which have been tested multiple times. Compressive strength results obtained from the rebound hammer test at a certain location of testing had a coefficient of variation less than 5%.

Figure 3-30: Distance Measuring Caliper

Figure 3-31: Rebound/ Schmidt Hammer Test

3.4.1. Out of Plane Measuring Instruments

The out of plane measurement used on the trial beam consisted of three holes located at three different distances along the longitudinal axis of the beam. Two of the holes were located at the center of the 45^{o} shear critical failure line running from the support to the loading point where maximum shear is expected to happen and the third hole was at the center of the beam where maximum flexural stress is expected to happen.

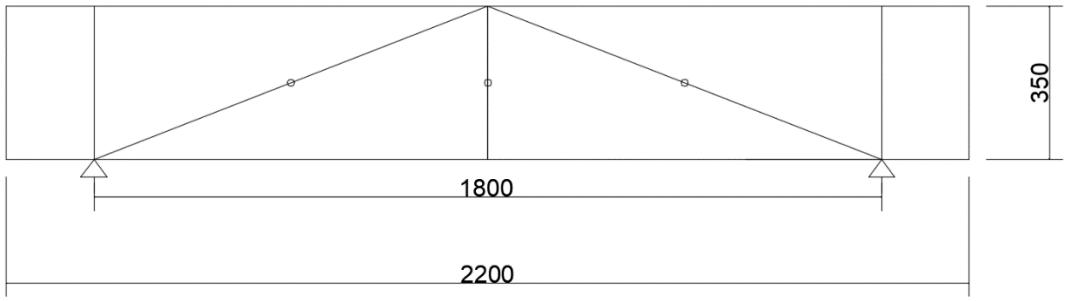

Figure 3-32: Out of Plane Deformation Measurement Holes (Trial Beam)

After testing the trial beam, the middle hole at the longitudinal center of the beam was deemed unnecessary. The results obtained from the two holes created in the shear critical plane led to the realization that additional information could be obtained if multiple holes were created at the same shear critical plane used on the trial beam. Thus, the use of three vertical holes was implemented in the main specimens.

As mentioned earlier, 16mm diameter holes passing through the width of the beam were created by plastic conduits as a way to measure the out of plane deformation the beam experiences. The holes were located in between the support and loading point. On one side of the beam three vertically lined holes were prepared. Each hole was located on each stress zone, one at compression zone, one at the neutral axis and one at tension zone. On the other side of the beam separated by the longitudinal midspan, again three holes were prepared one at each zone but placed along a 135-degree angle diagonal instead of a vertical line. These holes were put if other options of instrumentations were to be thought after casting and if there comes a need for extra holes. However, in this experiment only the three vertical holes were used to measure the out of plane deformation of specimens.

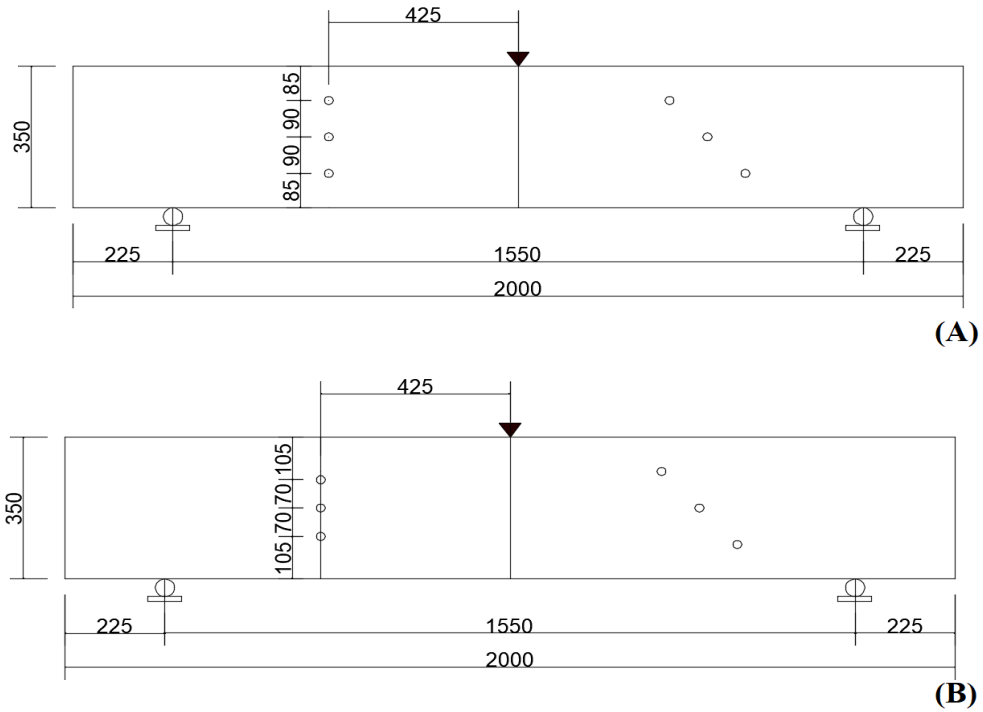

Figure 3-33: Out of Plane Deformation Measurement Holes (A) For two Layer Longitudinal Reinforcement (B) For Three Layer Longitudinal Reinforcement

Inside the holes are 1mm thick aluminum plate strips with an average 10mm width attached to two other strips on each side and were attach by an adhesive (Epoxy) to the outer surface of the beam.

Figure 3-34: Aluminum Strips used for Out of Plane Strain Measurement

Strain gauges were attached to these aluminum strips. In the trial beam strain gauges were placed at the middle and edge of the aluminum plate in each hole to see if the deformation has variation along its length. But it was observed the aluminum strips had similar deformation along their length therefore, for the main specimens only one strain gauge was attached to each aluminum strip.

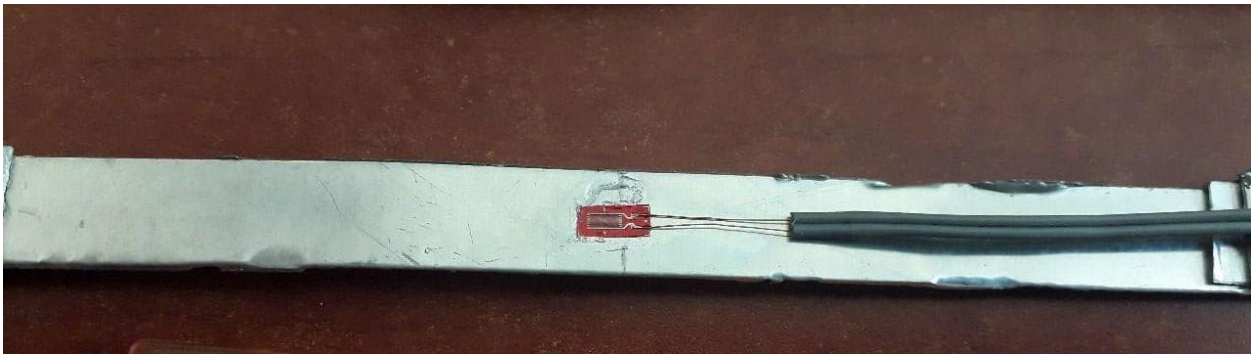

Figure 3-35: Strain Gauge Attached in the Middle of Aluminum Strip

These aluminum plates, in the trial beam were attached to the beam surface vertically which was later changed to horizontal attachment for the main specimens to get the pure behavior of the zone it is attached to.

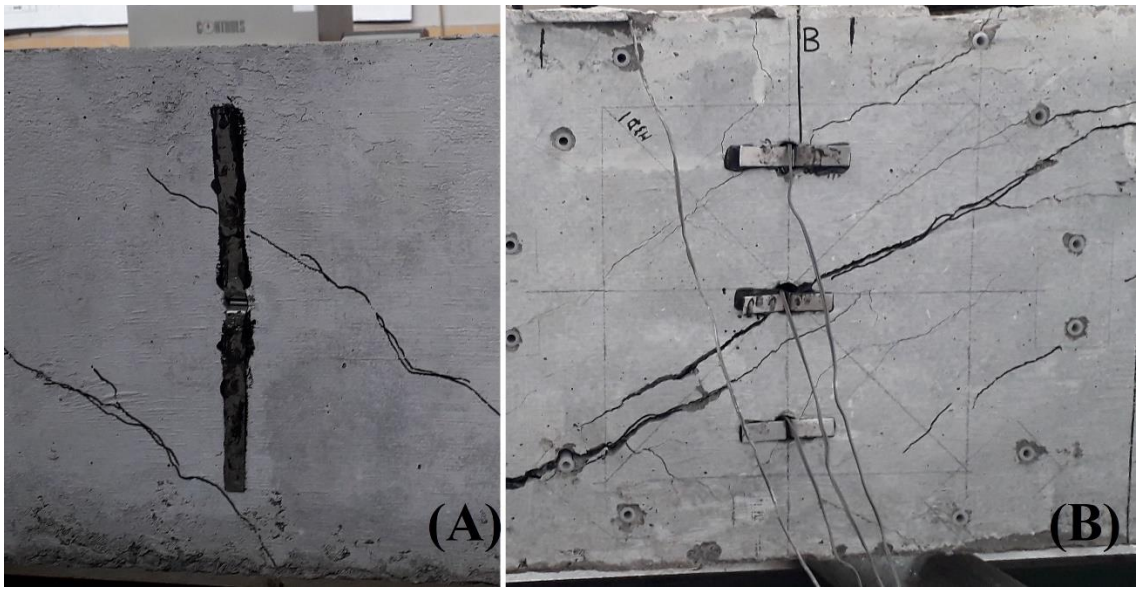

Figure 3-36: Aluminum Strip Plates Attached to Beam (A) Trial Beam (B) Main Specimens

Aluminum plates with a thickness of 1mm are chosen for their better flexibility and lower modulus of elasticity as compared to using steel. The aluminum plates were placed in the universal testing machine to quantify its mechanical properties but unfortunately the sample failed locally before being loaded when the machine grabbed it for testing. Hence no data regarding the plate's mechanical property was recorder as the plate's failure load was way below the machine's sensitivity. After examining the plates manually, it was seen that their flexibility was suitable for

the desired purpose. The strain gauge attached would sense even the smallest bit deformation since the plate thickness used allows a deformation to happen even at smaller load.

3.4.2. Surface Mounted Displacement Measurements

A 240mm*240mm square grid with a diagonal length of 340mm was used as a guide to place surface displacement measuring instruments. This square grid was positioned in a region where shear failure is expected to govern, it was placed between the support and loading point on the beam symmetrically in two alternative sides. Linearly varying differential transformers (LVDT) (Displacement Transducers) were installed along the two diagonals put at 45º and 135º degree angles and one horizontal installation was placed at the midline of the proposed grid.

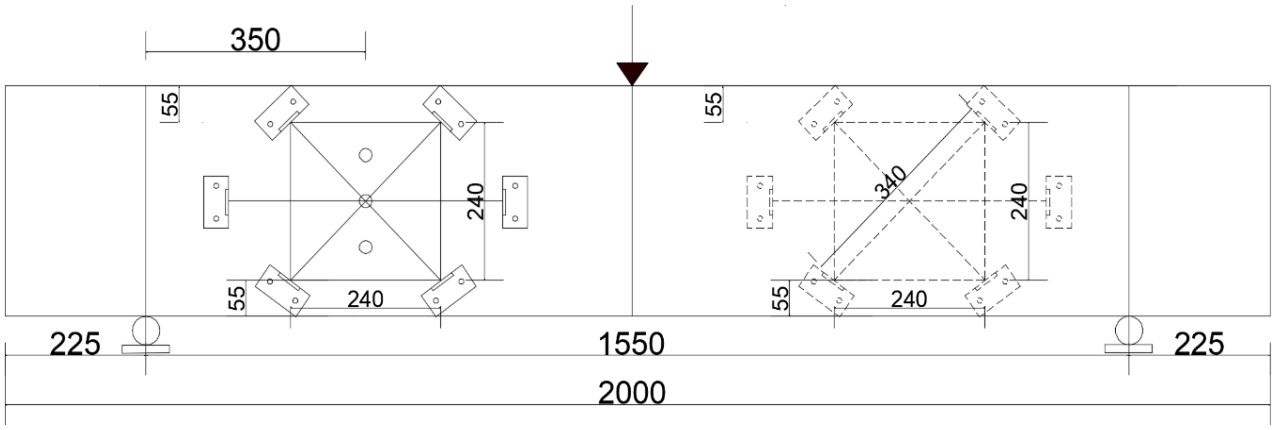

Figure 3-37: Surface Mounted Displacement Measuring Instrument Setup

Holes for mounting instrumentation steel plates were pre-drilled in each specimen prior to installation of test assembly components. The displacement transducers were logged in to the geodatalog which is connected to a computer data acquisition system named “Datacom”, which was tailored to record data in 1 second interval to match with the TDS-630 data logger. The results obtained were then collected in an excel format from the connected computer. A total of three LVDTs were used on one side of the beam, the average surface shear strain was obtained from the relative movement of the two diagonally placed displacement measurements while longitudinal displacement was obtained from the horizontally placed LVDT. The same set up is reciprocated at the alternative side.

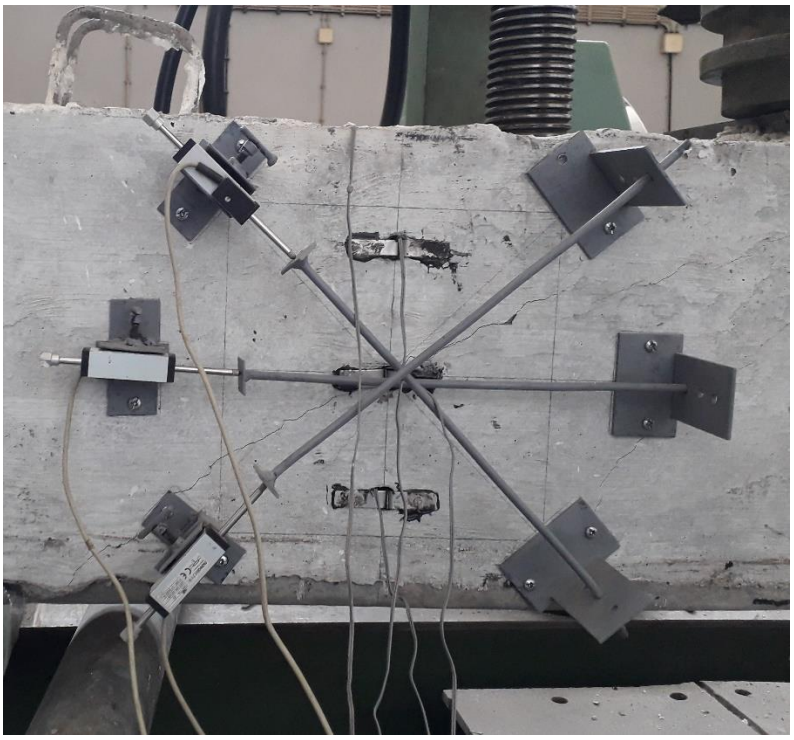

Figure 3-38:Surface Mounted Displacement Measuring Instruments

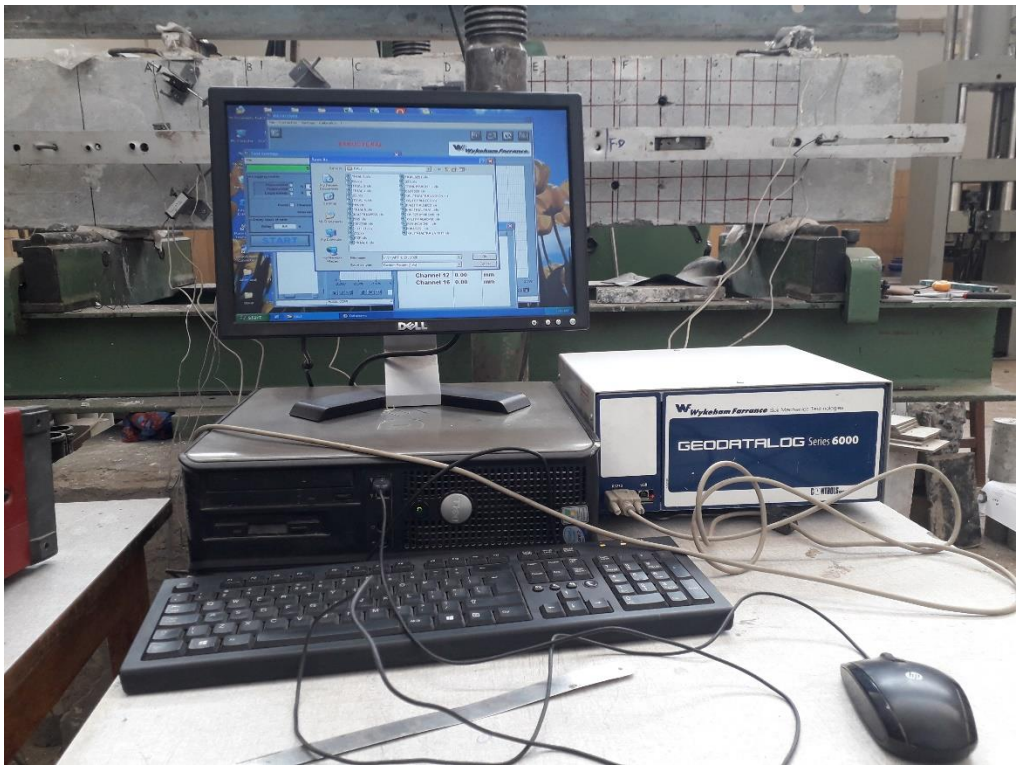

Figure 3-39: Geodatalog Connected to a Computer Data Acquisition System

4. TESTING OF SPECIMENS

4.1. Testing Procedure

Once the beams were ready for testing, they were transported from the casting area to the construction material laboratory by using a pickup vehicle. Within the laboratory, heavy lift equipments and hydraulic floor cranes were used to place the beams on the reaction frame. The reaction frame had two roller supports which were adjusted for the required testing length of the beam. After placement, the beam alignment was then adjusted to the center of the reaction frame.

The test assembly followed a thorough procedural set of steps to avoid eccentric loading and to ensure proper reading of measuring instruments for their intended purpose. Primarily, the holes for mounting surface displacement measuring instruments were drilled. After that, aluminum strip plates with strain gauges attached in the middle were anchored through the width of the beam by using an Epoxy adhesive followed by placement of surface displacement measuring instruments mounted on to the drilled holes by screws.

Plumb bob and bubble level were used while setting up for the loading platform above the beam which included the load cell, hydraulic jack and thick load bearing/distributing plates which were used in between for an even load distribution and to avoid local crushing on the beam surface.

Since the setup and preparation prior to testing required a lengthy amount of time, it took two days to complete the testing of one specimen. The first day, the beam is setup for the planned measurements and the instruments are installed. Testing took place the second day after the setup instruments were properly connected to their respective data recording systems. After initializing readings, the beam is loaded to failure under monotonic loading. During testing the beam was monitored distantly for safety reasons but a camera was mounted nearby to document the tests. At the end of each test day the accessories for loading and instrumentations were removed and post failure status of the beam was documented by taking pictures and measuring crack properties.

4.2. Test Observation - TRIAL Beam

As detailed in Figure 3-5, the trial beam was designed with two different side covers of 50mm and 75mm on each side of the beam's cross section. Additionally, for the same web reinforcement ratio of 0.74% two different stirrup spacing of ϕ8 c/c 60mm and ϕ10 c/c 100mm were used on the left and right side of the beam, making it a specimen with four different test regions, as shown in Figure 3-5. The beam had a flexure to shear over strength factor of 1.25. It went through 9 cycles of loading in multiple days before finally being loaded to failure. This was due to loading problems regarding the load applying hydraulic jack. Three different hydraulic jacks were used consecutively in multiple attempts to achieve the expected failure load but were inadequate to

apply load greater than 500kN. The expected failure load of the specimen under one-point monotonic loading was 682.5kN (CSA).

The trial beam had a test day concrete compressive strength of 26.15MPa. On the first testing day the specimen was subjected to 3 cycles of monotonic loading at a maximum of 348kN, 458kN, and 461kN. On the second testing day the beam was loaded only up to 500kN and the hydraulic jack couldn't load any further. Hence the need for another loading jack that can deliver up to 650kN.

On the third testing day a new hydraulic jack was tried and the specimen was again subjected to 3 cycles of monotonic loading each at a maximum of 64kN ,57kN, and 112kN, the hydraulic jack needed modifications as it was not possible to load greater than 112kN. After modifying the new hydraulic jack to best fit the loading purpose, 2 cycles of loading were undertaken at a limited peak load of 439kN and 469kN. Unfortunately, the modifications made were unable to apply the required failure load leading to the final 10th cycle.

After the first 9 cycles flexural and diagonal cracks of width less than 0.8mm were observed on all four test regions and were marked with a black marker for better visibility. No significant damages had occurred to the physical surface of the beam.

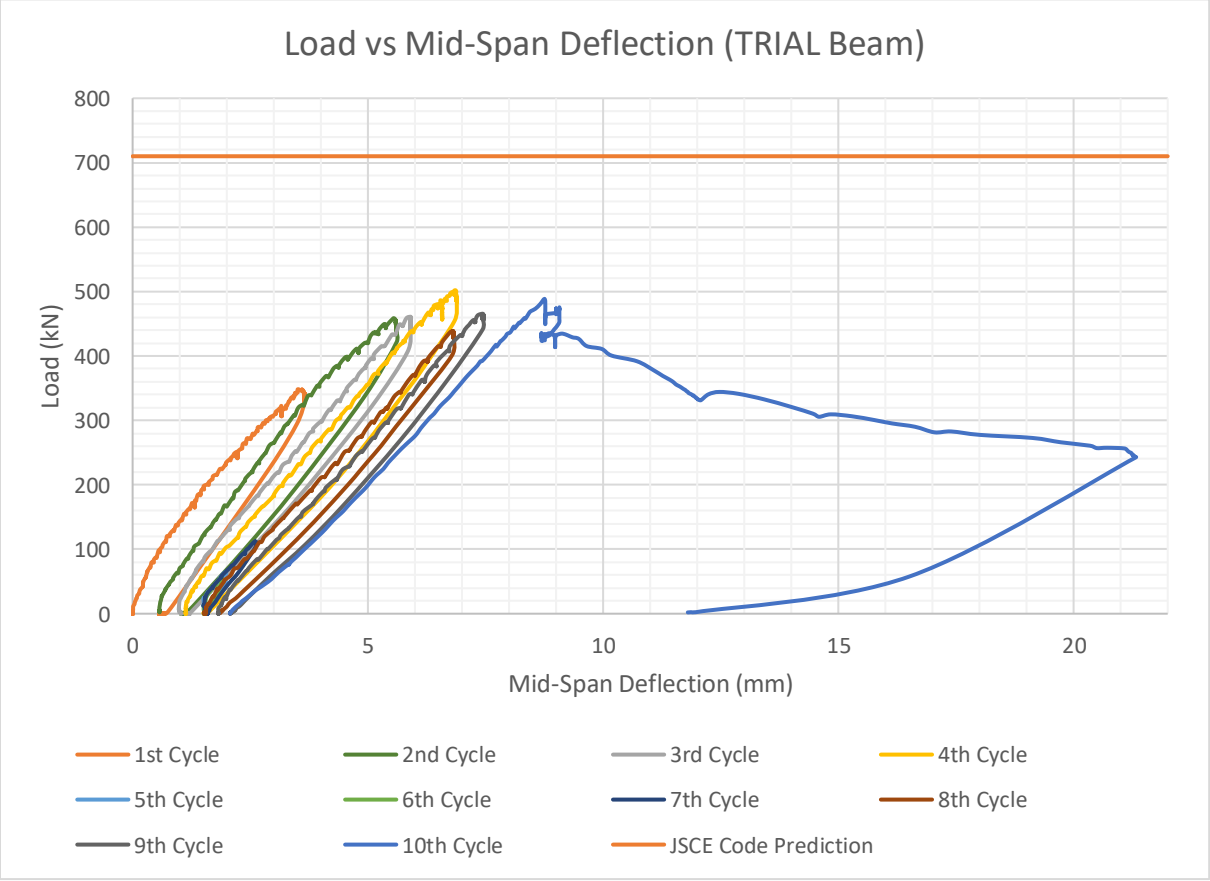

Figure 4-1: Load Vs. Mid-Span Deflection for TRIAL Beam

Figure 4-2: Trial Specimen After the First 9 Cycles of Loading (A.TR 8-50 / B.TR 8-75 / C.TR 10-50 / D.TR 10-75)

After six months, the trial beam was loaded to failure and failed in shear. With a test day concrete compressive strength of 35.3MPa the specimen failed at 488.6kN which is below the predicted failure load even after considering the beam's previous history of loading. During the first loading stages, the diagonal shear cracks created previously started to widen, especially on the left side (8 c/c 60/ 50) where the failure happened. As loading progressed, the diagonal cracks near the bottom tension side showed a greater increase in crack width as compared to the ones propagating to the top loading point. This was followed by a peculiar longitudinal cracking on the top surface of the beam originating from the loading point.

As the beam approached failure it was accompanied by multiple closely spaced diagonal cracks increasing in width and detaching from the concrete core. At failure the concrete cover was detached from the core at exactly where the diagonal compression cracks of failure had occurred. The top longitudinal crack also split outward creating an out of plane deformation.

Figure 4-3: Top Longitudinal Crack at Failure (TRIAL Beam (TR 8-50/75))

A clear difference in diagonal compression crack width and spacing was observed from the two sides having 50mm and 75mm side cover. The side with 50mm side cover had a closely spaced diagonal cracks with a relatively smaller crack width. The side with 75mm side cover however had fewer cracks with larger crack width.

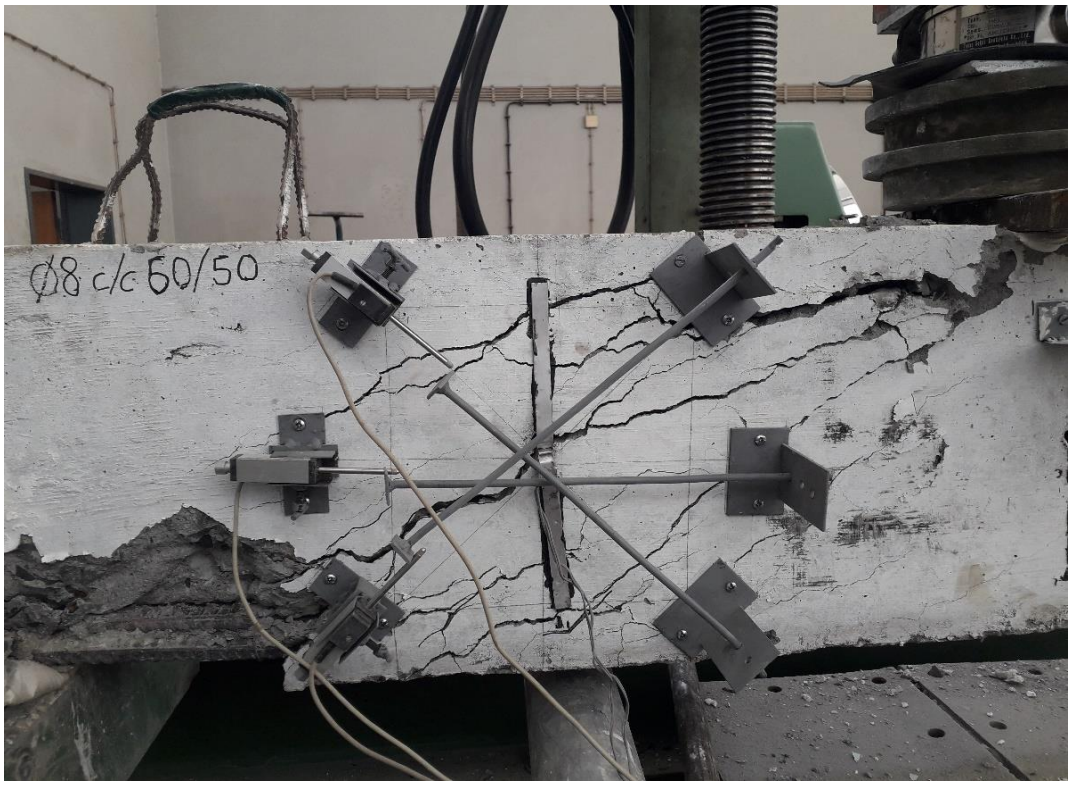

Figure 4-4: Diagonal Shear Cracks at Failure, 50mm Side Cover (TRIAL Beam (TR 8-50))

Figure 4-5: Diagonal Shear Cracks at Failure,75mm Side Cover (TRIAL Beam (TR 8-75))

The side cover provided on each side had completely delaminated on the area of maximum shear following the diagonal compression cracks. After the surface measuring instruments were taken off the beam, the loose side cover detached from the core section was effortlessly removed by hand picking.

Figure 4-6: Side Cover Spalled ,50mm Side Cover (TRIAL Beam (TR 8-50))

Figure 4-7: Side Cover Spalled, 75 mm Side Cover (TRIAL Beam (TR 8-75))

It can be seen that the concrete side cover within the diagonal compression zone had spalled off, including the cover in the top and bottom faces of the beam. The concrete core confined inside the stirrup cage was however intact.

Figure 4-8: Side Cover Spalled, Top View (TRIAL Beam (TR 8-50/75))

Figure 4-9: Final State of Beam After Failure (TRIAL Beam)

4.3. Test Observation - Specimen SI8-25

Specimen SI8-25 was designed with a side cover thickness of 25mm with a web reinforcement ratio of 0.71%, a stirrup ϕ8 c/c 60mm was used throughout the beam's length. The beam had a flexure to shear over strength factor of 1.18. Before being loaded to failure the beam went through 22 cycles of loading, due to problems of the loading jack the test had to be reloaded multiple times. SI8-25 had a test day concrete compressive strength of 36.8MPa and failed at 639kN.

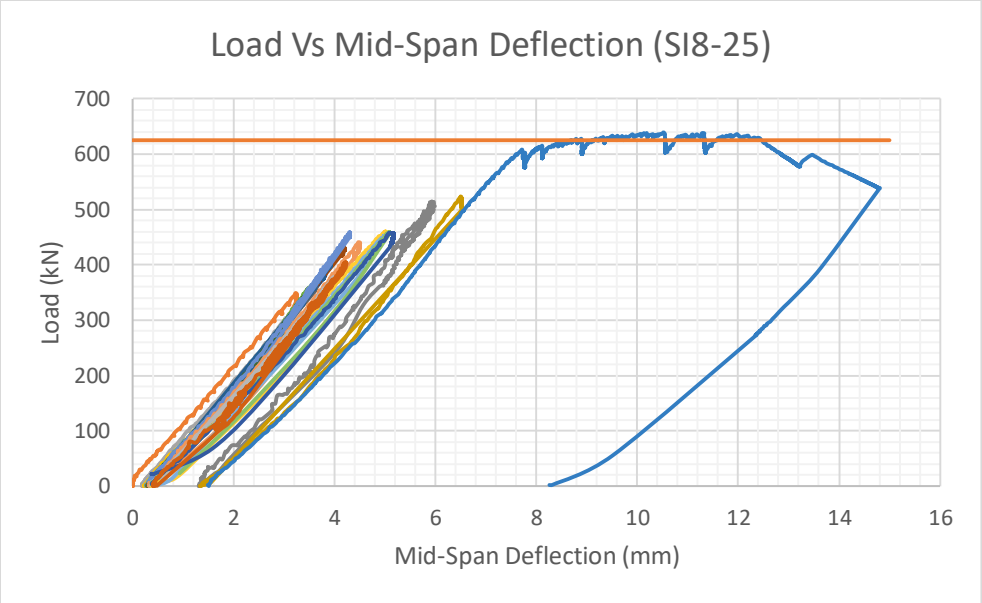

Figure 4-10: Load Vs. Mid-Span Deflection for SI8-25

At earlier load stages diagonal shear cracks started forming following flexural cracks at the bottom of the beam. As loading progressed, the diagonal cracks on the left side (the side where failure had propagated) showed a greater increase in crack width as compared to the one on the right. Similar to the trial beam, top longitudinal crack originating from the loading point along the center was also observed in this specimen. In addition, top crack following the stirrup cage was observed but it was limited to a shorter length. However, at failure load this top crack did not widen as much as it did on the trial beam.

Figure 4-11: Top Longitudinal Crack (SI8-25)

At peak load the main diagonal crack causing failure had a width of 9.3mm near the bottom while the flexural cracks opened up to 1.9mm. The top longitudinal crack near the edge of the beam led to spalling of the side cover near the top loading region.

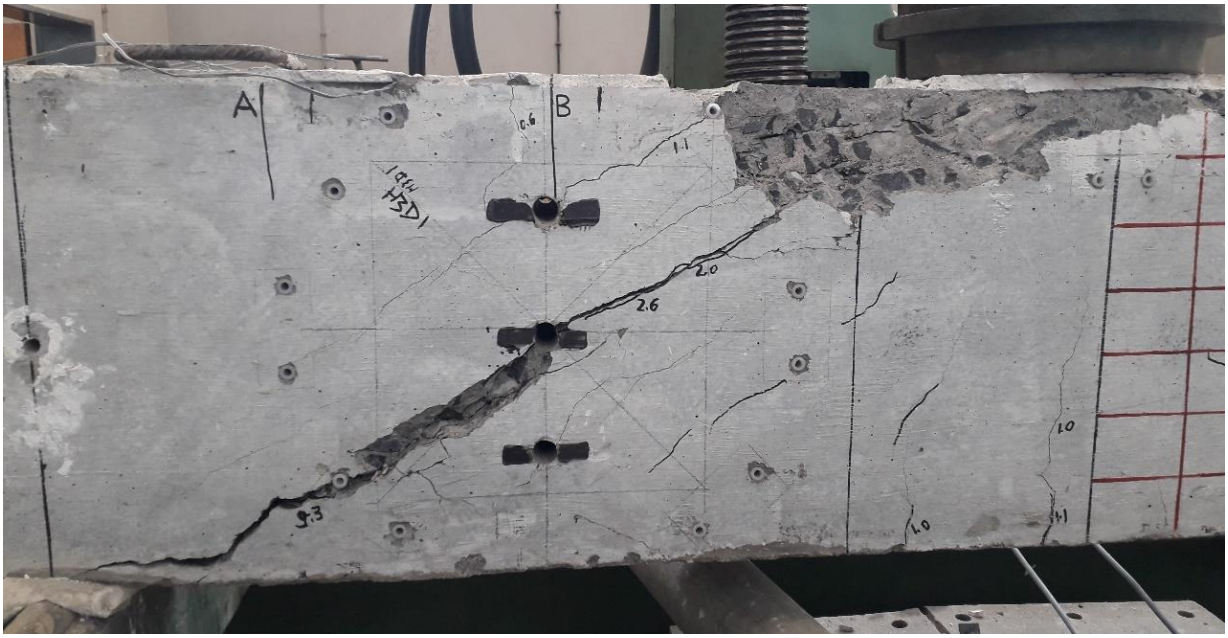

Figure 4-12: Side Cover Spalling Limited at the Top (SI8-25)

Similar behavior is reciprocated at the back of the beam as well. Although not accompanied by spalling, the top cover had detached from the concrete core.

Figure 4-13: Back Side Diagonal Compression Cracks at Failure (SI8-25)

This specimen showed a typical shear failure with an average diagonal shear crack spacing of 9.5cm on each side. Spalling was observed near the top at peak load.

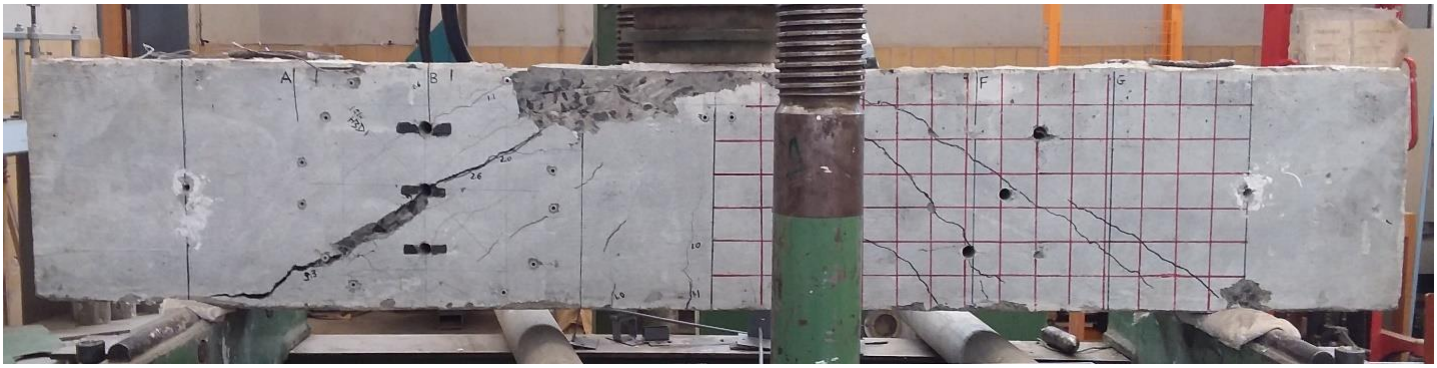

Figure 4-14: Final State of Beam After Failure (SI8-25)

4.4. Test Observation - Specimen SI8-50

Specimen SI8-50 was designed with a side cover thickness of 50mm and a web reinforcement ratio of 0.57%, a stirrup ϕ8 c/c 60mm was also used throughout the beam's length. The beam had a flexure to shear over strength factor of 1.17. With a test day concrete compressive strength of 35.1MPa the specimen failed at 681kN.

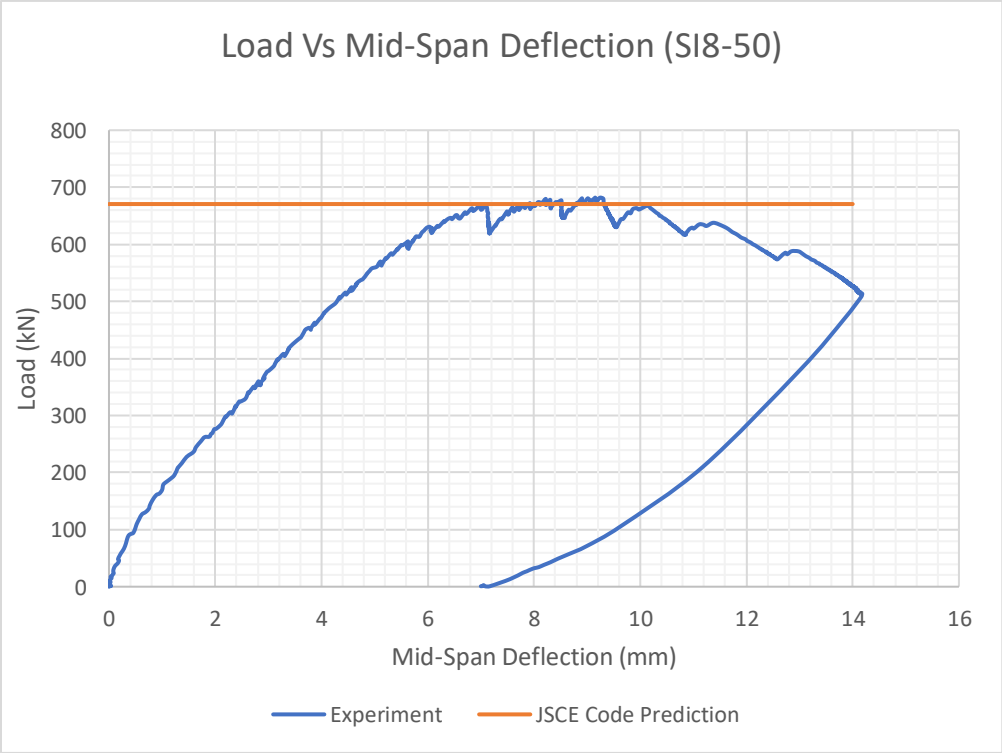

Figure 4-15: Load Vs. Mid-Span Deflection for SI8-50

Diagonal compression cracks formed at a spacing of 12.5cm from each other. The failure crack propagated on the right side of the beam.

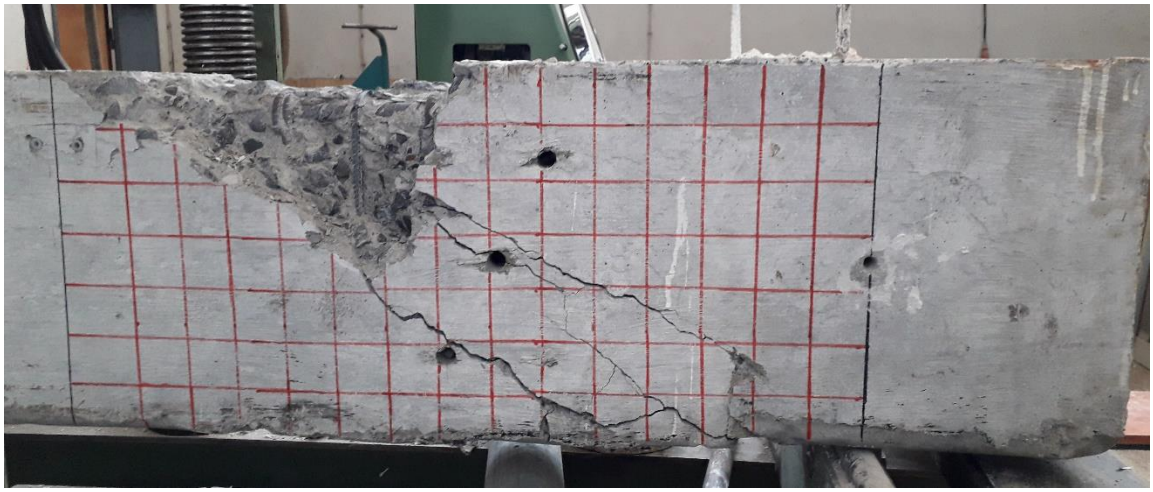

Figure 4-16: Diagonal Compression Crack at Failure (SI8-50)

Top longitudinal cracks were observed following the edge of stirrup cage. The concrete side cover in both sides near the top had completely detached from the core and loose concrete was hand-picked after the test instruments were removed off the beam.

Figure 4-17: (A) Top Longitudinal Cracking (B) Spalled Section Top View (SI8-50)

Although the observed spalling was limited to the top section of the beam, the section had experienced an out of plane deformation. In Figure 4-17(B) it can be seen that cracks along the

stirrup cage had progressed downward indicating the cover has detached from the concrete core. After failure it can also be seen that the surface mounted displacement measurements were misaligned to their respective paired plate due to the beam's out of plane thrust.

Figure 4-18: Misalignment of Surface Measurements due to Out of Plane Deformation I (SI8-50)

Figure 4-19: Misalignment of Surface Measurements due to Out of Plane Deformation II (SI8-50)

The specimen failed in shear with spalling along the shear failure region, mainly at the top, exposing the stirrups.

Figure 4-20: Final State of Beam After Failure (SI8-50)

4.5. Test Observation - Specimen SII10-50

Specimen SII10-50 was designed with a side cover thickness of 50mm and a web reinforcement ratio of 0.57%, a stirrup ϕ10 c/c 110mm was used throughout the beam's length. This specimen is designed as replica of SI8-50 only differing in stirrup spacing. The beam had a flexure to shear over strength factor of 1.15. With a test day concrete compressive strength of 35.1MPa the specimen failed at 674kN.

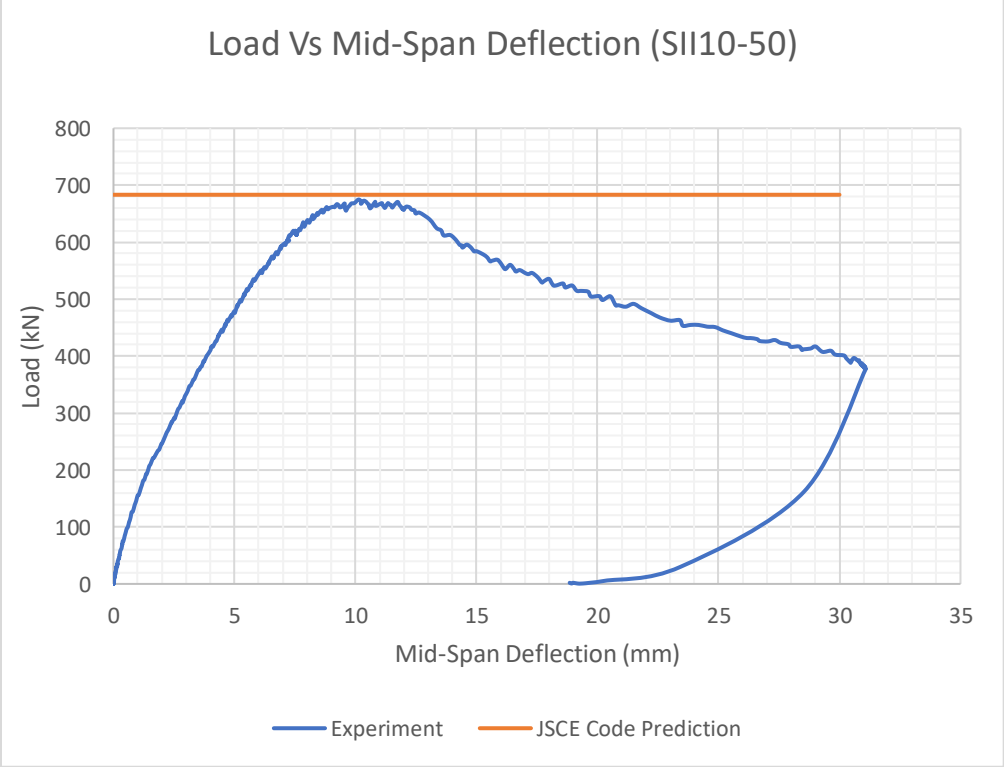

Figure 4-21: Load Vs. Mid-Span Deflection for SII10-50

Widening of diagonal compression cracks at an average spacing of 10.5cm led to propagation of failure to the right side of the beam. This was accompanied by top cracks, as shown in Figure 4-22, situated at the maximum shear area between the support and loading point.

Figure 4-22: Top Longitudinal Cracking (SII10-50)

For the purpose of documenting it's post peak behavior, the specimen was loaded further after ultimate load was reached. This led to the widening of already created diagonal compression cracks and increase in out of plane expansion making the concrete side cover loose enough to fall off.

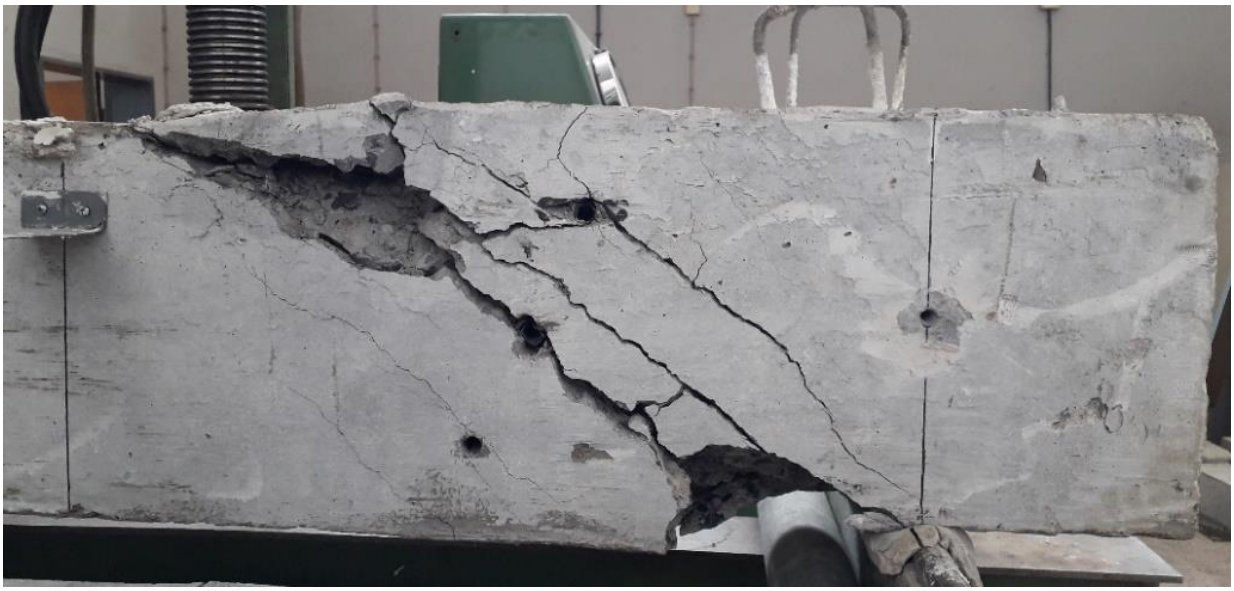

Figure 4-23: Diagonal Compression Crack and Top Spalling at Failure Front Side (SII10-50)

Figure 4-24: Diagonal Compression Crack and Top Spalling at Failure Back Side (SII10-50)

Concrete cover section in the entire diagonal compression region was detached from the core. The loose concrete cover was hand-picked as it was completely separated from the concrete core. Concrete covers (including top and bottom covers) were wholly spalled at the maximum shear stress area of the beam.

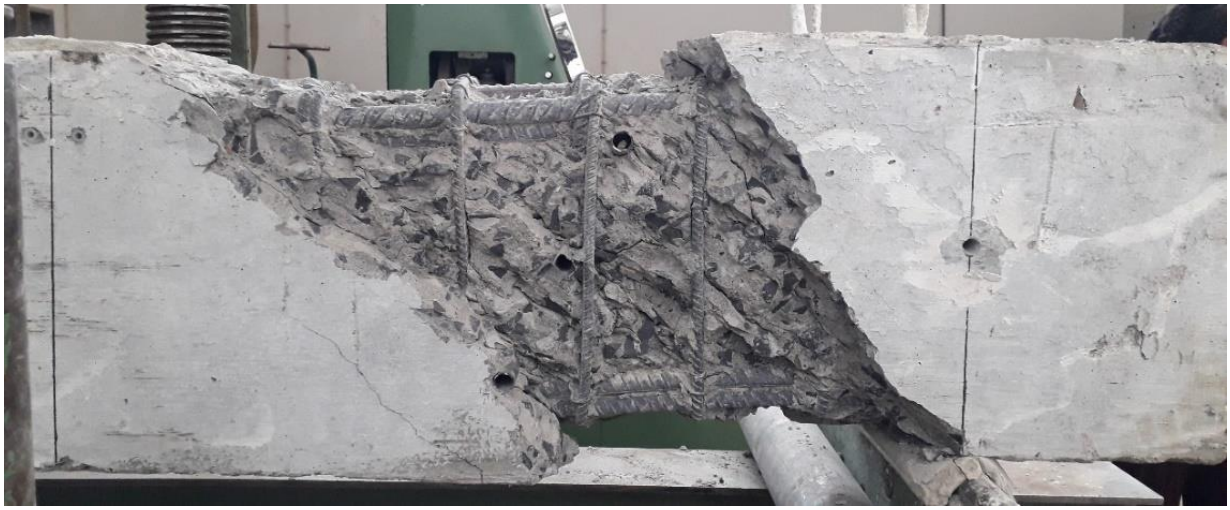

Figure 4-25: Spalled Section Front Side (SII10-50)

The concrete core between stirrups is seen to be affected by the spalling as some parts of it's section were detached along with the delaminated side cover. The longitudinal reinforcement bending was also seen clearly at the spalled sections.

Figure 4-26: Spalled Section Back Side (SII10-50)

Figure 4-27: Final State of Beam After Failure (SII10-50)

4.6. Test Observation - Specimen SIII10-75

Specimen SIII10-75 was designed with a side cover thickness of 75mm and a web reinforcement ratio of 0.57% (similar to SI8-50 and SII10-50, and SIII8-75), a stirrup ϕ10 c/c 110mm was used throughout the beam's length. This beam also had a reduced stirrup cage width of 100mm.The beam had a flexure to shear over strength factor of 1.15. With a test day concrete compressive strength of 35.1MPa the specimen failed at 455kN.

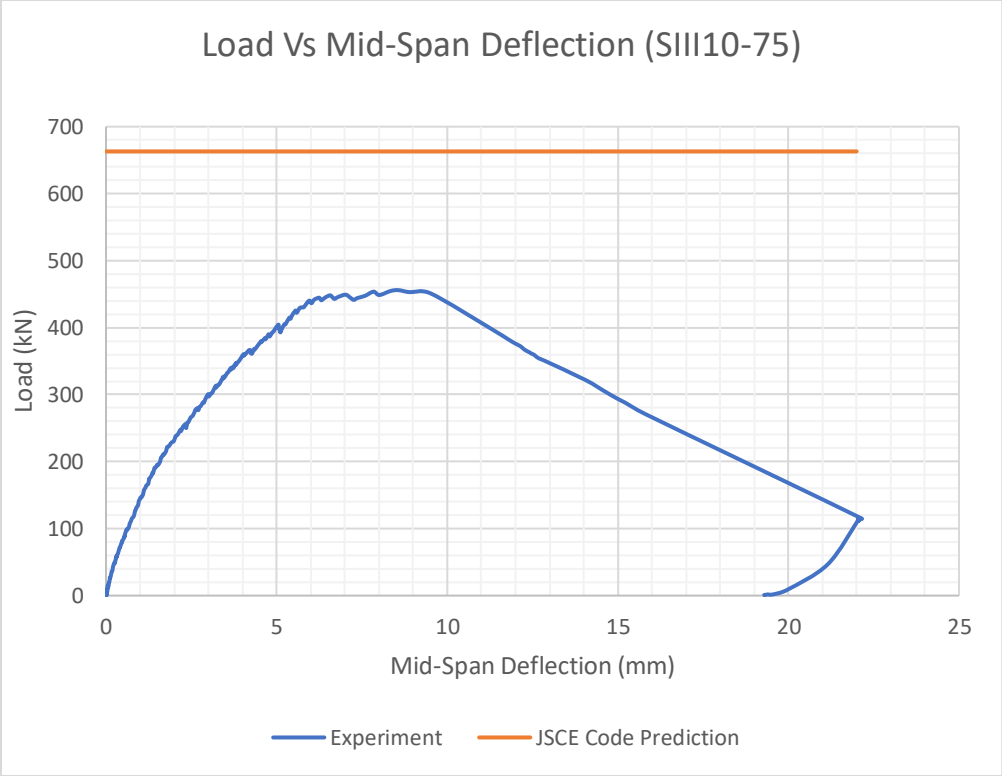

Figure 4-28: Load Vs. Mid-Span Deflection for SIII10-75

The diagonal compression crack that led to failure happened in the right side of the beam. Once the diagonal crack was created, its widening happened quickly. It had a width of 15mm.

Figure 4-29: Diagonal Compression Crack at Failure Front Side (SIII10-75)

In addition to diagonal cracks from loading point to the support, splitting cracks were observed at the rear section of the beam as shown in Figure 4-30. The top longitudinal cracks had continued to the sectional part for this specimen.

Figure 4-30: Splitting Crack Rear Section of the Beam (SIII10-75)

Cracks observed at the rear end cross section of the beam were continuation of the top longitudinal crack as shown below in Figure 4-31.

Figure 4-31: Top Longitudinal Crack (SIII10-75)

The loose concrete side cover was then removed and was observed that the front side had completely spalled above the failure diagonal crack while the back side was relatively intact as the spalling was situated only around the end of the beam. It can be seen that spalling happened at the interface caused by stirrups.

Figure 4-32: (A) Spalling on the Rear End of the Beam (B) Spalled Section Back Side (SIII10-75)

Figure 4-33: Spalled Section Front Side (SIII10-75)

The detached side cover from the front side came out in one piece without crushing.

Figure 4-34: Spalled Piece of Side Cover (SIII10-75)

It was observed from this detached piece that the plane of spalling was not necessarily a straight line following the stirrups. As seen in Figure 4-34, in between stirrup planes concrete sections from the core are seen detached. Roughness valleys penetrating into the core concrete confined within the stirrups were also observed in the final spalled state of the beam.

Figure 4-35: Final State of the Beam (SIII10-75)

4.7. Test Observation - Specimen SIII8-75

Specimen SIII8-75 was designed with a side cover thickness of 75mm and a web reinforcement ratio of 0.57% (similar to SI8-50, SII10-50 and SIII10-75), a stirrup ϕ8 c/c 70mm was used throughout the beam's length. This beam from the third set differs from the specimens of the other two sets such that it had a reduced stirrup cage width of 100mm.The beam had a flexure to shear over strength factor of 1.17. With a test day concrete compressive strength of 35.1MPa the specimen failed at 541kN.

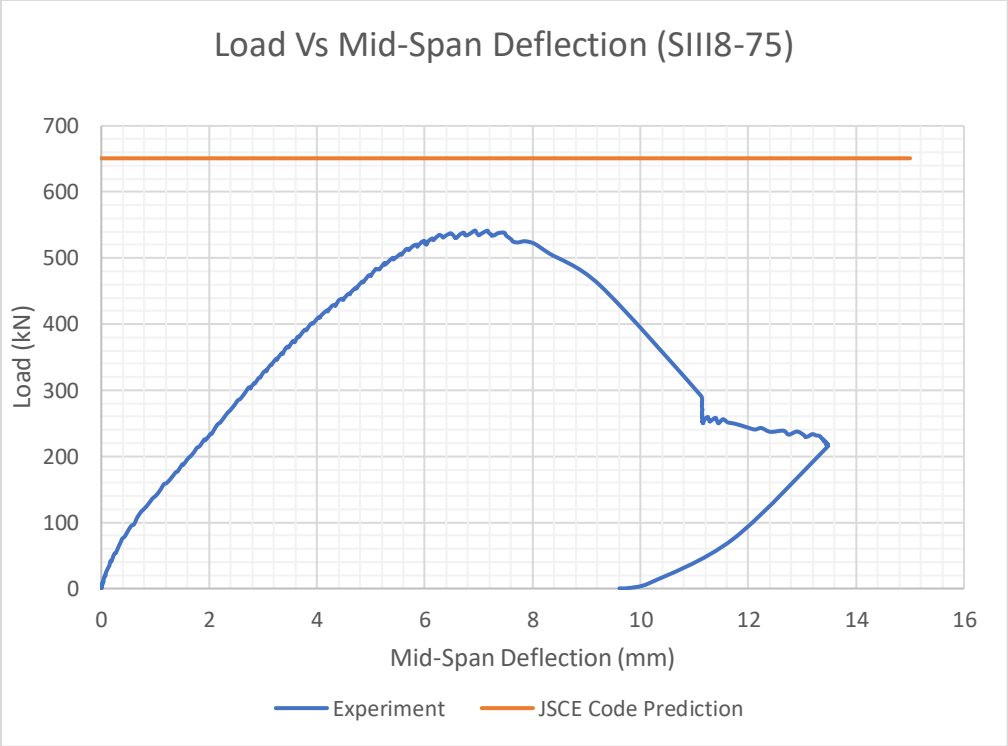

Figure 4-36: Load Vs. Mid-Span Deflection for SIII8-75

After reaching the peak load, the cover on the rear left side fell off. Failure started at the left support from the front side and propagated diagonally along the section, leading to a sudden detachment. This incident prevented post peak loading as the detached section created a loss of confinement near the support and the concrete directly above the support had crashed following the fall-off.

Figure 4-37: Concrete Cover Spalling at the Rear Left End (A) Front View (B) Sectional View (C) Back View (SIII8-75)

In Figure 4-37 (B) clear spalling of side cover from a cross sectional point of view can be seen as a crack of width 5mm splits through the interface of the stirrup cage and side cover.

The spalled section was intact and in one-piece resembling a pure anchorage failure.

Figure 4-38: Spalled off Section (SIII8-75)

The diagonal compression cracks and the top longitudinal crack propagated as the peak load was reached. The diagonal crack had a crack width of 0.6mm.

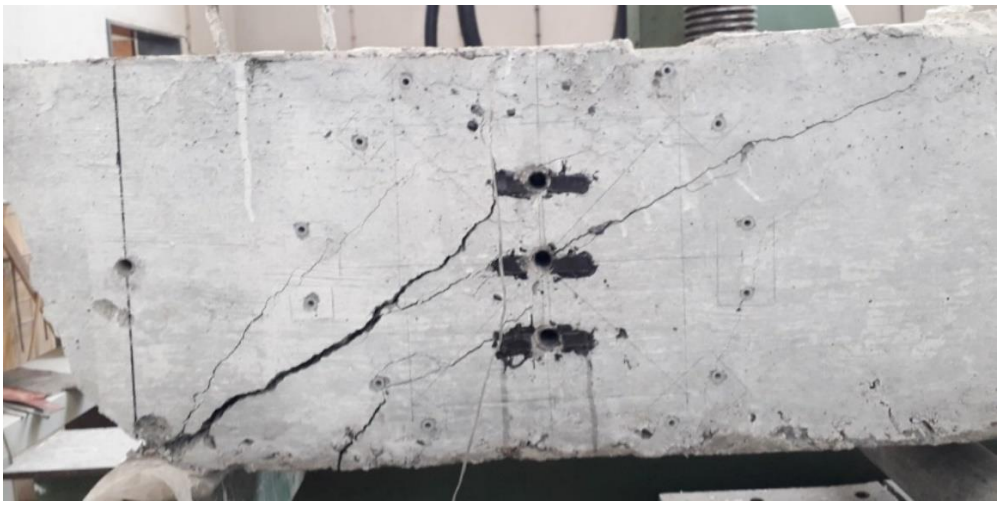

Figure 4-39: Diagonal Compression Cracks at Failure Front Side (SIII8-75)

Due to localization of stress near the end of the beam caused by loss of cross section, nearly vertical cracks originating from the support are observed at the back of the failure region.

Figure 4-40: Diagonal Compression Cracks at Failure Back Side (SIII8-75)

The front section of the failure zone had a side cover that was completely detached from the core above the diagonal compression crack.

Figure 4-41: Spalled Section Front Side (SIII8-75)

Spalling strictly followed the interface plane created by stirrups by creating a relatively smooth surface of concrete between stirrups.

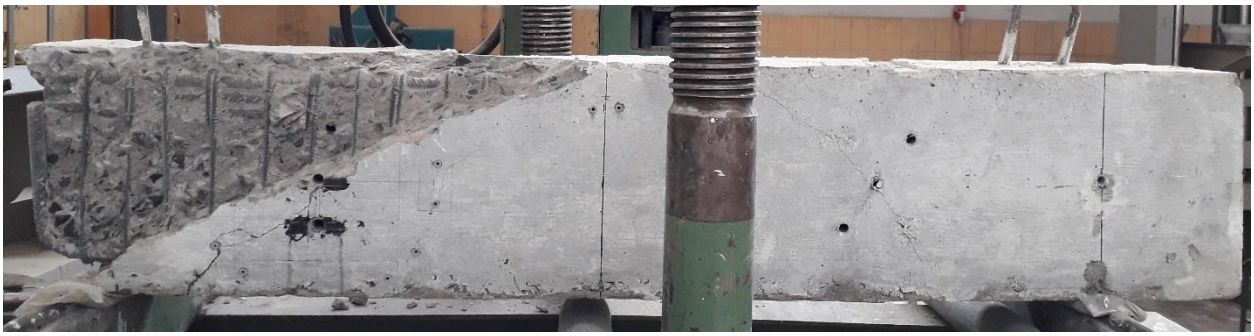

Figure 4-42: Final State of Beam (SIII8-75)

4.8. Test Observation - Specimen SII10-75

Specimen SII10-75 was designed with a side cover thickness of 75mm and a web reinforcement ratio of 0.48%, a stirrup ϕ10 c/c 110mm was used throughout the beam's length. It had the largest beam width and largest expected failure load from all the test specimens. The beam had a flexure to shear over strength factor of 1.17. With a test day concrete compressive strength of 35.1MPa the specimen failed at 727kN.

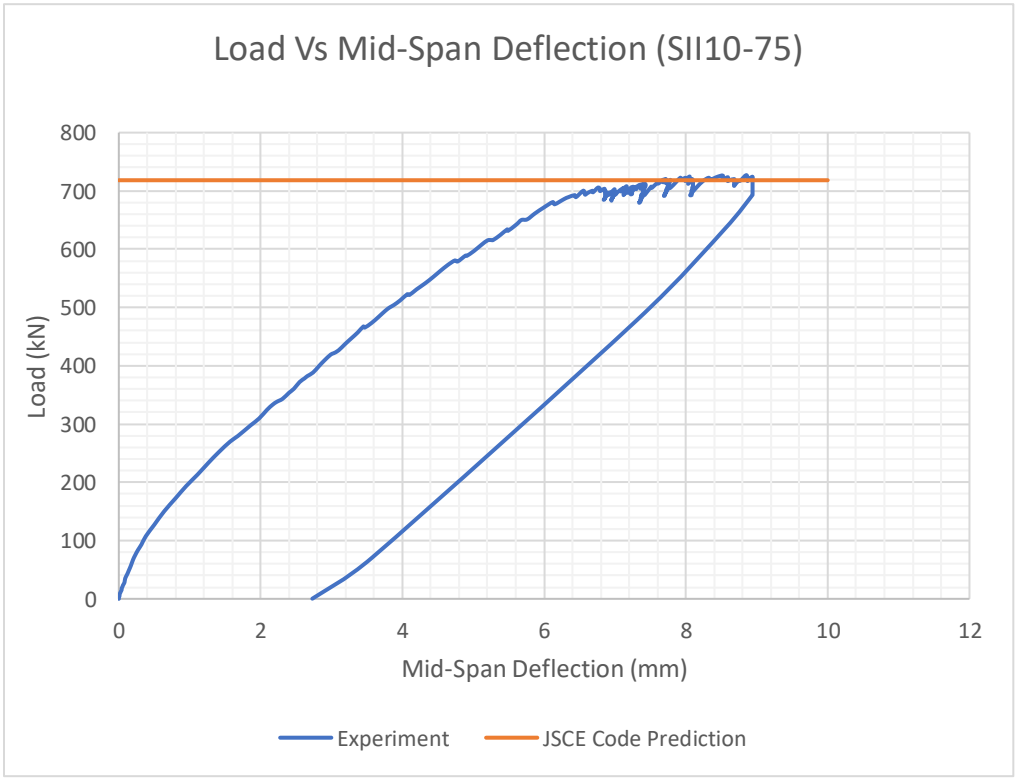

Figure 4-43: Load Vs. Mid-Span Deflection for SII10-75

Due to load limitations of the reaction frame, the testing had to stopped just at the ultimate load and post peak behavior couldn't be documented. Diagonal cracks were observed in the same failure manner as the previously tested specimens. Failure propagated at the left side of the beam with a diagonal crack width of 2mm.

Figure 4-44: Diagonal Compression Crack at Failure Back Side (SII10-75)

As in the case of the previously tested specimens, top longitudinal cracks originating from the loading point were observed.

Figure 4-45: Top Longitudinal Crack (SII10-75)

At failure the beam had an average diagonal crack spacing of 10cm and flexural cracks of width 0.3mm.

Figure 4-46: Diagonal Compression Crack at Failure Front Side (SII10-75)

Figure 4-47: Final State of Beam After Failure (SII10-75)

5. NON-LINEAR FINITE ELEMENT ANALYSIS

5.1. 2D NLFEA Using Vector 2

The specimens defined for the experimental program are modelled using a two-dimensional non-linear finite element analysis tool called Vector 2. Vector 2 is a program based on the modified compression field theory and disturbed stress field model for predicting the response of reinforced concrete elements subjected to in-plane normal and shear stresses under quasi- static or dynamic load conditions.

It uses a pre-processor software program called FormWorks and the software Augustus provides graphical post processing for the analysis results. Augustus provides post-analysis visualization of results such as the load-deformation response, element stress and strain conditions, crack patterns, and other data. The output data has separate files for each load stage, describing the state of the nodes and elements. It also includes the material properties utilized, finite element model, and the analysis.

5.1.1. Material Definition

5.1.1.1. Concrete

Two types of concrete materials were defined for each model, plain concrete used for concrete covers and concrete with smeared reinforcement for part of the beam that includes web reinforcement. Concrete regions were modeled with Plane Stress Rectangular Elements with uniform thickness in the out-of-plane direction. The width of the beams were therefore defined as thicknesses for each model. Both compressive and tensile strength of concrete were taken from the experimental program.

5.1.1.2. Reinforcement

Similar to the concrete material, two types of reinforcements were used, longitudinal flexural reinforcements were modelled as discrete ductile truss elements while web reinforcements were modeled as smeared reinforcement within the concrete by specifying the web reinforcement ratio. Yield and ultimate strength of reinforcements were taken from rebar tests conducted in the laboratory. In addition, smeared reinforcements in the out of plane direction were defined for the plain concrete used in the cover parts of the beam to avoid localized failures.

5.1.1.3. Structural Steel

Steel supports serving as reactions in the actual experiment were also incorporated in the modelling by defining structural steel as one of the materials. Its thickness was defined the same as the width of the beam used.

5.1.2. Modelling

In modelling the specimens, first, geometry of the element is defined by creating regions. Regions are created by defining four nodes, assigning material and defining mesh parameters. For a more accurate result a finer mesh grid of 10mm by 15mm (x, y) was defined for each specimen. Then reinforcements were defined as truss elements between two nodes by assigning previously defined reinforcement material. Finally, the mesh was created and added to the defined structure.

Boundary conditions were set for the defined structure before analysis by adding support restraints at the two sides where structural steel supports were defined. Aimed to create a simply supported one pin and roller supports were used at alternative supports of the beam model. Monotonic loading was applied by assigning a fixed support displacement.

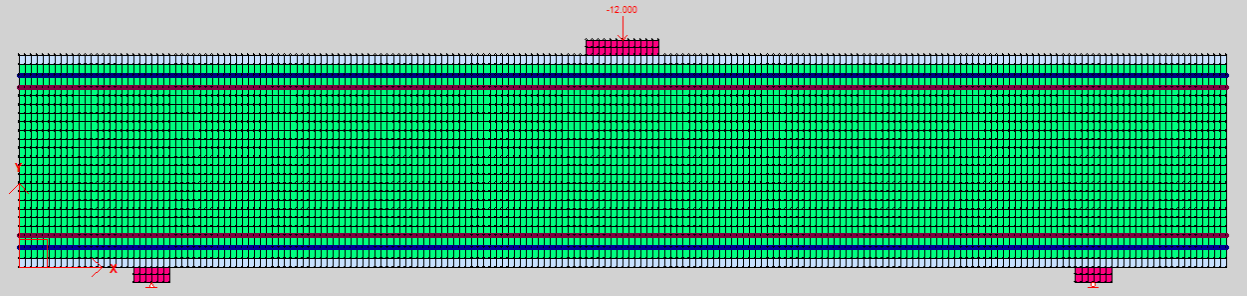

Figure 5-1: Typical VecTor 2 Modelling for Specimens

One load case with a monotonic loading type with an iteration of 50 load stages was defined. Vector processor is then run for analysis and results were graphically illustrated by the post processor, Augustus.

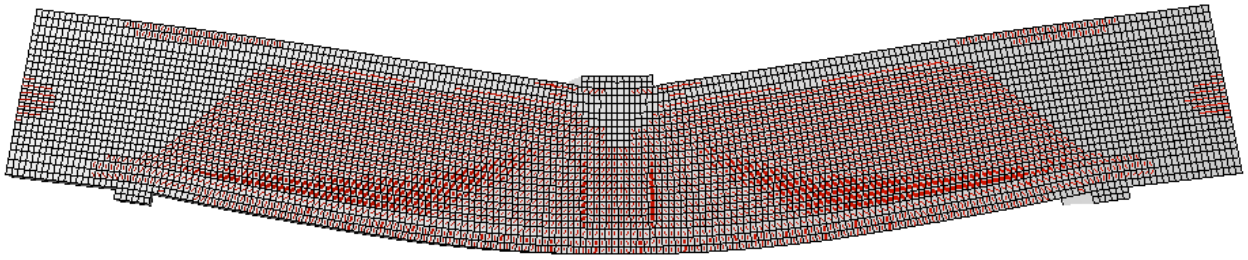

Figure 5-2: Displacement and Crack Pattern at Failure Displayed by Augustus

6. RESULT AND DISCUSSION

Seven slender RC Beams were tested to failure and all specimens failed in shear. The full response and prediction of each specimen is reported and discussed in this section based on the collected data. Software simulations, and building code predictions are reported and further explanations are given based on their responses. The effect of different variables used are also discussed thoroughly by making equivalent comparisons.

6.1. Building Code Predictions

Based on the material property of the web reinforcement used, longitudinal reinforcement ratio and the beam's test day concrete strength from corresponding cube and cylinder samples, ultimate load resistance capacity was predicted using the four building codes reviewed in section 2.2 and by the MCFT reviewed in section 2.1.2. For building code predictions hand calculation procedures were followed according to their respective design equations included in APPENDIX while the program RESPONSE 2000 was used to determine predictions based on MCFT.

Table 6-1 below summarizes predictions made by Eurocode (EC), ACI Standard (ACI), Canadian Standard (CSA), Japanese Code (JSCE) and the program RESPONSE 2000 which is based on MCFT.

Table 6-1: Building Code Prediction for Ultimate Load Resistance

	Experimental Results					Ultimate Static Failure Load Prediction (kN)				
Specimen	fc (MPa)	ϱl (%)	fyd (MPa)	ϕ (mm)	Failure Load (kN)	MCFT (RESPONSE)	EC	ACI	CSA	JSCE
SI8-25	36.82	2.5	520.08	8	639.51	673.4	535.9	586.5	624.8	625.2
SI8-50	35.1	2.4		8	681.77	764.4	558.2	610.1	666.6	669.1
SII10-50	35.1	2.4	544.48	10	674.77	771.6	571.5	624.5	678.7	681.7
SII10-75	34.59	2		10	727	871	589.5	653.3	726.9	715.1
SIII8-75	35.1	2.4	520.08	8	541.72	764.4	541.1	590.2	644.9	649.5
SIII10-75	35.1	2.4	544.48	10	455.93	771.6	553.9	603.9	656.5	661.5
TR8-50/75	26.15	3.3	515.8	8	488.6	690	619.1	660.6	682.5	710.9
TR10-50/75			534.7	10	488.6					

Accordingly, the experimental test to prediction ratio is presented below:

Table 6-2: Experimental Test to Prediction Ratio

	Test to Prediction Ratio				
Specimen	MCFT (RESPONSE)	EC	ACI	CSA	JSCE
SI8-25	0.95	1.19	1.09	1.02	1.02
SI8-50	0.89	1.22	1.12	1.02	1.02
SII10-50	0.87	1.18	1.08	0.99	0.99
SII10-75	0.83	1.23	1.11	1	1.02
Average	**0.9**	**1.2**	**1.1**	**1.01**	**1.01**
SIII8-75	0.71	1	0.92	0.84	0.83
SIII10-75	0.59	0.82	0.75	0.69	0.69
TR8-50/75 TR10-50/75	0.71	0.79	0.74	0.72	0.69

The above results indicate that for four of the specimens with stirrup cage width of 150mm (SI8-25, SI8-50, SII10-50, SII10-75) CSA and JSCE codes gave an accurate ultimate failure load prediction while both Eurocode and ACI underestimated the capacity. For the remaining three specimens, SIII8-75, SIII10-75 and TRIAL Beam with a reduced stirrup cage width of 100mm, 100mm, and 85mm respectively, Eurocode gave a relatively closer prediction than the rest due to its conservative nature.

MCFT predictions were obtained from the sectional analysis program RESPONSE 2000 which gave an over estimated result for the four specimens with an average test to prediction ratio of 0.9.

From the four building codes used, the ultimate load predictions calculated using Eurocode were the least accurate with an average test to prediction ratio of 1.2. The code gave low failure predictions underestimating the section's resistance. The main cause for these low predictions is the restricted value designated for the concrete resisting shear (Vc) limited by the crushing of concrete.

With a test to prediction ratio of 1.01, CSA and JSCE were found to give the most accurate failure load predictions for the specimens with "typical" stirrup cage width (150mm) and hence are used as a guideline for design code comparisons for all tested specimens.

6.2. Experimental Results

Experimental results of the seven tested beams (including the TRIAL Beam) are reported below. All specimens failed in shear characterized by diagonal compression cracking, and yielding of web reinforcement. It was also observed that spalling had occurred near peak load for most of the specimens.

This section will present the full response of each specimen with respect to the different data obtained from the experiment. It will also elaborate on how the defined variables affected the failure and general behavior of each specimen. As the failure of most specimens was accompanied by spalling, this section will also explain the out of plane deformation of the specimens along with interesting findings.

6.2.1. Load Deformation Curves

Load deformation curves for specimens are plotted directly from readings obtained from load cell and displacement transducer. The load cell placed right below the loading hydraulic jack gave load readings while the displacement transducer placed at the mid longitudinal section of the beam gave mid span deflection. No calculation or data manipulation was required as the data logger was calibrated to record load in *kN* and displacement in *mm* units.

6.2.1.1. TRIAL Beam

The TRIAL Beam was primarily designed to check the adequacy of the planned instrumentations and observe the effects of each defined variable in a nutshell. The specimen had four different test regions differing in stirrup spacing and side concrete cover, ϕ8 c/c 60mm and ϕ 10 c/c 100 were used on each half of the beam's longitudinal direction. Each of them had 50mm and 75mm side cover on their alternative sides. The specimen had a relatively reduced stirrup cage width of 85mm.

As mentioned in section 4.2 the trial beam had been tested multiple times (unintentionally) at different load levels before its final failure loading. A total of 10 cycles of loadings were performed. Softening of the specimen after each cycle can be seen from the load vs mid span deflection plot.

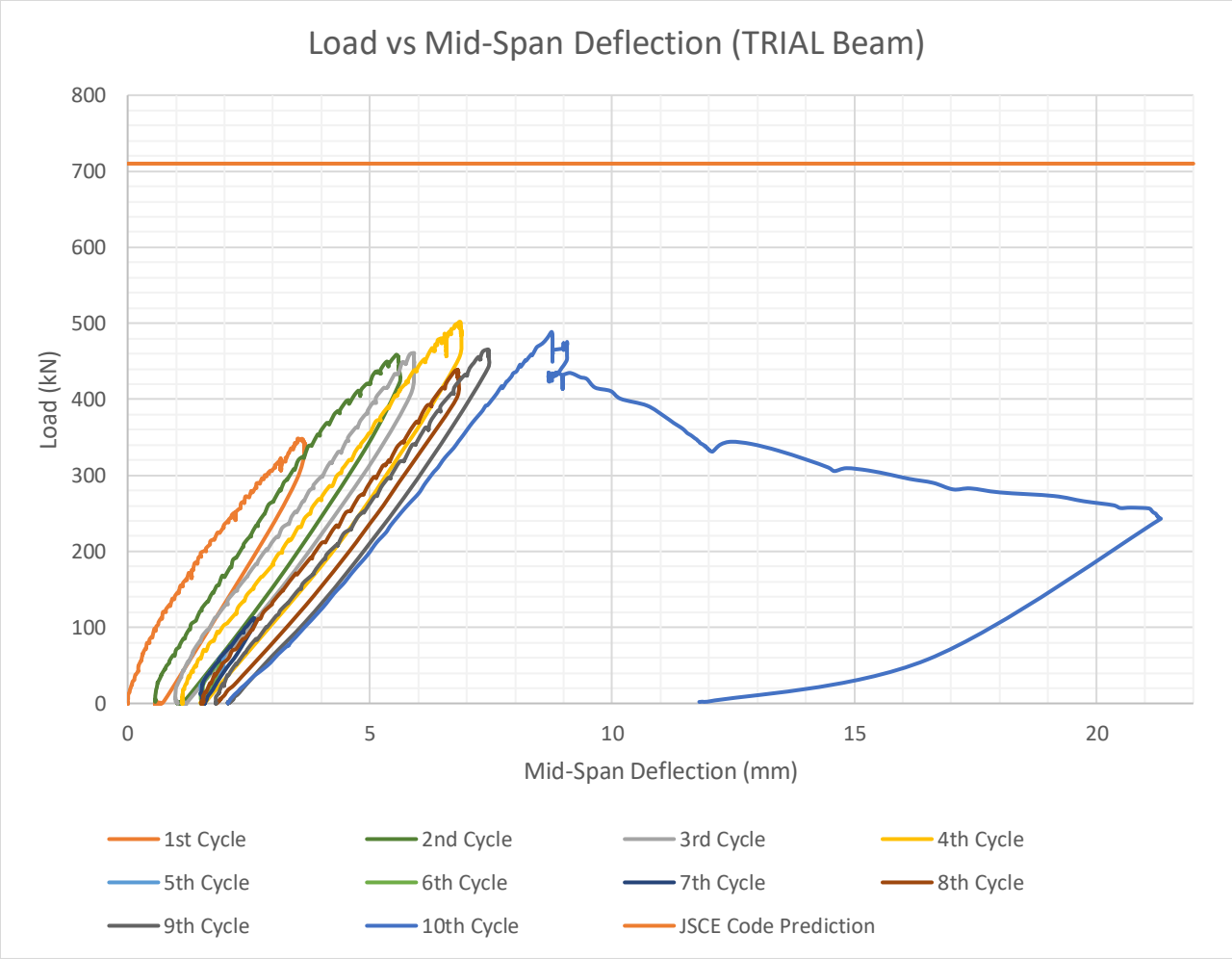

Figure 6-1: Load Vs. Mid-Span Deflection for TRIAL Beam

The first nine cycles with a maximum load experienced being 500kN had caused a cumulative of 2.07mm permanent mid-span deflection prior to the final loading that led to failure. For the 10th and final loading cycle, at 488.6kN the specimen had reached its peak load with a corresponding mid-span deflection of 8.75mm. The specimen was loaded post peak until the side cover delamination was clearly seen and in doing so, a maximum mid-span deflection of 21.3mm was reached. As explained in the observation, section 4.2, the failure had propagated on the ϕ 8 c/c 60mm spacing side causing spalling in both 50mm and 75mm side covers. The concrete core confined within the stirrups was however intact and successfully resisted the applied load without crushing.

Although the strain gauge attached on the stirrup did not function well enough to give reinforcement strain results to ensure yielding of web reinforcement, it can be clearly observed that shear was mainly resisted by the yielding of stirrups. In addition, comparisons made with analyzed data made it possible to obtain equivalent vertical stirrup strain results from the surface

strain measurements. This is later explained more on section 6.2.4.2 with reference to vertical surface strain quantifying that indeed stirrups had yielded.

The beam had a constant web reinforcement ratio of 0.74% throughout its longitudinal axis. The diagonal crack chose the side of the beam where diameter 8 stirrups were put to form its failure path. In a typical beam where stirrups are put symmetrically along the longitudinal axis with a constant spacing, the choice of failure path may not be of concern. But for this particular specimen the failure path followed begs the question if stirrups are actually planes of weaknesses triggering side cover spalling as mentioned in literatures. And this is based on the assumption that loading and support conditions, alignment, eccentricities, and general test setup has a very minimum margin of error.

Although the beam had experienced multiple cycles of loading before failure, the load repetitions were all under 500kN and well within the elastic range of the beam causing flexural and shear cracks of width less than 1mm showing no signs of failure. However, this doesn't disregard the fact that the beam had experienced a certain amount of damage at a low stress level but it was not significant enough to reduce the beams overall resistance capacity.

The expected failure load according to JSCE was 710.9kN. The final loading leading to failure had a maximum load resistance of 488.6kN which was 31% less of the expected resistance. This indicates that the beam had failed prematurely before attaining its full capacity as calculated by the code. The premature failure can be attributed to the loss of cross section due to spalling of side cover or the unusually reduced stirrup cage width or a combination of both.

6.2.1.2. Main Specimens

SI8-25

Specimen SI8-25 had a stirrup cage width of 150mm with a web reinforcement ratio of 0.71%. The specimen had a typical shear failure with concrete spalling limited at the loading area. The specimen had experienced 22 cycles of loading (unintentional) to different load stages before failure. Softening of early-stage load deformation behavior can be seen on the last failure loading.

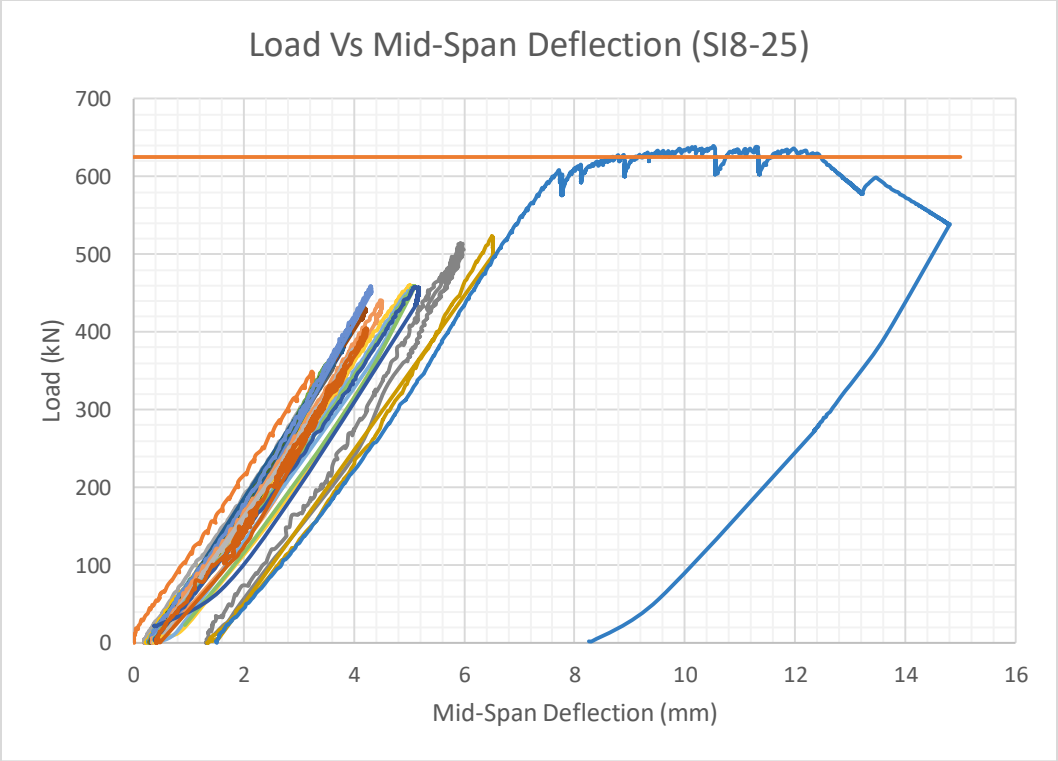

Figure 6-2: Load Vs. Mid-Span Deflection for SI8-25

The first 21 cycles of loading with a maximum of 523.7 kN of applied load had caused a cumulative mid span deflection of 1.46mm prior to the final loading leading to failure. These cycles had only caused flexural and shear crack widths of less than 1mm. The final failure load was 639.5 kN with a corresponding mid span deflection of 10.5mm.

Since it was the first specimen to be tested that had a failure load greater than 500kN (the reaction frame's previous capacity before being strengthened) it was loaded with great caution. After reaching 600kN the test was paused at certain load stages to monitor the modified reaction frame's safety. Low amplitude cyclic patterns can be seen in the load deflection graph near peak load. The post peak loading was limited to a maximum deflection of 14.8mm.

Similar to the trial beam the failure load recorded in the last cycle is directly compared to JSCE code's static load prediction since the previous cycles were within the elastic range of the beam affecting only the initial load stage of the failure loading. The final loading leading to failure had a maximum load resistance of 639.5kN which was accurately predicted by JSCE code of 625.2kN with only a 2% decrease. The beam failed after attaining its full capacity as calculated by the code.

SI8-50

Specimen SI8-50 had a stirrup cage width of 150mm with a web reinforcement ratio of 0.57%. It was brought to failure in one monotonic loading. The specimen had a typical shear failure with concrete spalling.

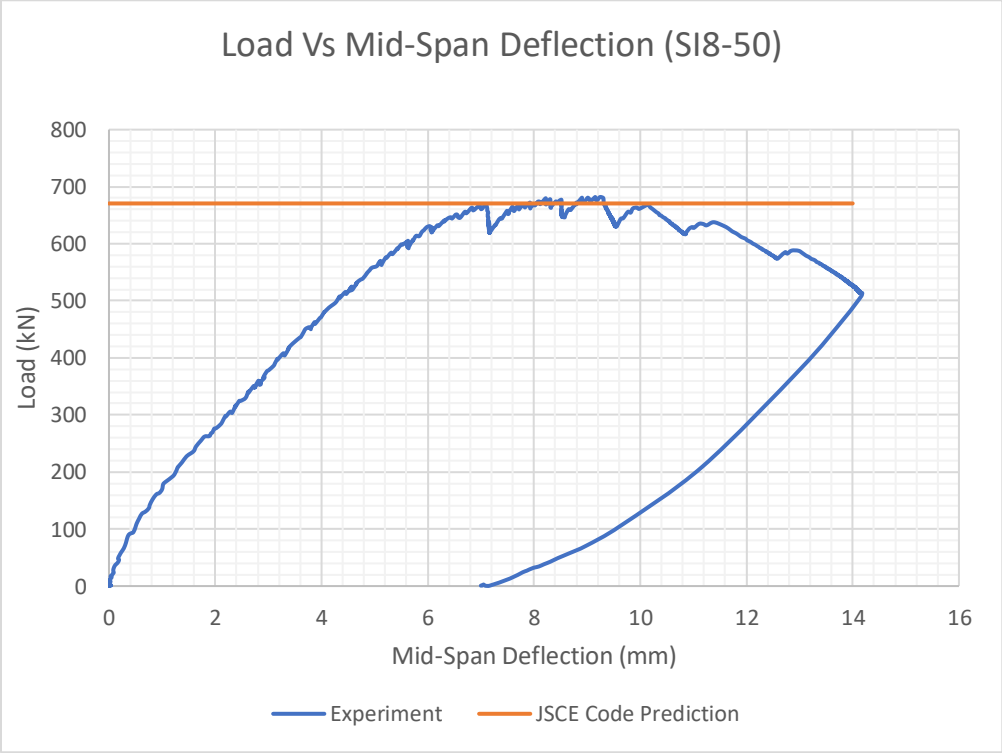

Figure 6-3: Load Vs. Mid-Span Deflection for SI8-50

The specimen reached a peak load of 681.77 kN with a corresponding mid span deflection of 9.2 mm. Similar to specimen SI8-25 the loading procedure above 600kN was carried out while monitoring the modified reaction frame and hence testing was paused at different load stages.

The specimen was loaded post peak until a maximum deflection of 14.18 mm was reached.

JSCE code prediction gave an accurate ultimate load prediction of 669.1 kN with a 2% variation from the test result of 681.77kN. Although side cover spalling was experienced near ultimate load it did not lead to the premature failure of the specimen. The section had delivered the required amount of resistance.

SII10-50

Specimen SII10-50 had a stirrup cage width of 150mm with a web reinforcement ratio of 0.57%. The specimen had a typical shear failure accompanied by side concrete cover spalling. This

specimen had similar side cover, beam width, stirrup cage width and web reinforcement ratio as SI8-50 only differing in stirrup spacing.

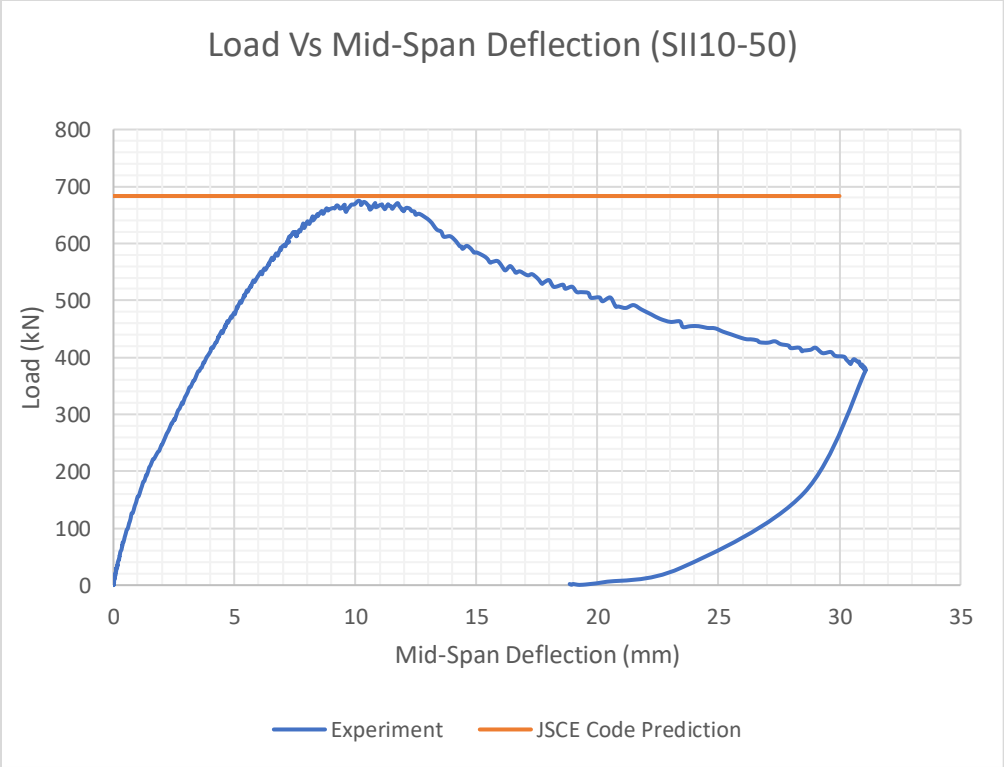

Figure 6-4: Load Vs. Mid-Span Deflection for SII10-50

The specimen had a failure load of 674.77 kN with a corresponding mid span deflection of 10.12mm. It was loaded post peak until a deflection of 31.08mm was reached.

JSCE code gave an accurate prediction of 681.7 kN which was only 1% greater than the experimental result. Similar to specimen SI8-50, even though severe spalling of side cover was observed near ultimate load the specimen resisted the required amount of load adequately.

SII10-75

Specimen SIII10-75 had a stirrup cage width of 150mm with a web reinforcement ratio of 0.48%. The specimen had a typical shear failure.

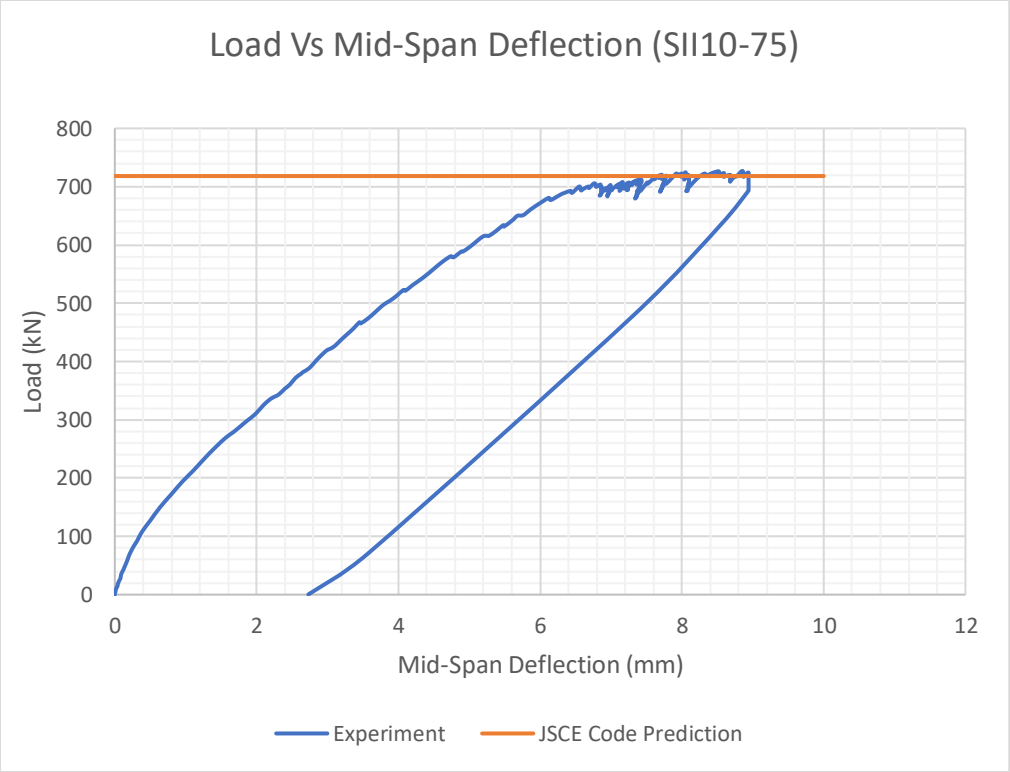

Figure 6-5: Load Vs. Mid-Span Deflection for SII10-75

The specimen had a failure load of 727 kN with a corresponding mid span deflection of 8.85mm. Post peak loading was limited to a deflection of 8.94mm since the specimen's capacity was a safety threat to the reaction frame's test setup. Loading was stopped almost immediately after peak load was reached. Side cover spalling was not observed for this specimen.

JSCE code gave an accurate prediction of 715.1 kN which was only 2% less than the experimental result. The beam resisted the required amount of load sufficiently.

SIII8-75

Specimen SIII8-75 had a reduced stirrup cage width of 100mm with a web reinforcement ratio of 0.57%. The specimen had a typical shear failure with concrete spalling. This specimen had similar beam width and web reinforcement ratio as SII8-50 differing in stirrup cage width and side cover. These two specimens also had similar ultimate load prediction according to design codes.

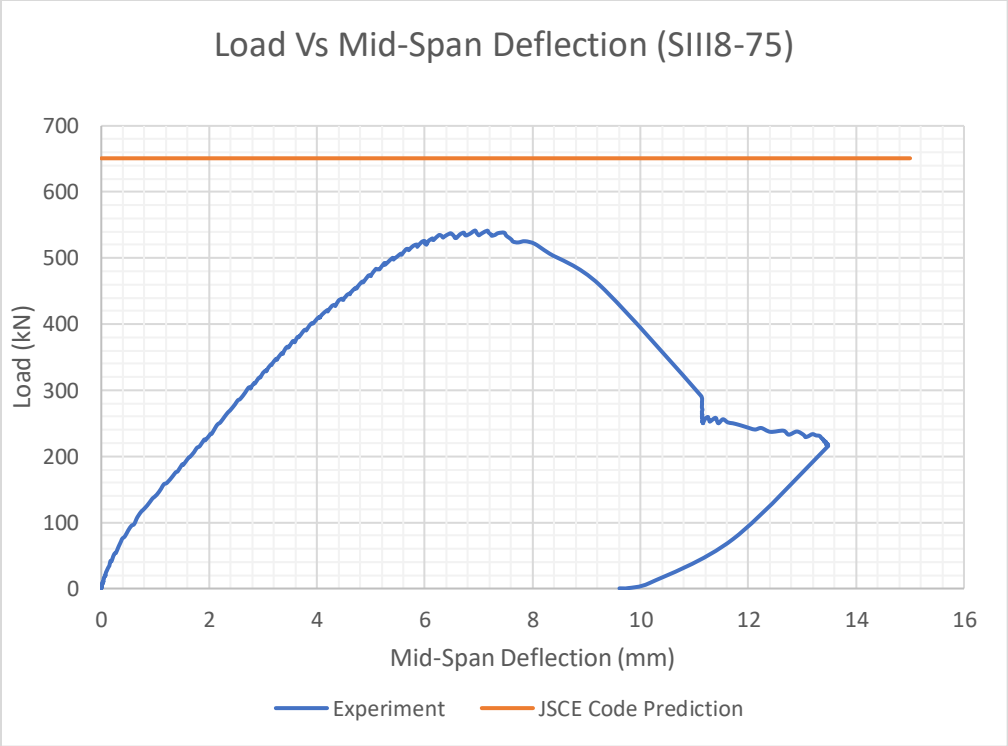

Figure 6-6: Load Vs. Mid-Span Deflection for SIII8-75

The specimen had a failure load of 541.72 kN with a corresponding mid span deflection of 6.93mm. It was loaded post peak until a maximum deflection of 13.48mm was reached. The specimen had severe spalling on the side of the beam where diagonal failure cracks had propagated.

JSCE code predicted a failure load of 649.5 kN, while the section had a 27% reduced resistance as reported from the experimental result.

SIII10-75

Specimen SIII10-75 had a reduced stirrup cage width of 100mm with a web reinforcement ratio of 0.57%. The specimen had a typical shear failure with concrete spalling. This specimen had similar beam width and web reinforcement ratio as SII10-50 differing in stirrup cage width and side cover. These two specimens also had similar ultimate load prediction according to design codes.

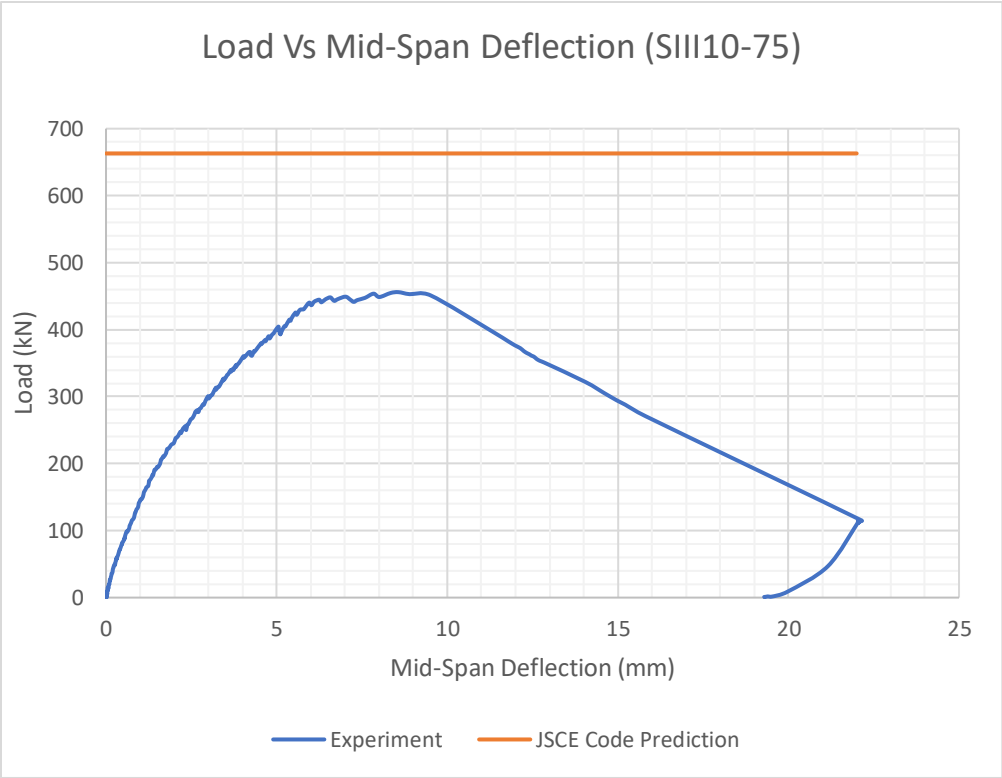

Figure 6-7: Load Vs. Mid-Span Deflection for SIII10-75

The specimen had a failure load of 455.93 kN with a corresponding mid span deflection of 8.57mm. It was loaded post peak until a maximum deflection of 22.15mm was reached. The specimen had severe spalling on the side of the beam where diagonal failure cracks had propagated.

JSCE code predicted a failure load of 661.5kN, while the section had a 31% reduced resistance as reported from the experimental result.

6.2.2. Web Reinforcement Strain

Local web reinforcement strains were obtained from strain gauges attached mid-height of the stirrup legs. A stirrup in between the loading point and beam support along the 45° expected failure crack line as illustrated in Figure 3-14 was chosen to take strain readings in each specimen. The measured strains at each load stage are plotted against applied load from readings obtained from strain gauge and load cell respectively. No calculation or data manipulation was required as the data logger was calibrated to record applied load in **kN** and strain in **με** units.

Out of the seven test specimens strain gauges were attached to, only three of them gave measurement outputs. For the rest four specimens the strain gauges were possibly damaged during casting and couldn't give readings due to malfunction or wires breakage.

For Specimen **SI8-25** strain gauge was attached on a stirrup found on the side of the beam where failure had happened**.** Stirrup yielded prior to reaching the peak load. Yield strain was obtained from tensile test results of the stirrups used. Strain gauge measurements during the post-peak loading were unreliable due to large reinforcement strains and deterioration of the concrete around the strain gauges. Post-peak strains presented here are therefore used for visual demonstration purposes only.

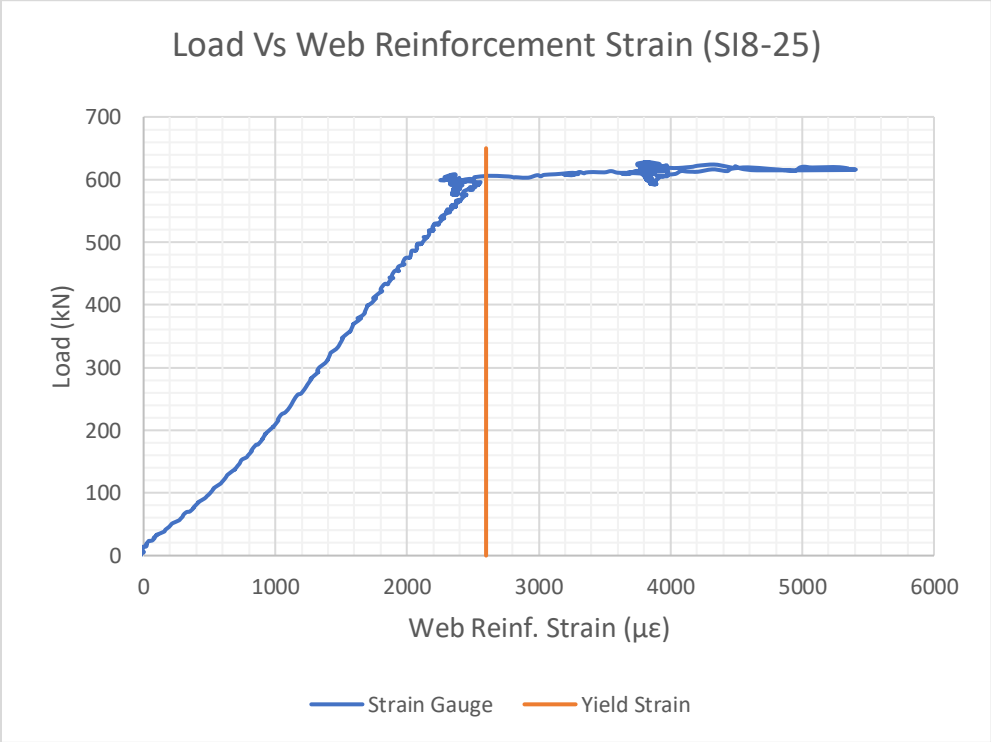

Figure 6-8: Load Vs. Web Reinforcement Strain for SI8-25

Specimen **SI8-50** also had strain gauge attached on a stirrup found on the side of the beam where failure had happened**.** Fluctuations in the strain measurements were observed at each load stage due to signal disturbances from the strain gauge. These disturbances had an average strain variation of 800με. At the beginning of loading (Applied load=0kN) a corresponding strain measurement of zero was recorded at the lower bound of the variation, therefore, for the purpose of analysis the lower bound strain is taken into consideration.

Similar to specimen SI8-25, stirrup yielded prior to reaching the peak load. Strain reading was however abruptly stopped right after reaching yield. This discontinuity of reading is sought to be due to detachment of strain gauge from the stirrup surface as deformation of the reinforcement progressed.

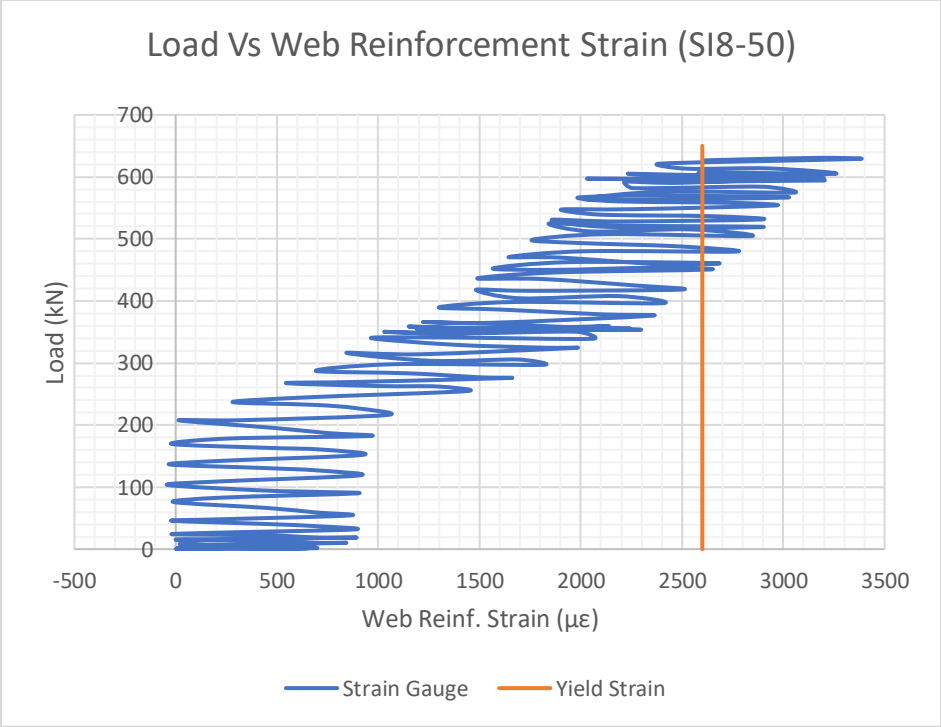

Figure 6-9: Load Vs. Web Reinforcement Strain for SI8-50

For specimen **SII10-50** strain reading was interrupted shortly after reaching peak load before attaining yield capacity. Strain reading dropped suddenly after the specimen reached peak load and soon after stopped giving readings at all. Similar reason given to specimen SI8-50 can be put here as well.

Specimen **SII10-50**'s strain gauge was attached to a stirrup placed at the opposite side of the diagonal failure crack. The fact that this particular stirrup did not attain yield doesn't imply the shear failure of this specimen is not characterized by yielding of web reinforcement. Stirrups that resisted the diagonal shear failure on the other side show clear signs of yielding as presented in section 4.5 and the failure of the specimen was not controlled by crushing of concrete in compression as the concrete confined within the stirrups was intact and had no sign of crushing.

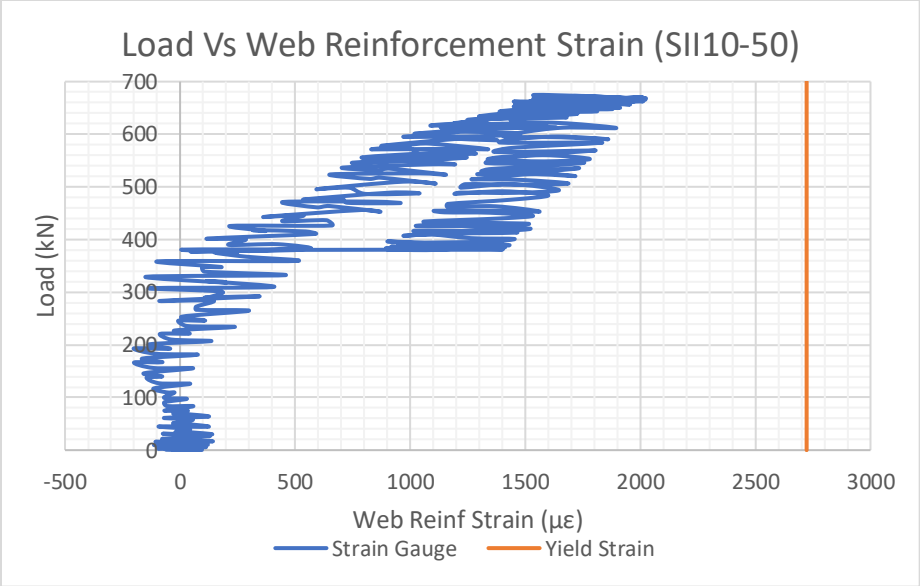

Figure 6-10: Load Vs. Web Reinforcement Strain for SII10-50

6.2.3. Out of Plane Deformation/ Strain

Out of plane deformation was obtained from strain gauges attached on aluminum strip plates going through out of plane holes created for measurement. Strain measurements from strain gauges were obtained directly from the data logger in **με** units. The gauge factor for the strain gauges was calibrated in such a way that positive strain measurements were translated to tension reading while negative ones were to compression.

6.2.3.1. TRIAL Beam

The trial beam had three holes created into the section of the beam for the purpose of measuring out of plane deformation. The holes were located at the mid-section of the beam as illustrated in Figure 3-32. Out of plane deformation instrumentations used in the trial beam gave strain results of six strain gauges that were attached to three aluminum strip plates. Each aluminum strip had two strain gauges attached, one attached to the middle (M) and other near the end of the strip (E). This was done to check which location of strain gauge attachment had a better representation of the average out of plane strain.

As mentioned in section 3.4.1 strain measurements were obtained from three holes. After testing the trial beam, it was observed that the strain measurements from the middle hole were very erratic due to the region being highly stressed and the results couldn't be interpreted in a logical manner. And hence, the strain results from the middle hole of the specimen were removed from the analysis. Strain measurements for the first three cycles of loading from the two holes (Hole 1 and Hole 3) located at the shear critical regions are presented below in Figure 6-11 with reference to applied load.

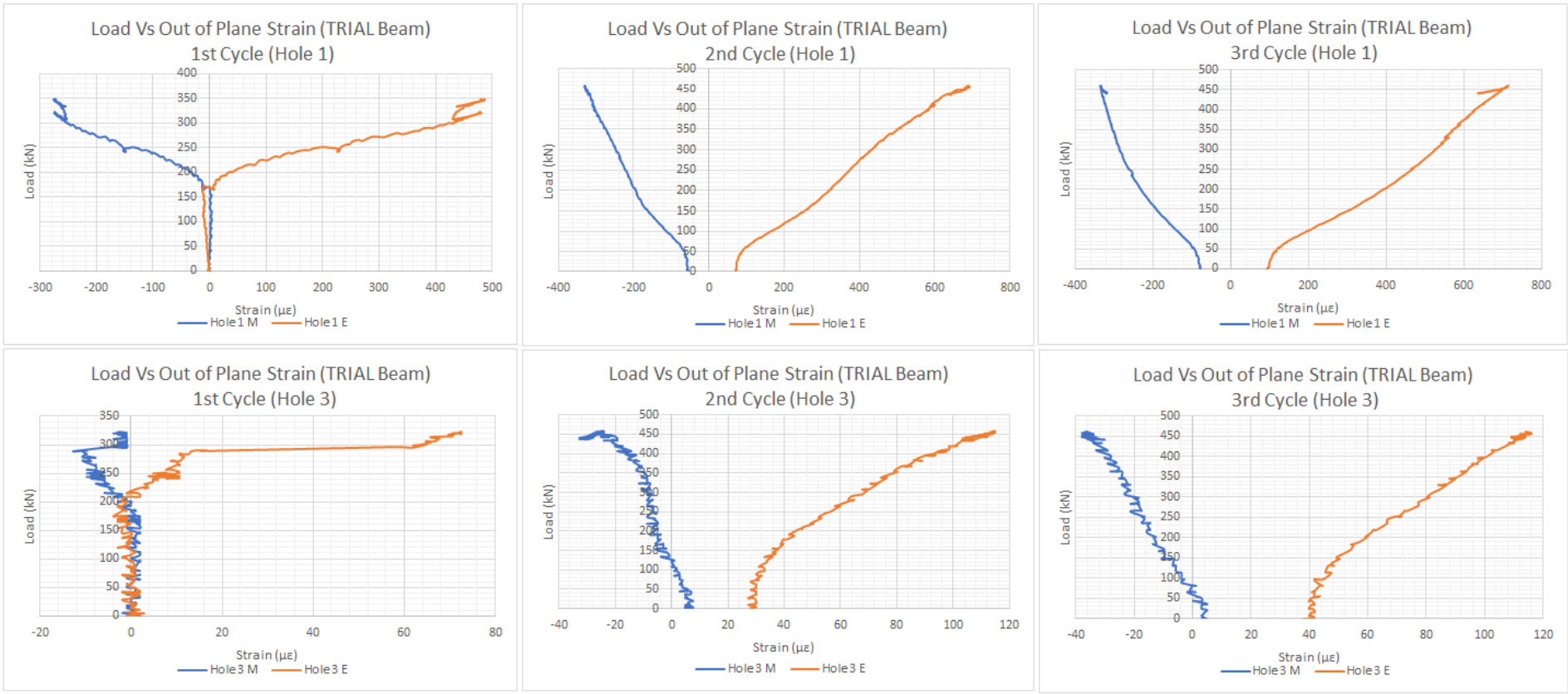

Figure 6-11: Load Vs Out of Plane Strain (TRIAL Beam)

Strain measurements attached to the middle of the aluminum strip, designated by M, show compressive strain in all cycles of loading while the strain gauge attached to the end of the strip, designated by E, shows tensile strain in all cycles. From the first loading cycle it can be seen that out of plane deformation started around 160kN for both hole 1 and 3. Strain measurements progressed from 0 to a maximum of 500 με in hole 1 and around 70 με in hole 3. These strain values have increased with each cycle of loading indicating that there is indeed a quantifiable amount of out of plane deformation for a beam member subjected to an in-plane loading.

Similar responses for both hole 1 and 3 from the remaining seven cycles are presented in APPENDIX. For the last 10th cycle however strain measurement from only hole 3 were presented as strain gauges on hole 1 were damaged. At peak failure load aluminum inside hole 3 broke at the edge where connection has been made to the wings.

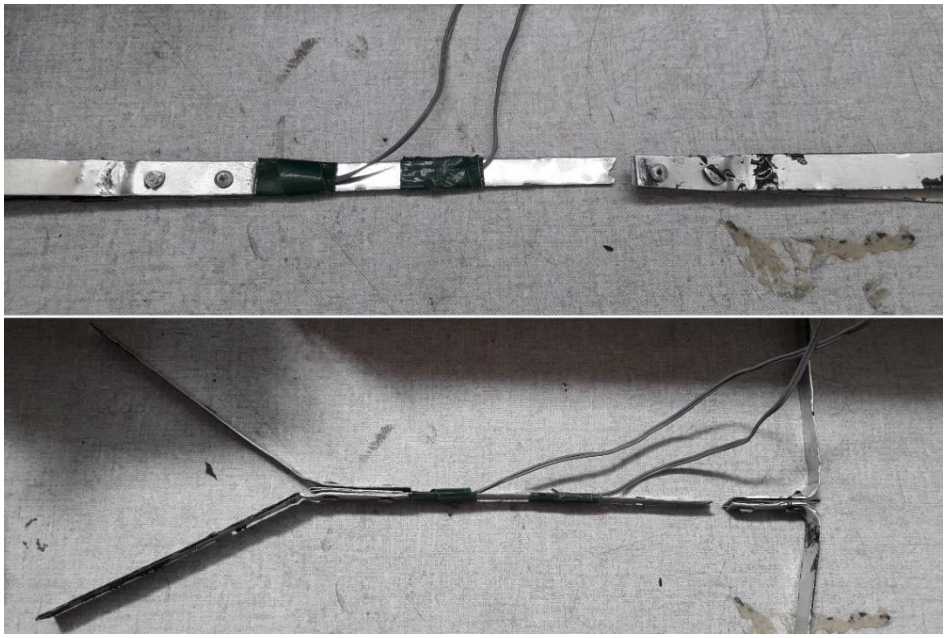

Figure 6-12: Aluminum Strip at Failure (TRIAL Beam)

Strain measurements from the end attached strain gauge were affected by stress localization as it was mounted near the stiffened section of the aluminum strip. Therefore, a more representative strain result of the out of plane deformation of the beam is obtained from the strain gauge mounted at the middle. The choice in instrumentation location needed a modification as the one implemented on the trial beam gave justifiable but incomparable results. The modified instrumentation used the location of maximum shear but instead of one hole in the mid-section two more holes were created in the same cross-sectional plane at the compression and tension regions of each specimen. This gives comparable strain values and a better idea on how out of plane deformation and eventually spalling happens.

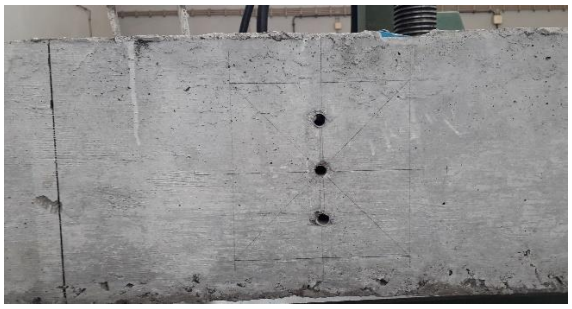

Figure 6-13: Modified Out of Plane Instrumentation Holes for Main Specimens

6.2.3.2. Main Specimens

Out of plane strain measurements were obtained from strain gauges attached to aluminum strip plates going through the holes created for testing. Prior to loading, all tested beam specimens were assumed to have a very small out of plane strain, which for the sake of this experimental data analysis is taken as 0. Measurements are reported after the onset of loading. The holes created for testing are assumed to be representatives of compression zone, mid-section and tension zone of the beam section.

Presented below in Figure 6-14 are the load vs out of plane deformation plots for the six main specimens. Three holes found on the same cross-sectional plane at compression zone, mid-section and tension zone of the beam were used to obtain out of plane deformation in terms of strain.

The out of plane deformation measuring aluminums were attached to the concrete surface at the left side of the beam for all specimens, where all three holes are found on the same cross-sectional plane. However only in specimens SI8-25, SII10-75, and SIII8-75 did failure happen on the instrumented side, for the rest of the beams (SI8-50, SII10-50 and SIII10-75) failure happened on the unmonitored side of the beam. Therefore, although recorded responses represent the beam's behavior, they aren't exactly representatives of the actual failure side.

Positive strain results represent tensile strain while negative strain results represent compressive strain. Tensile strains are recorded when the specimen experiences out of plane deformation away from the confined concrete core leading to spalling of side cover when strain results are greater than the cracking strain of concrete. As stated in the Crack control report by Leonhardt F. 1998 [29] the cracking strain of concrete is found within the range of 90 to 120.

Negative strain results represent compressive stains. These are recorded when the out of plane deformation of the specimen is directed towards the core concrete. For the purpose of illustration strain values less than 0 are considered as sections that haven't experienced spalling and are presented as the original section dimension. The instrumentation gave average strain result for side cover delamination on both sides.

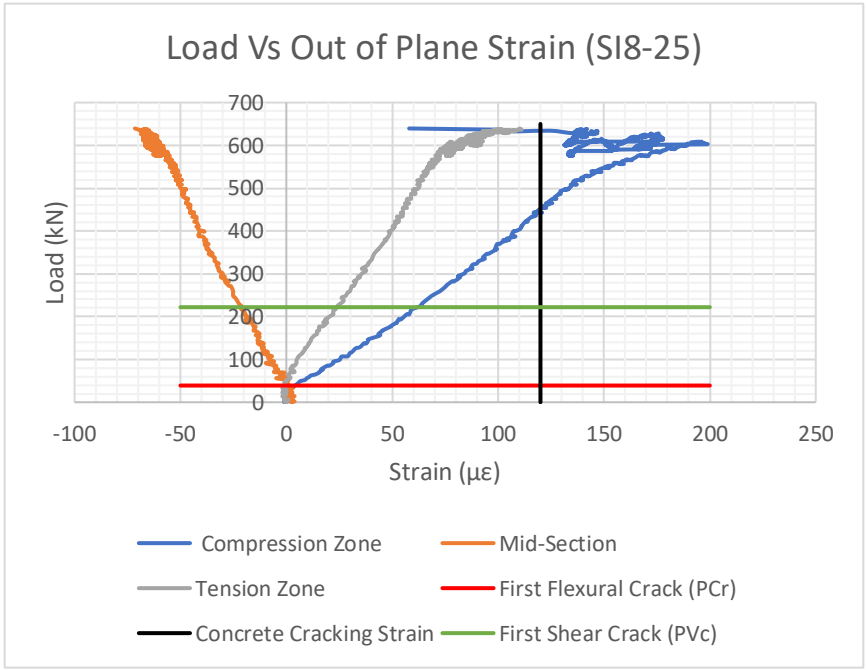
Load Vs Out of Plane Strain (SI8-25)
Load (kN)
Strain (με)
Compression Zone
Mid-Section
Tension Zone
First Flexural Crack (PCr)
Concrete Cracking Strain
First Shear Crack (PVc)

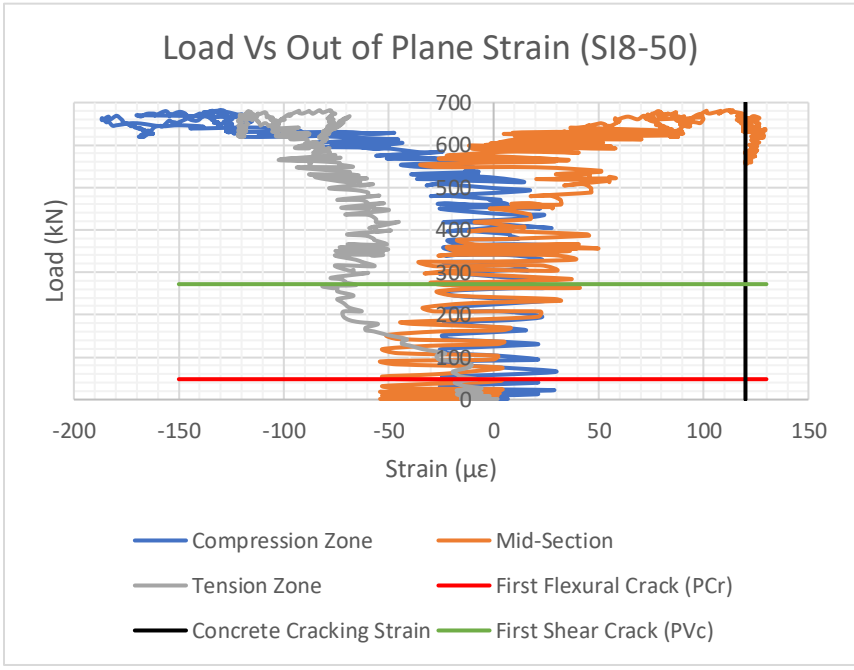
Load Vs Out of Plane Strain (SI8-50)
Load (kN)
Strain (με)
Compression Zone
Mid-Section
Tension Zone
First Flexural Crack (PCr)
Concrete Cracking Strain
First Shear Crack (PVc)

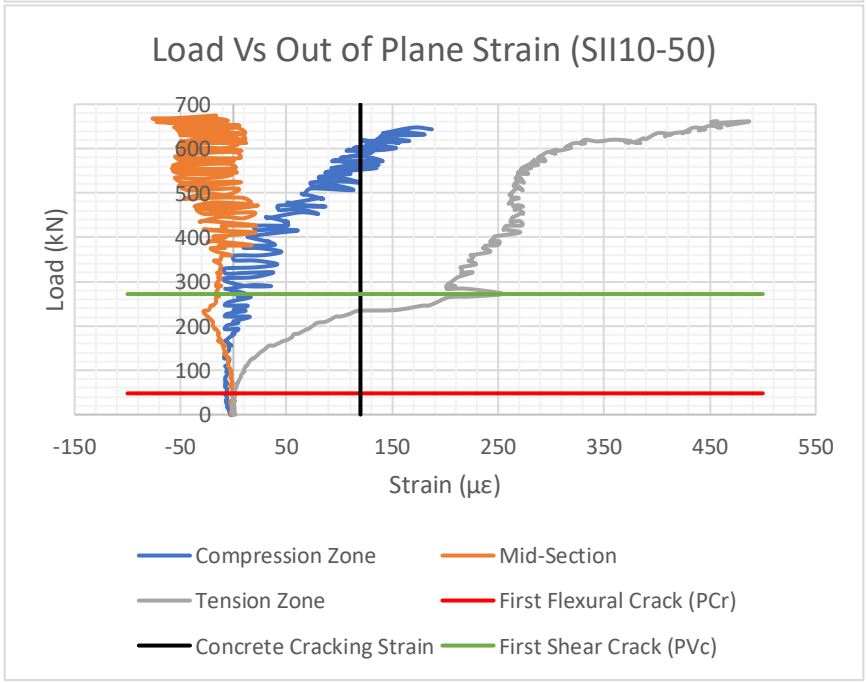
Load Vs Out of Plane Strain (SII10-50)
Load (kN)
Strain (με)
Compression Zone
Mid-Section
Tension Zone
First Flexural Crack (PCr)
Concrete Cracking Strain
First Shear Crack (PVc)

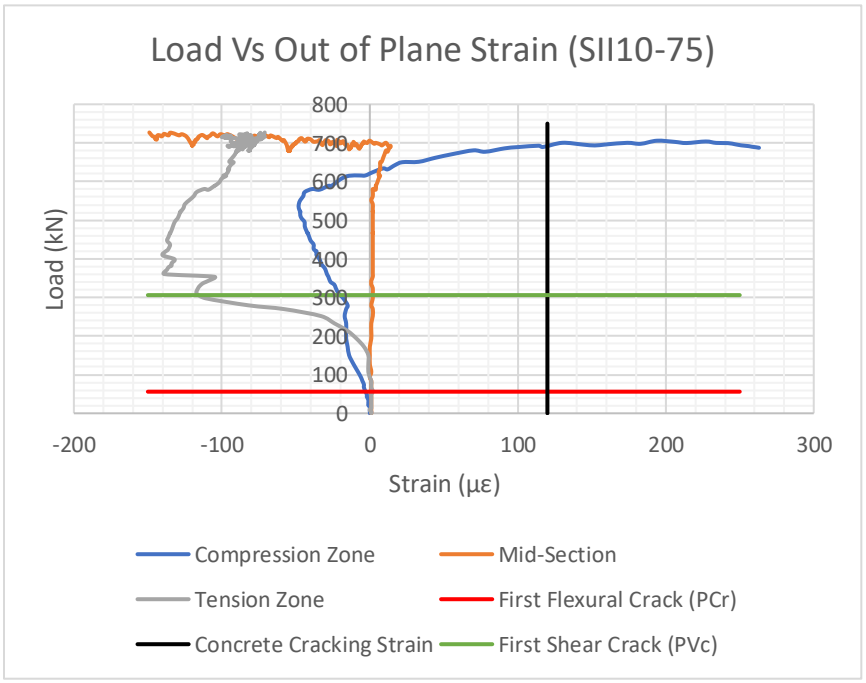
Load Vs Out of Plane Strain (SII10-75)
Load (kN)
Strain (με)
Compression Zone
Mid-Section
Tension Zone
First Flexural Crack (PCr)
Concrete Cracking Strain
First Shear Crack (PVc)

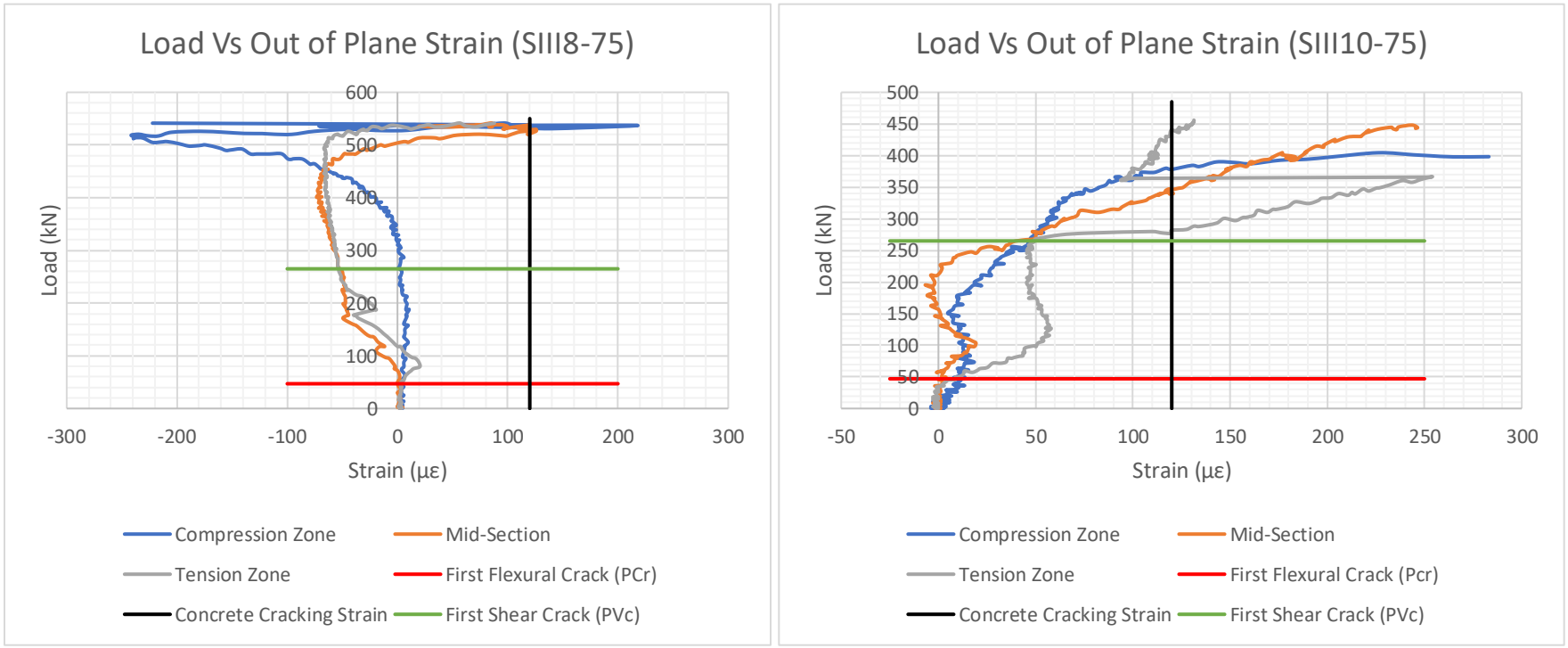

Figure 6-14: Load Vs Out of Plane Strain for Main Specimens

In each plot presented in Figure 6-14, in addition to the out of plane strain results, the theoretical load at which the first flexural crack is expected to happen (Pcr), the theoretical diagonal concrete cracking load (Vc) as calculated by the design code, and cracking strain of concrete (120με) are included as a reference for better interpretation of results.

The gauge calibration factor for the strain gauges was set up in the data logger in such a way that tension readings gave positive strain values while compression readings gave negative strain values. Correspondingly both tensile and compressive strain values were recorded as a response to each specimen's out of plane deformation.

Disturbed/fluctuating strain results are seen on specimen SI8-50 from onset of loading and on specimen SII10-50 after diagonal cracking. The reason behind these disturbances is attributed to local stress induced cracks at the concrete surface where the aluminums were mounted. The fluctuation had a minimized average amplitude as compared to the stirrup strain measurements. For the purpose of analysis, the average response was taken into consideration.

Out of plane deformation was initiated at the load at which the first flexural crack had happened. In all specimens it can be observed that exactly after passing this load point, strain measurements gave strain results differing from zero. This deformation was pronounced after reaching the diagonal cracking load. Strain results obtained post peak were excessive and unreliable and hence were not presented in the analysis.

As mentioned earlier in this section, not all failures happened on the instrumented side of the out of plane deformation measurements and as observed from the out of plane strain plots concrete cracking strain of 120με was reached at different load stages for each specimen. Table 6-3 below summarizes these two parameters.

Table 6-3: Out of Plane deformation Measurement Details

Specimen	Failure on the Instrumented Side?	Cracking Strain Reached
SI8-25	YES	After Vc
SI8-50	NO	At Peak Load
SII10-50	NO	Before Vc
SII10-75	YES	At Peak Load
SIII8-75	YES	At Peak Load
SIII10-75	NO	After Vc

Although all specimens had experienced significant amount of out of plane deformation leading to spalling, the responses obtained from the three different cross-sectional zones for each specimen is different. Except for specimen SI8-50 and SII10-50, positive out of plane strain in the compression zone is seen to be significantly higher than the corresponding mid-section and tension

zone. On the contrary specimen SII10-50's response led to tensile strain being significantly higher in the tension zone of the beam.

For specimen SI8-50 the strain along the mid-section had the maximum tensile strain, while strain results from both the compression zone and tension zone indicated that they were in compression.

These different out of plane strain responses can be attributed to different factors. The first and important factor is the unpredictability of shear failure in general. Shear failure doesn't follow a certain defined failure path with consistent responses, and its mechanism of load transfer within the section is complex specially when web reinforcements are involved. In addition, the fact that the tested specimens had a span to depth ratio of 2.5 doubles the complication of load transfer. a/d ratio of 2.5 is a borderline transition from short to slender members, load resisting mechanism can be a combination of direct strut formation and inclined diagonal cracking. The specimens also had varied shear responses among one another due to the use of different variables like web reinforcement ratio, stirrup spacing, stirrup cage width, and side cover width. Varying side cover not only affects the mechanism of cover spalling but also causes variation in the shear cracking behavior (Shear crack width, spacing, propagation) of the beams. The other reason is that not all responses reported are the exact representations of the shear failure and spalling experienced by the specimen. Since the out of plane strain measuring holes were prepared on only one side of the beam, the failure response was not always captured. Three of the specimens as specified in Table 6-3 had shear failure on the un-instrumented side as presented in Figure 6-15.

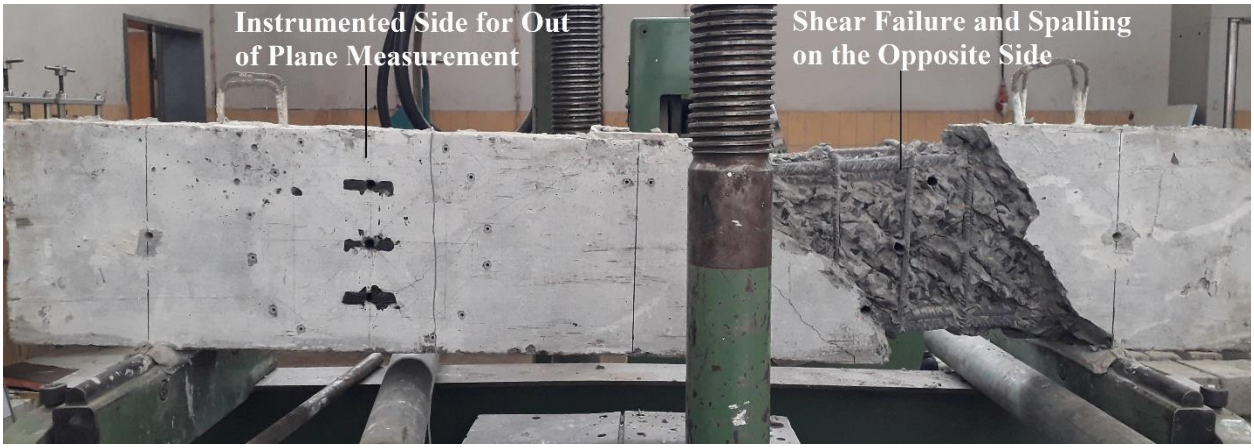

Figure 6-15: SII10-50's Failure Opposite to the Instrumented Side

Local disturbances around the aluminum plates caused by internal cracks passing through the holes of testing, and surface diagonal cracks passing through the mounted aluminum also cause inconsistencies in the out of plane deformation of the specimens.

The graphical illustration in Figure 6-16 demonstrates the out of plane deformation of each specimen at the three selected load points, first flexural cracking load, first diagonal cracking load and peak load. These drawings were made by converting the out of plane strain at each load stage into an equivalent displacement in mm. A similar scale factor was used to multiply the obtained

displacement for better visualization. Details of conversion are included in APPENDIX. The illustration is based on the assumption that the strain recorded is equally divided for both side cover delamination, and hence equivalent displacements are split to both sides.

	First Flexural Crack	First Diagonal Shear Crack	Peak Load
SI8-25	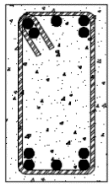	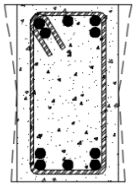	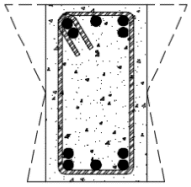
SI8-50	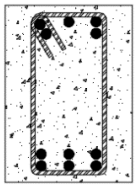	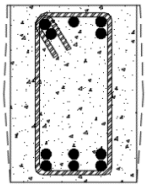	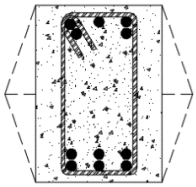
SII10-50	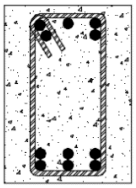	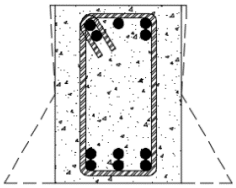	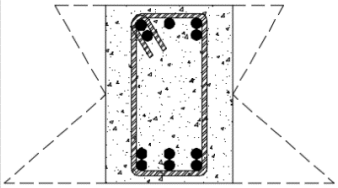
SII10-75	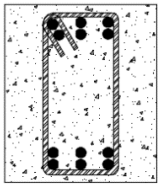	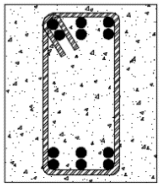	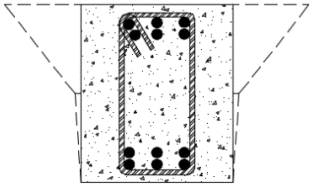
SIII8-75	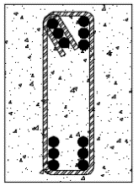	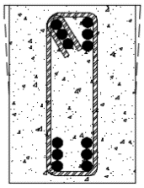	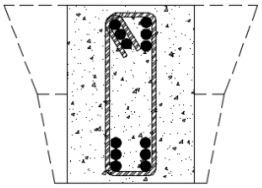
SIII10-75	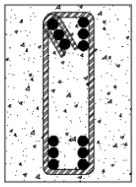	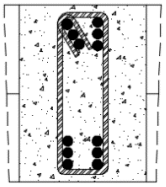	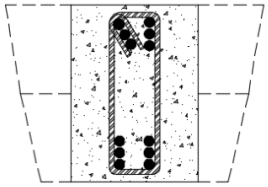

Figure 6-16: Out of Plane Strain Illustration for Main Specimens

6.2.4. Surface Strain Measurements

Two similar surface displacement measuring setups were put at alternative sides of a beam, namely H3 and H1 found at the left and right side of the specimen respectively. The surface measurement setup includes two diagonals D1 and D2 put at 45° and 135° respectively, and one horizontal measurement (H). A total of six LVDT (3 on each alternative side) were used for each specimen including the TRIAL beam.

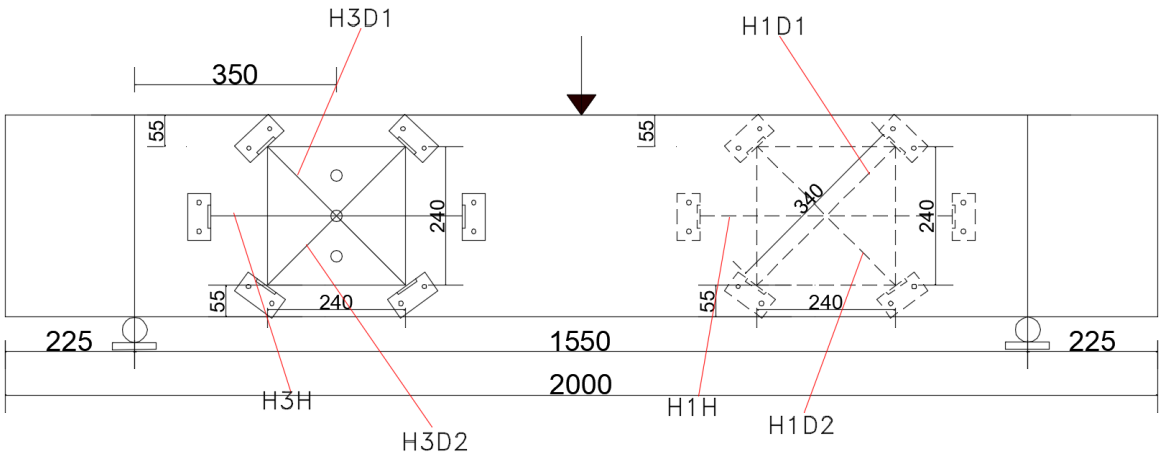

Figure 6-17: Surface Displacement Measurement Setup Detail

Displacement data from each LVDT was acquired from the Geodatalog system in *mm* units per one second interval. These displacement units were converted to an equivalent strain unit by dividing the displacement recorded (change in length) to the original length (340mm). Negative strain results are interpreted to compression while positive ones are for tension.

6.2.4.1. Surface Shear Strain

Surface shear strain is calculated from the displacement measurements obtained from the two diagonals put at 45° and 135°, their difference gave shear strain within the grid of instrumentation, which is an area where shear is critical. Presented below in Figure 6-18 are the load vs shear strain plots of all tested specimens.

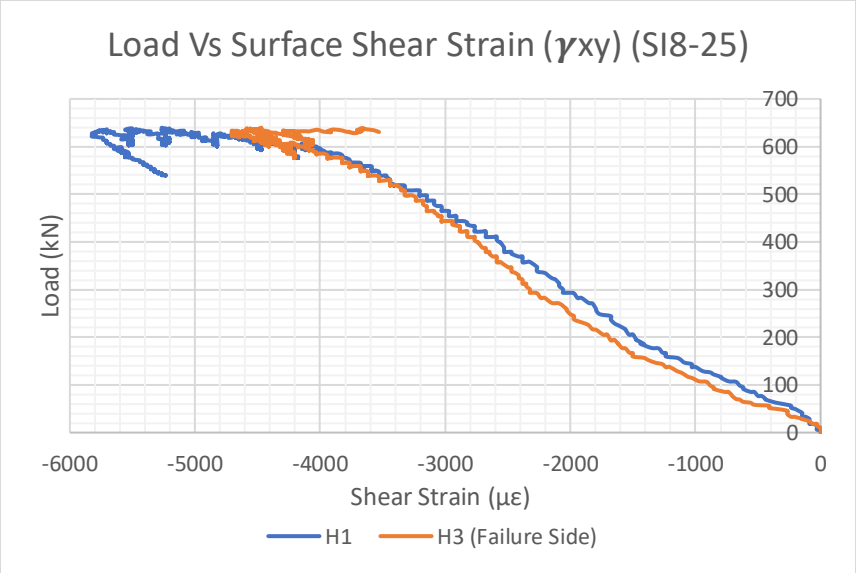
Load Vs Surface Shear Strain (γxy) (SI8-25)
Load (kN)
Shear Strain (με)
H1
H3 (Failure Side)

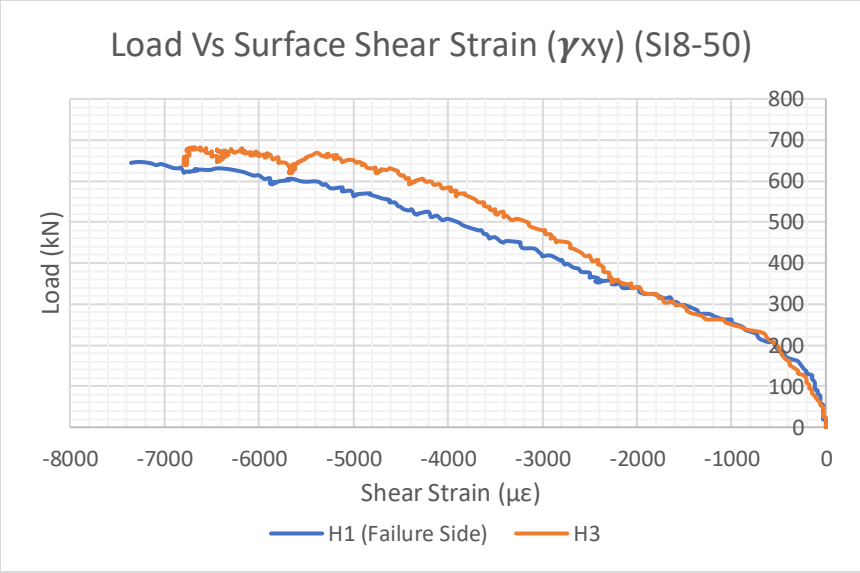
Load Vs Surface Shear Strain (γxy) (SI8-50)
Load (kN)
Shear Strain (με)
H1 (Failure Side)
H3

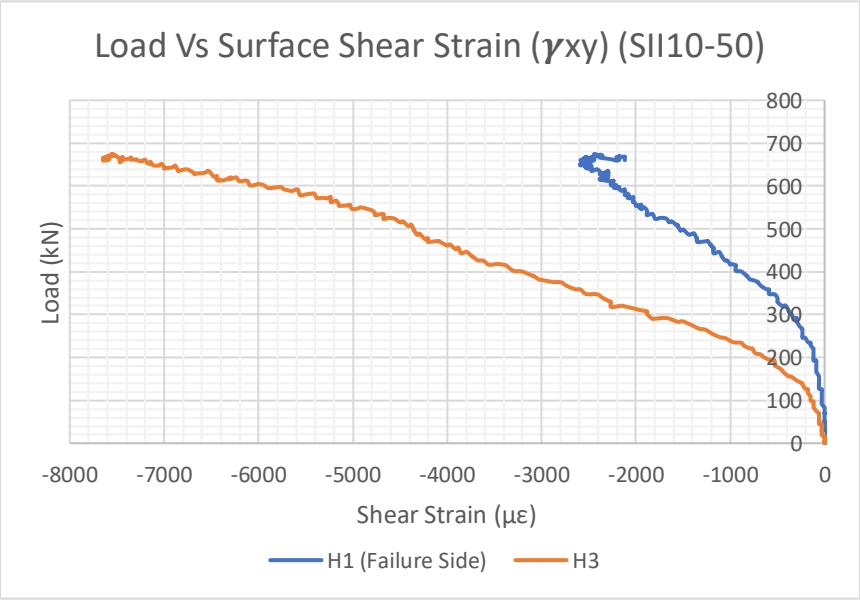
Load Vs Surface Shear Strain (γxy) (SII10-50)
Load (kN)
Shear Strain (με)
H1 (Failure Side)
H3

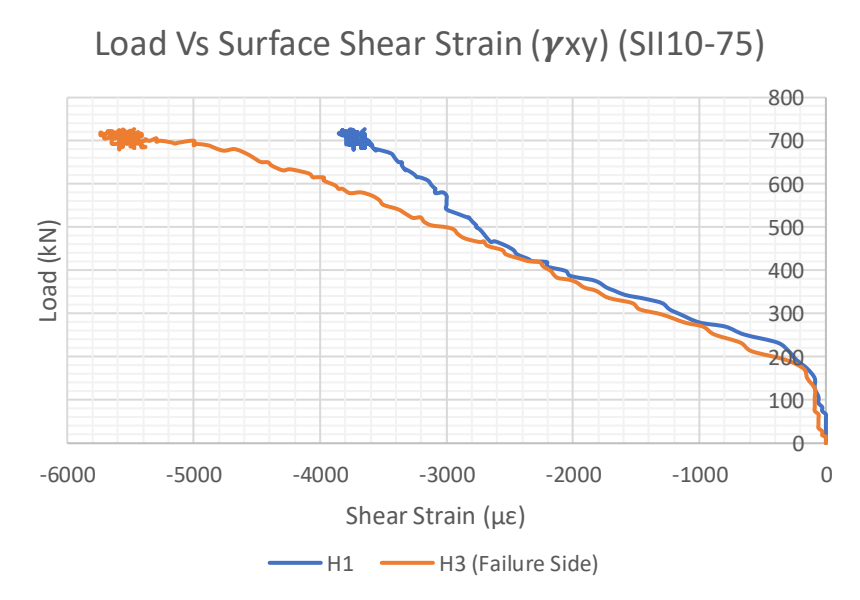
Load Vs Surface Shear Strain (γxy) (SII10-75)
Load (kN)
Shear Strain (με)
H1
H3 (Failure Side)

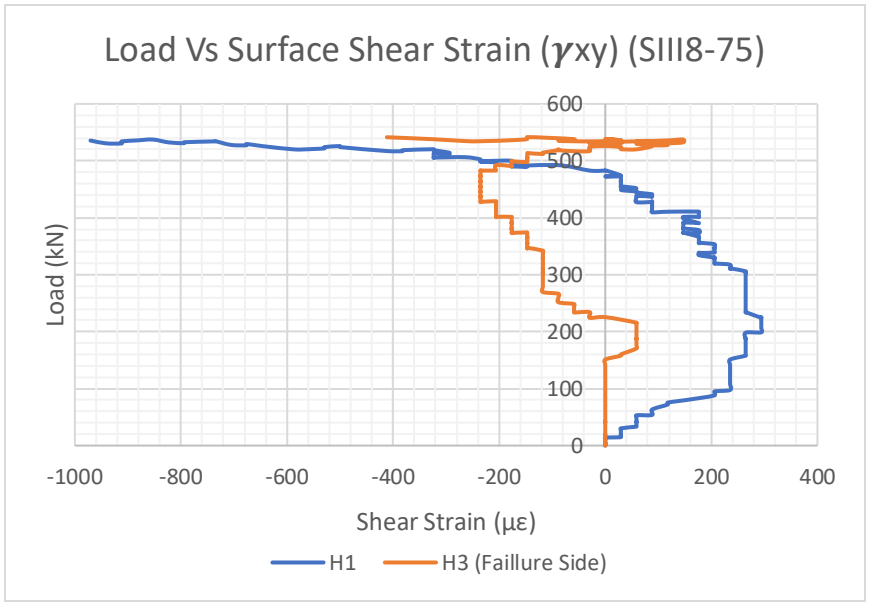

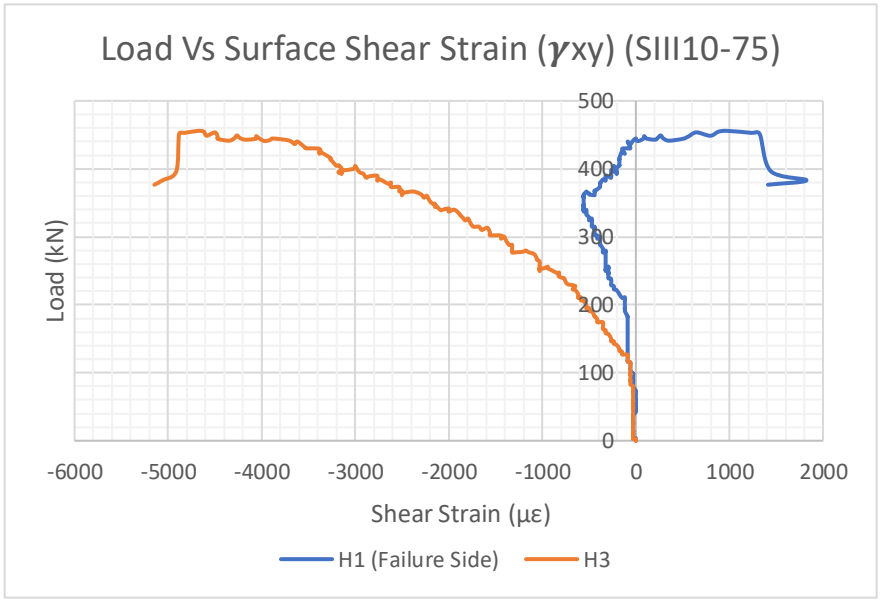

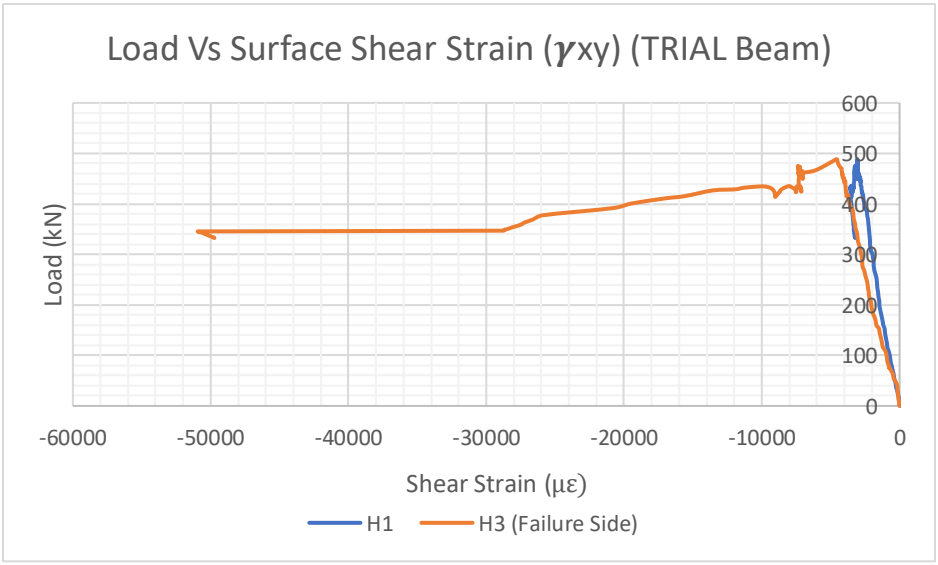

Figure 6-18: Load Vs Surface Shear Strain for Main Specimens and TRIAL Beam

For Specimen SI8-25, having a side cover of 25mm and a minimal cover spalling limited to the top compression region, although failure propagated on one side shear strain measurements on both shear critical sides have the same response throughout the test. For the rest of the specimens with side covers of 50mm and 75mm which have experienced spalling, a clear difference is seen on the shear strain response at a certain load stage. A relatively softened shear strain response is observed for surface measurement obtained from the failure side.

All readings show negative shear strain meaning compressive strain in the shear critical area, in specimen SIII8-75 and SIII10-75 however positive strain readings were observed. These erratic readings are caused by local failures affecting both the stability and fixity of the surface mounted instruments. Disrupted test result or infinitely increasing strain values are also a result of these anomalies. LVDTs mounted on the beam surface were being pushed out of their plane of measurement due to spalling of side concrete cover, and were also being affected by the local surface cracks forming directly through the mounted instruments.

Figure 6-19: Out of Plane Deformation Disrupting Surface Displacement Measurements

6.2.4.2. Vertical Strain

From the defined surface measurement grid, vertical strain had to be computed from strain relationship formulas in Eq. (6.1) as no LVDT was mounted in the vertical direction for direct measurement. By using the diagonal strain at 45°, horizontal strain ($\boldsymbol{\epsilon}_x$) from the horizontally mounted LVDT and the shear strain ($\boldsymbol{\gamma}_{xy}$) computed from 45° and 135° mounted measurements, into the strain relationship formula below the vertical strain ($\boldsymbol{\epsilon}_y$) was determined.

$$\epsilon_y = \frac{\epsilon_\Theta - \epsilon_x cos^2\Theta - \gamma_{xy} \sin\Theta \, cos\Theta}{sin^2\Theta} \tag{6.1}$$

This gave an average vertical strain result of each specimen over the defined area of surface measurement. Vertical strain results for all specimens were positive indicating tensile strain in the vertical direction of the shear critical area. Load vs vertical strain plots for all specimens are presented in APPENDIX. Similarly, from the surface mounted displacement measurements Horizontal strain ($\boldsymbol{\epsilon}$x), Principal Strain ($\boldsymbol{\epsilon}$1 & $\boldsymbol{\epsilon}$2), and Principal Angles (Θ) were all obtained. Procedures followed, formulas used and plots with respect to applied load are included in APPENDIX.

Presented below in Figure 6-20 , for three of the specimens with stirrup strain readings, comparisons were made against their corresponding vertical strain results as quiet interesting observation had been made between vertical strain on the failure side and strain results from strain gauges attached on vertical stirrups.

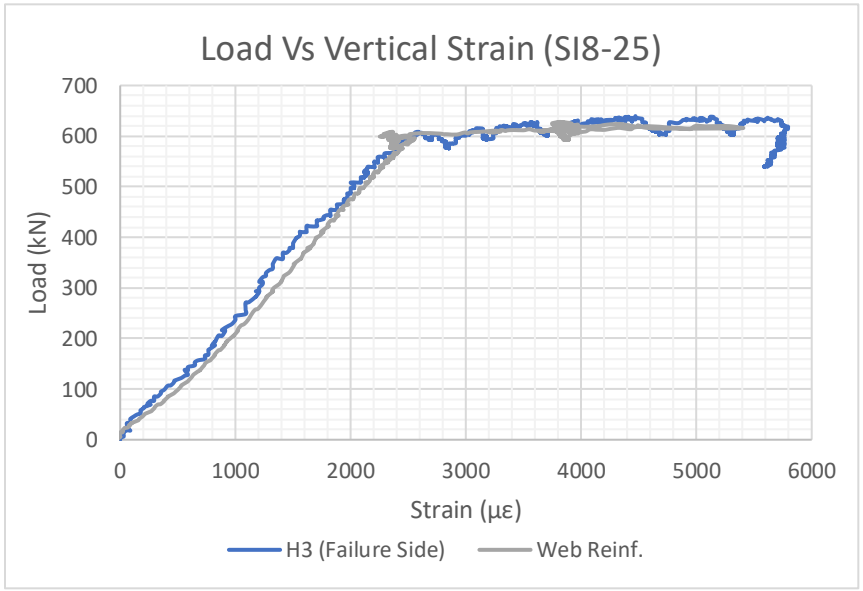

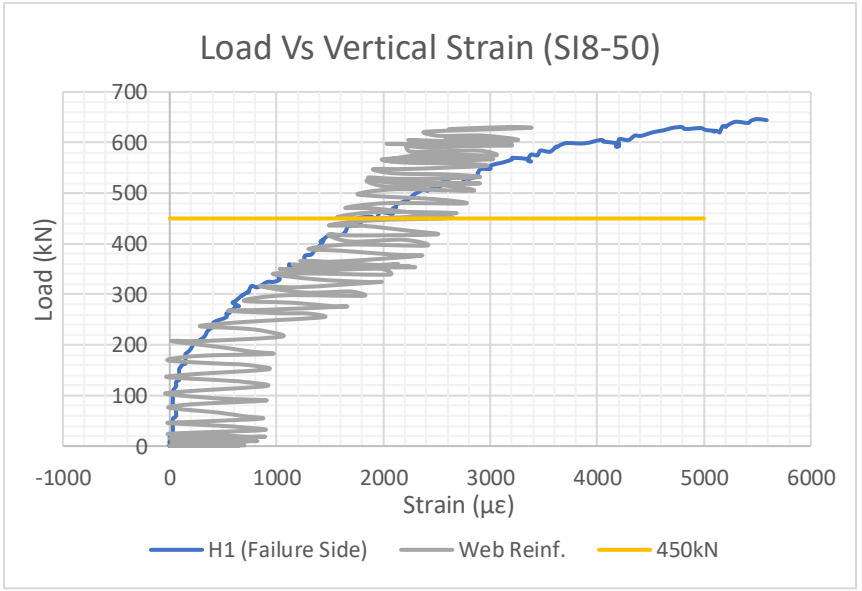

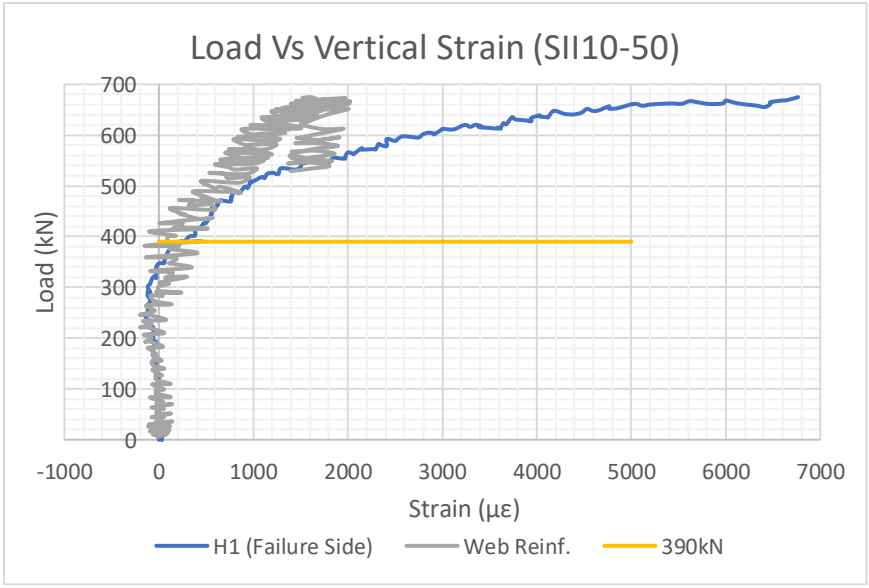

Figure 6-20: Load Vs Vertical Strain Plots for SI8-25, SI8-50, and SII10-50

For specimen SI8-25 web reinforcement strain attached on a stirrup and the average surface vertical strain have exactly the same response from onset of loading up to failure. The fact that this specimen had a thin side cover of 25mm and had suffered less from spalling as compared to the other specimens, might just be the reason as to why a local stirrup strain measurement result is the same as the surface measured average vertical strain. This result also serves the purpose of verifying the accuracy of the surface displacement measurements and strain relation equations used.

For specimen SI8-50, and SII10-50 both with side covers of 50mm and severe spalling at failure, the stirrup strain and average vertical strain did not have a synced response for the entire loading curve as for specimen SI8-25. During the initial loading stages, up to 65% and 60% of the ultimate load for specimen SI8-50 and SII10-50 respectively, stirrup strain and vertical strain had similar responses. However, after reaching a certain load as indicated in a yellow line for both plots, the average vertical surface strain measurement is seen to have a softened response as the stirrup strain follows a steep slope to yielding.

Since the beam specimens are all subjected to shear and are resisting diagonal compression mainly by the yielding of stirrups, the response of stirrups represents the response of the core concrete confined within the stirrup. This indicates for specimens with thin side covers the concrete core confined within the stirrups represented by the stirrup strain and the outer section of the beam represented by the average vertical strain from the surface measurements have similar responses and that the entire beam section is contributing to the load resistance of the member. The core concrete and side cover outside of the stirrup act together throughout the loading scheme until failure.

However, for specimens with larger covers, the concrete core confined within the stirrups and side cover outside of the stirrup stop acting together at certain load stage. The side cover becomes less and less effective for load resistance as surface diagonal cracks widen and perpendicular stresses start accumulating to create out of plane deformations leading to spalling. Evidently this phenomenon can be observed from the softening of the surface average vertical strain from its corresponding stirrup strain plot. This is an indication that the entire beam section is not effective in resisting the applied load after a certain load stage is reached. The core concrete resists the applied load until failure while the outer section (side cover) becomes useless after detaching from the core.

This leads the vertical strain measurements to give a quantifiable indication that if the yield strain of the stirrup is reached on the surface strain measurements, the stirrup has definitely yielded. Because chances are either they have similar responses or the surface measurement has a softened result less than the stirrup strain. Either way if the surface strain had reached yield strain, then the stirrup within the grid of instrumentation it has definitely yielded.

6.3. Results from NLFEA

6.3.1. Results from Vector 2

Vector 2 is a finite element software program designed to analyze the response of two dimensional reinforced concrete members subjected to different types of loadings. For the two-dimensional NLFEA of the beam specimens in this study, one-point monotonic loading is applied to simulate the experimental program.

The details in the longitudinal direction of the beam are relatively well defined in the two-way axis of the program, as compared to the cross-sectional component which was defined in generalized terms. The overall cross-sectional width of the beam specimen was defined wholly, and web reinforcement details weren't specified as they were defined as smeared reinforcements within the concrete by assigning their reinforcement ratio alone. As one of the limitations of most two-dimensional finite element programs, this too lacks in considering the effects of discretized elements in the cross-sectional dimension neglecting the configuration and assortment of web reinforcement and the effects of side cover.

Inorder to quantify how Vector 2 accounts for the effect of concrete beam width, two different finite element models were simulated for each specimen, one with full beam width and the other with stirrup cage width without considering the side cover (assuming side cover had spalled and only the core incased within the stirrup cage is effective for load resistance). In these two modellings, the beam width is the only alteration, other variables are defined identical to the experimental program for both modellings.

Table 6-4: Vector 2 Predictions for Ultimate Load Resistance and Experimental Test to Prediction Ratio

	Ultimate Static Failure Load (kN)				Test to Prediction Ratio	
Specimen	Experiment	Vector 2 Full Section	Vector 2 Spalled Section	% Reduction	Vector 2 Full Section	Vector 2 Spalled Section
SI8-25	639.51	685.475	540.51	21%	0.93	1.18
SI8-50	681.77	726.14	488.542	33%	0.94	1.4
SII10-50	674.77	766.17	504.716	34%	0.88	1.34
SII10-75	727	815.67	462.9	43%	0.89	1.57
SIII8-75	541.72	770.27	352.229	54%	0.7	1.54
SIII10-75	455.93	774.379	356.571	54%	0.59	1.28

As presented in Table 6-4 the two-dimensional simulation done with the specimen's full width had an overestimated response while the simulation done with the stirrup cage width as the width of the beam gave an underestimated result. The decrease in beam width has caused a significant

decrease in the beam's ultimate load carrying capacity. This signifies that the software considers the entire beam width defined to be effective for resisting applied loads, hence decreasing resistance for a decreased width. Presented below are the load vs deformation plots for both types of VecTor 2 simulations along with the experimental result and sectional analysis result based on MCFT from RESPONSE 2000.

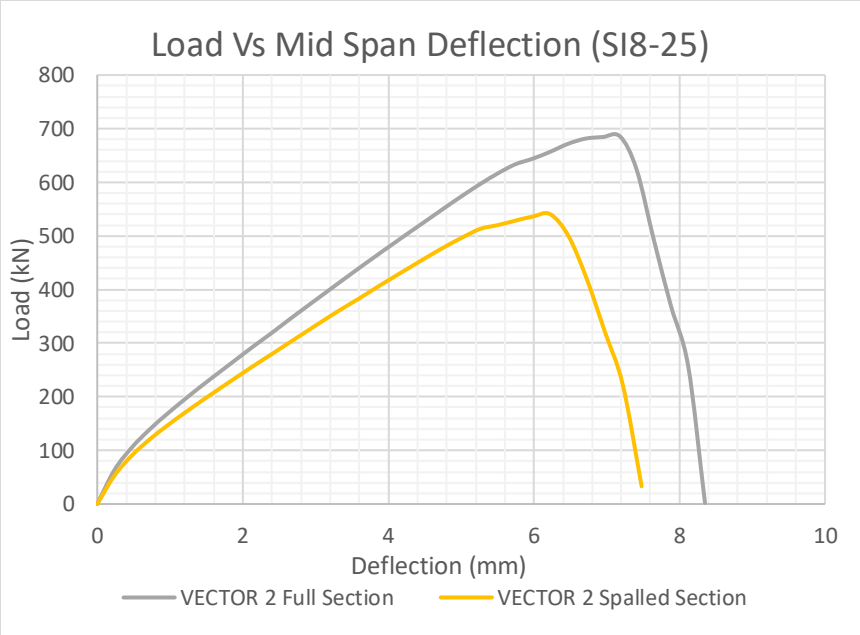
Load Vs Mid Span Deflection (SI8-25)
Load (kN)
Deflection (mm)
VECTOR 2 Full Section
VECTOR 2 Spalled Section

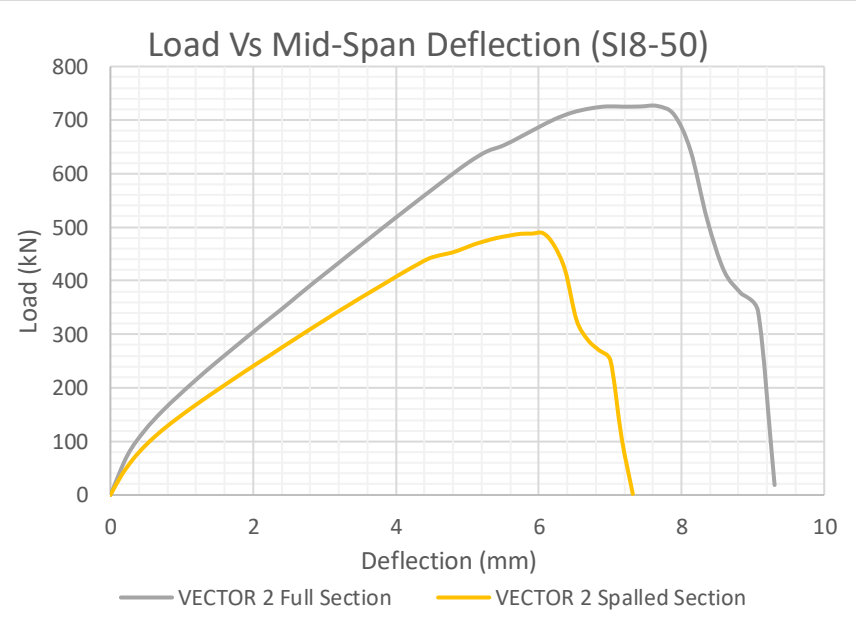
Load Vs Mid-Span Deflection (SI8-50)
Load (kN)
Deflection (mm)
VECTOR 2 Full Section
VECTOR 2 Spalled Section

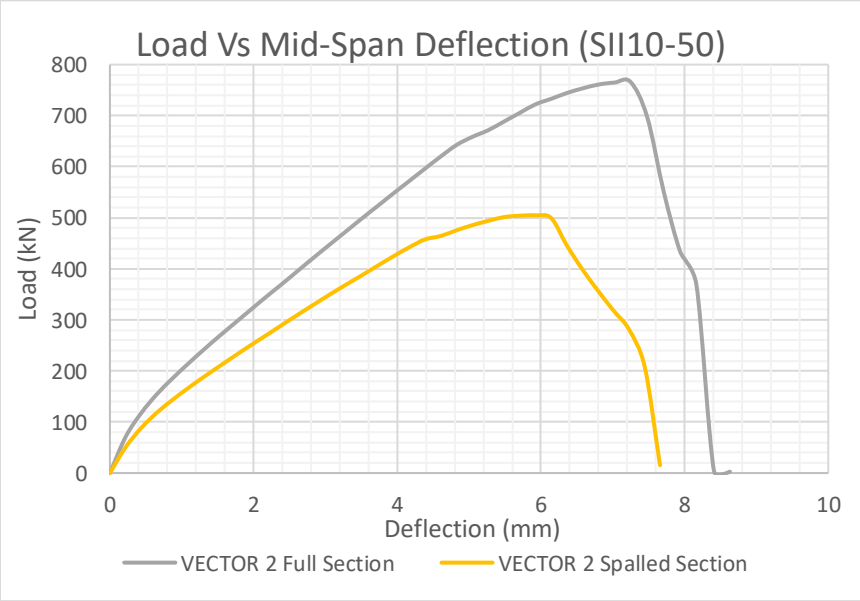
Load Vs Mid-Span Deflection (SII10-50)
Load (kN)
Deflection (mm)
VECTOR 2 Full Section
VECTOR 2 Spalled Section

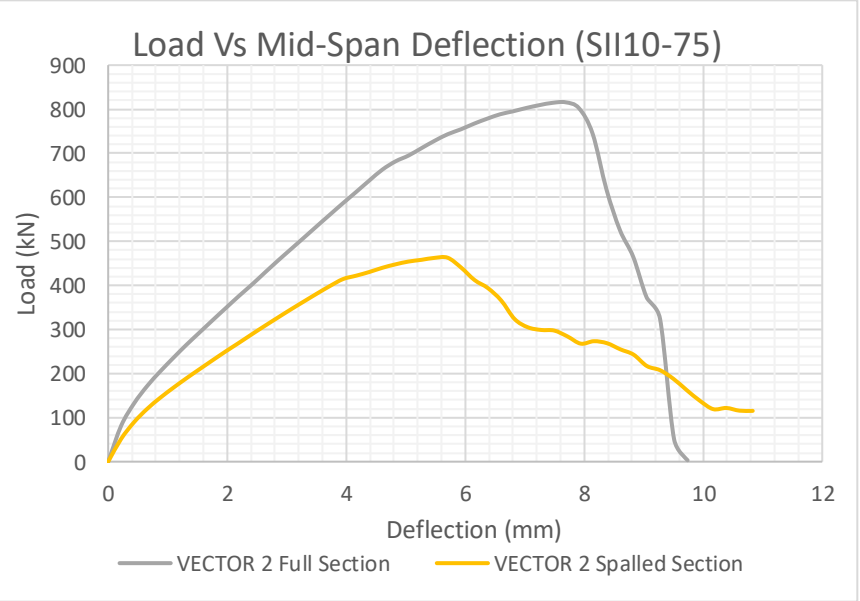
Load Vs Mid-Span Deflection (SII10-75)
Load (kN)
Deflection (mm)
VECTOR 2 Full Section
VECTOR 2 Spalled Section

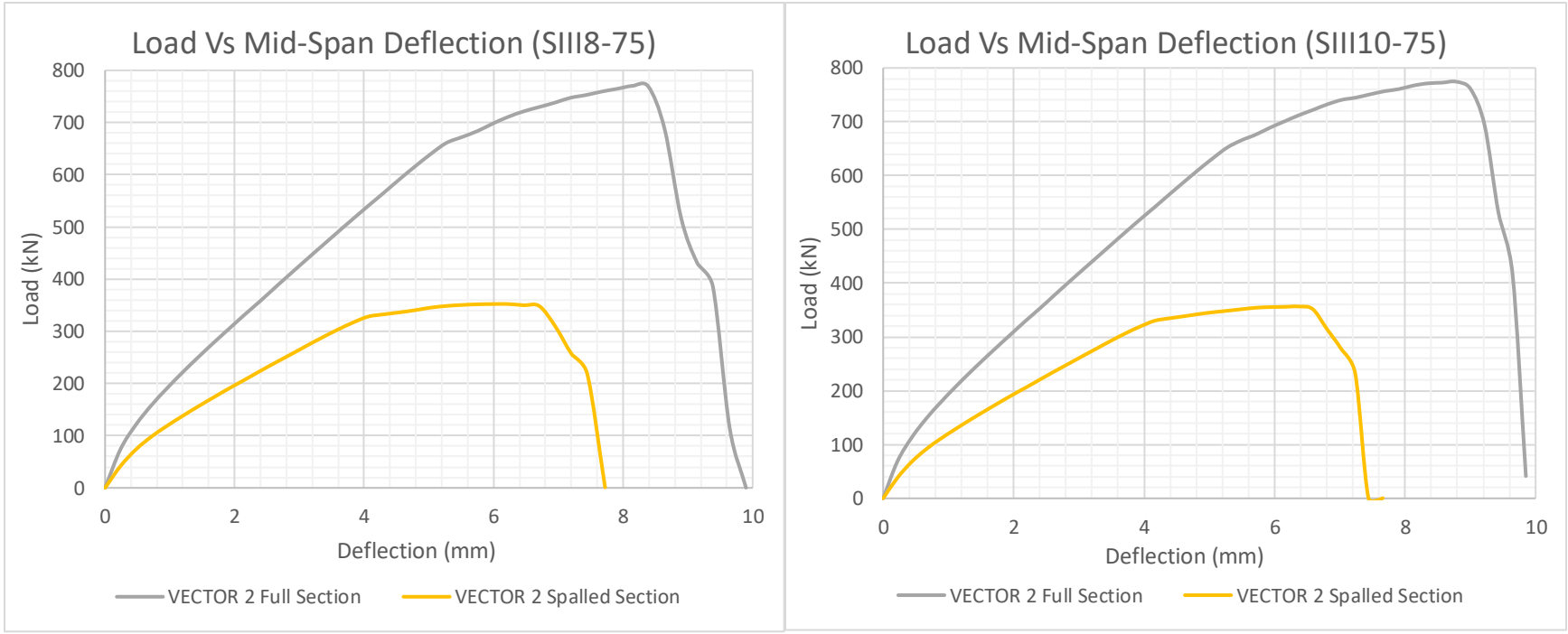

Figure 6-21: Load Deformation Results from VecTor 2

6.4. Comparison of Experimental Results to Software Simulations

In this section load deformation results from the experimental program are compared to deformation responses from the nonlinear two-dimensional VecTor 2 modellings and MCFT based sectional analysis done by RESPONSE 2000.

Plotted below in Figure 6-22 are four responses for each specimen. Similar responses are seen from VecTor full section modellings and RESPONSE 2000 load deformation results. Even though the modelling and analysis procedures followed are different both of these programs are mainly based on MCFT and rely on its basic concepts to relate stress and strains at various locations. These two responses over predicted the actual capacity of the specimens. The experimental result lies between the full section and spalled section of the VecTor modellings for each specimen with a closer initial loading response to the spalled section simulation. However, the spalled section simulation underestimated the specimen's capacity as it was defined with a minimized beam width.

VecTor 2, the two-dimensional non-linear finite element analysis couldn't correctly predict the specimen's ultimate failure load and overall load deformation response. The cross-sectional details included in the experimental program couldn't be incorporated in the modelling due to the limitations set by the program itself. Web reinforcement ratio is defined within the concrete properties as smeared reinforcement as it was not possible to discretely define stirrups as truss elements with their respective cage width.

The results of the experimental program clearly indicate that stirrup cage width has an effect on the shear resistance of beams. However due to the generalized definition of web reinforcement in the two-dimensional analysis this effect couldn't be captured and hence simulation predictions gave poor results to an unreliable extent.

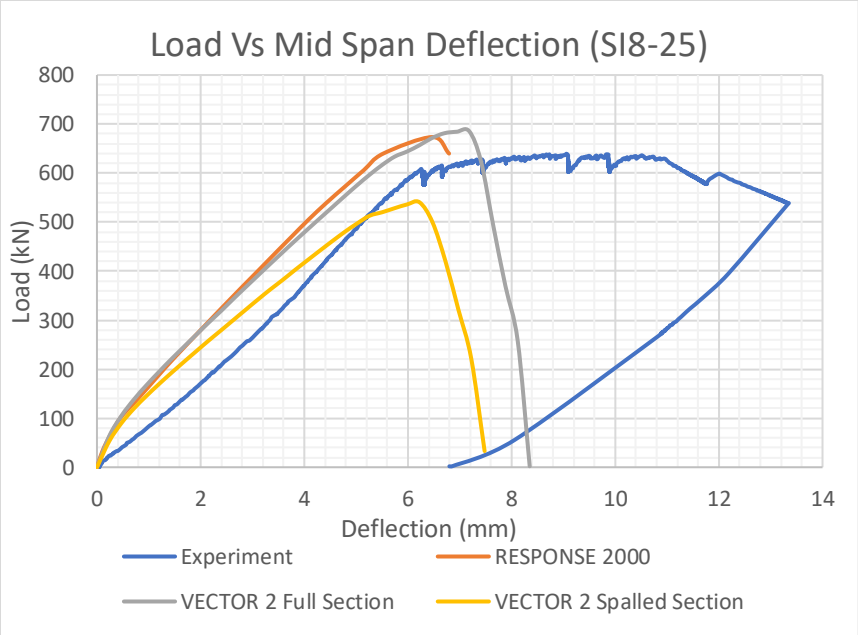
Load Vs Mid Span Deflection (SI8-25)
Load (kN)
Deflection (mm)
Experiment
RESPONSE 2000
VECTOR 2 Full Section
VECTOR 2 Spalled Section

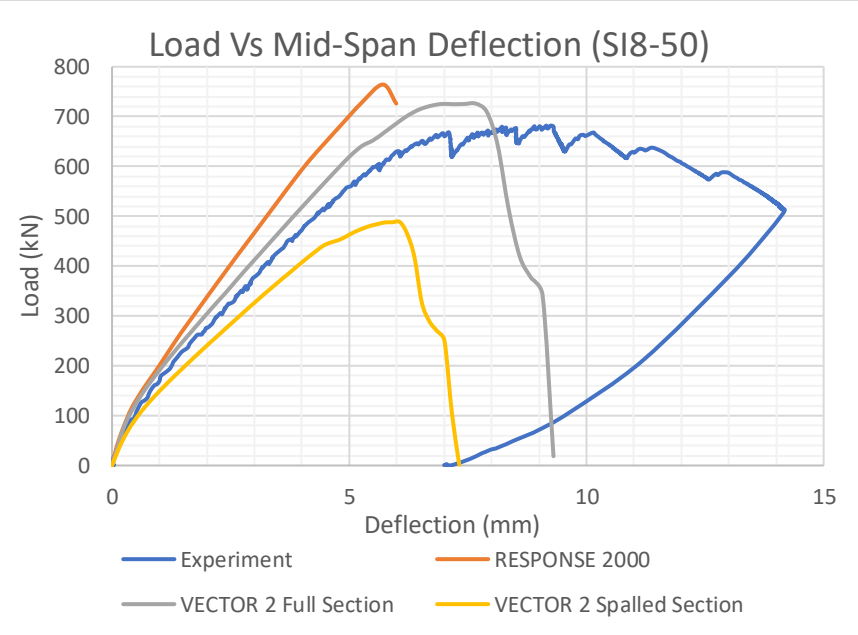
Load Vs Mid-Span Deflection (SI8-50)
Load (kN)
Deflection (mm)
Experiment
RESPONSE 2000
VECTOR 2 Full Section
VECTOR 2 Spalled Section

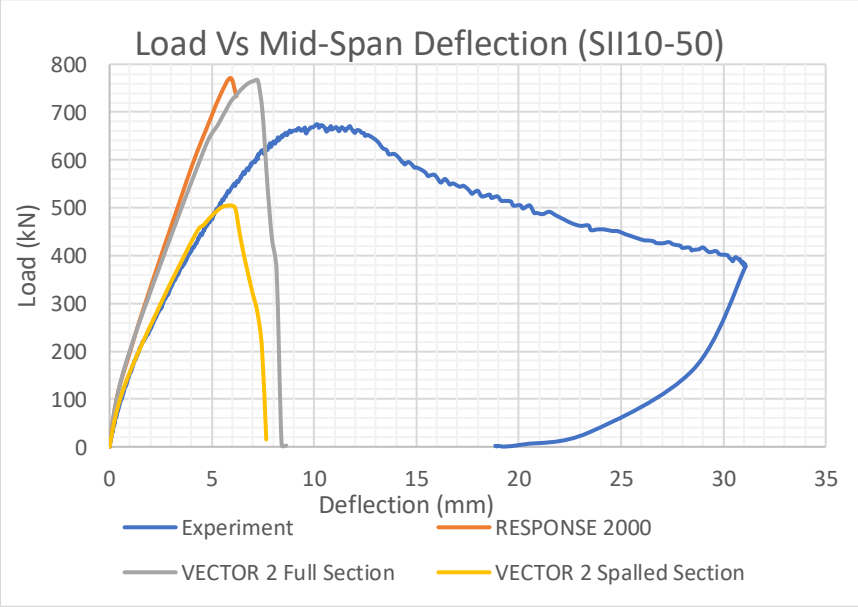
Load Vs Mid-Span Deflection (SII10-50)
Load (kN)
Deflection (mm)
Experiment
RESPONSE 2000
VECTOR 2 Full Section
VECTOR 2 Spalled Section

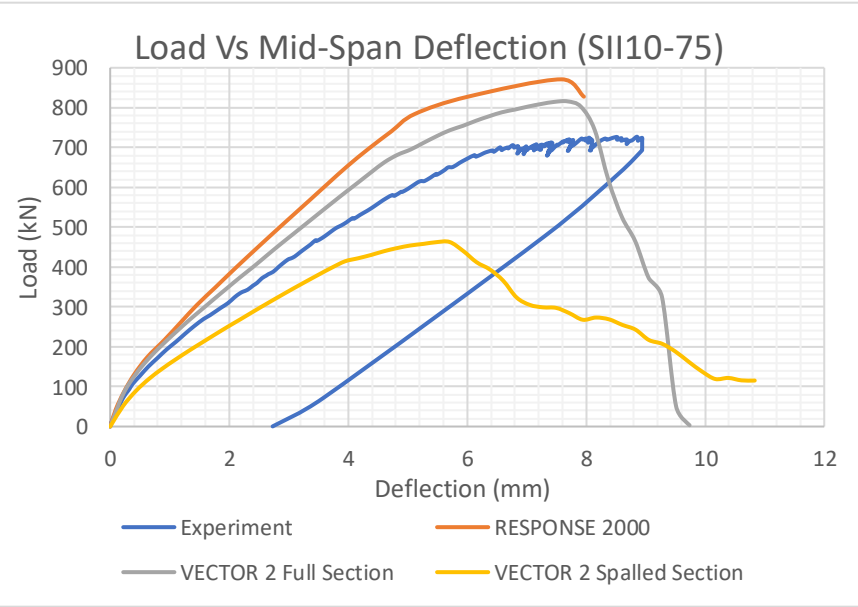
Load Vs Mid-Span Deflection (SII10-75)
Load (kN)
Deflection (mm)
Experiment
RESPONSE 2000
VECTOR 2 Full Section
VECTOR 2 Spalled Section

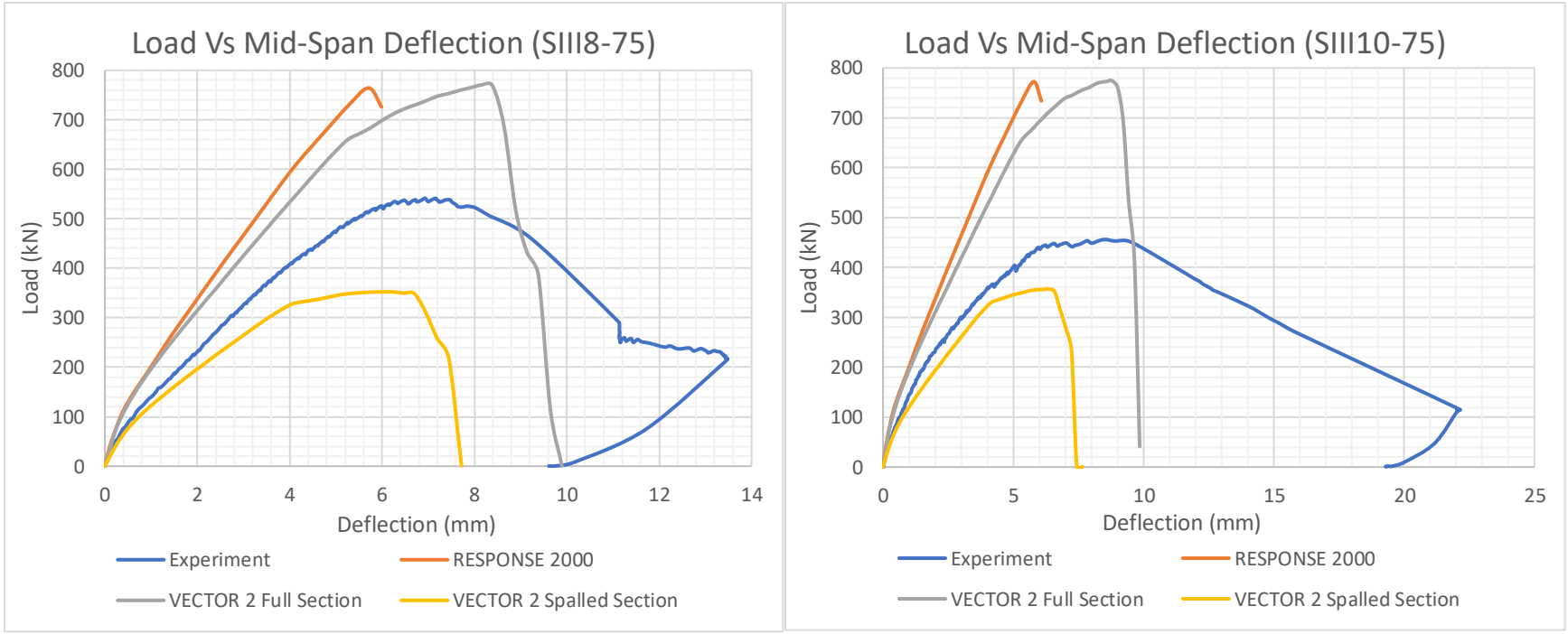

Figure 6-22: Comparison of Experimental Results to Software Simulations

6.5. Effect of Varying Side Cover Thickness and Stirrup Cage Width

Specimens defined in set I and II had stirrup cage width of 150mm while the two specimens defined in set III had a reduced stirrup cage width of 100mm. Side cover was varied with a constant cage width within a set for the first two sets. Varying side cover thickness for a constant cage width in the first two sets has shown no quantifiable strength difference within specimens as they were able to resist the predicted amount of load. However, variation of concrete side cover while also varying the stirrup cage width had a significant effect on the load resisting capacity of the specimen.

Compared below in this section are four specimens, SI8-50, SIII8-75, SII10-50 and SIII10-75. According to code predictions these four specimens all had similar load resistance capacities as they were design with the same web reinforcement ratio and beam width. However, the experimental result proved that the alternated variables should be given due attention as they've influenced the structural performance. For comparison load vs mid span deflection of paired specimens are plotted together.

Specimen SI8-50 and SIII8-75, in addition to having the same web reinforcement ratio and beam width these two specimens were also designed with the same stirrup spacing by using a diameter 8 rebar and had similar test day concrete strength of 35.1MPa.

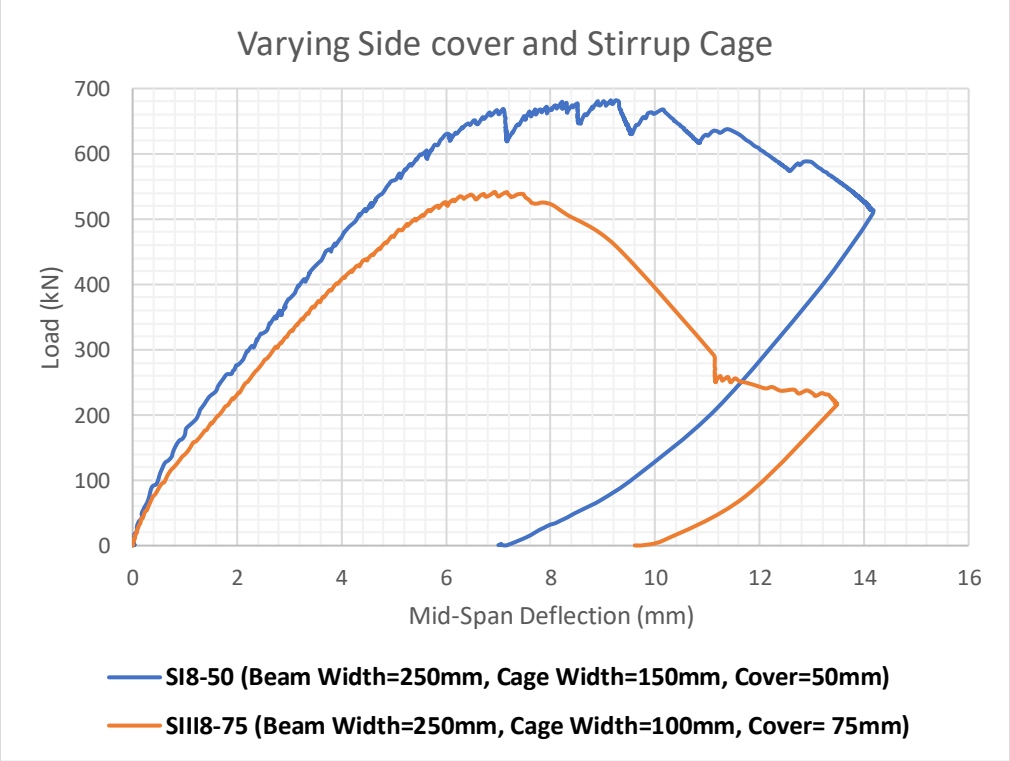

Figure 6-23: Comparison for Varying Side Cover and Stirrup Cage (SI8-50 and SIII8-75)

Apart from their stirrup cage width and their corresponding side cover variation they were identical and were expected to have similar responses. However, as plotted in Figure 6-23, due to the reduced stirrup cage specimens SIII8-75 had a **20.5%** less load resistance as compared to specimen SI8-50. Even though they had similar pre peak response, SI8-50 had a stiffer response throughout the loading scheme. Extensive spalling had occurred for SIII8-75 near peak load as compared to SI8-50.

Similarly, specimen SII10-50 and SIII10-75 had identical properties apart from their differing stirrup cage width. The specimens had identical response for the initial loading stage as seen in the comparison plot below in Figure 6-24.

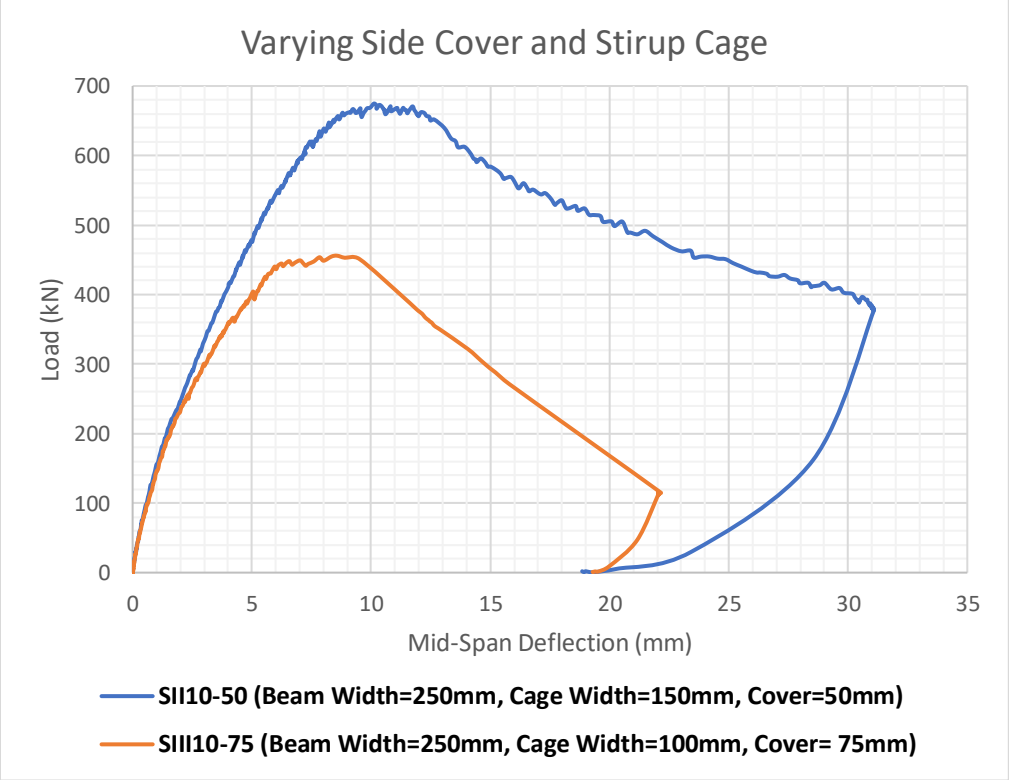

Figure 6-24: Comparison for Varying Side Cover and Stirrup Cage (SII10-50 and SIII10-75)

Specimen SIII10-75, with a reduced stirrup cage width of 100mm resisted a **32.4%** less load than SII10-50 (cage width=150mm). Similar to the comparison for Figure 6-23, the specimen with the largest cover had severe spalling near peak load as compared to the one with lesser side cover.

Side cover thickness variation within the first two sets brought up no reduction in ultimate capacity of the beams as the stirrup cage width was maintained even though side cover thickness had varied. This response was however changed when side cover was varied by reducing the stirrup cage width. Specimens with reduced stirrup cage width couldn't resist the expected load and failed prematurely indicating that ultimately a beam's shear resistance is dependent on the width of the stirrup cage and not the whole beam width.

6.6. Effect of Varying Stirrup Spacing

A total of four of the main specimens were defined with the same web reinforcement ratio. Comparisons were made in two pairs as the specimens had a varied cage width. In Figure 6-25 specimens from the first two sets having identical properties only differing in their stirrup spacing were compared. The failure load of specimen SI8-50 was **1%** higher than SII10-50 which can be considered a negligible difference.

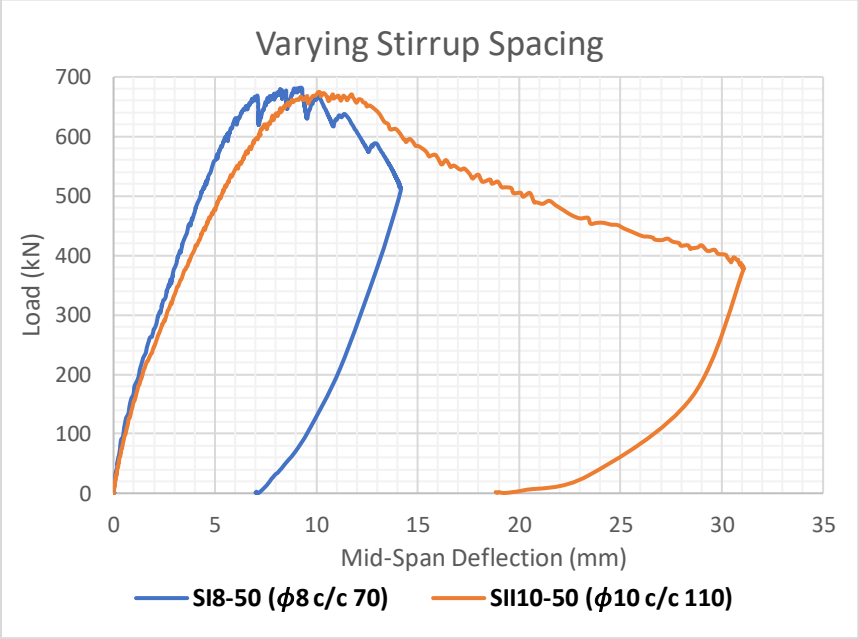

Figure 6-25: Comparison for Varying Stirrup Spacing (SI8-50 and SII10-50)

The two specimens had an equivalent ultimate resistance capacity and similar load deformation response as predicted by the design codes. However, for the comparison of specimen SIII8-75 and SIII10-75 as presented in Figure 6-26 a significant variation in load resistance capacity was recorded. Even though both specimens had failed prematurely as compared to their respective code predictions, their comparison to each other showed the specimen with tighter stirrup spacing (SIII8-75) had a **15.8%** higher load resistance capacity than the lightly spaced one (SIII10-75). Similar results were obtained from previous experimental researches[9] indicating that spacing and configuration of stirrups has an effect on the shear resistance of beams even when provided with the same web reinforcement ratio.

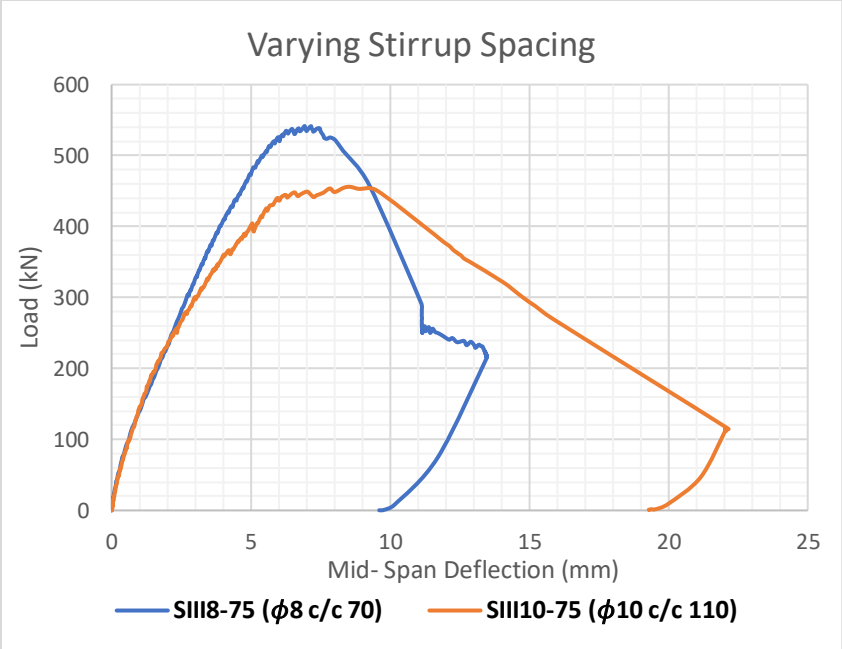

Figure 6-26: Comparison for Varying Stirrup Spacing (SIII8-75 and SIII10-75)

Varying stirrup spacing also had an observable effect on the mechanism of side cover spalling in terms of core concrete roughness in between stirrups. As presented in Figure 6-27, specimens with tightly spaced stirrups had a roughness that aligned with the plane of stirrups by creating a relatively smooth surface of concrete between stirrups. While for specimens with lighter stirrup spacing the concrete from the core is spalled along with the side cover causing valleys in between stirrups.

Figure 6-27: Spalled Section Roughness Variation (A) SIII8-75 (B) SIII10-75

6.7. Effect of Side Cover Thickness and Spalling

Cover provision for structural members is mainly concerned with durability requirements and is accordingly provided as per the need. Three different side cover thicknesses, all within the plausible range of cover provision according to the reviewed codes, were provided for the defined specimens. Effect of varying concrete side cover can be elaborated with regards to ultimate load resistance. The increase of side cover did not compromise the load resistance of specimens as long as the core concrete was adequate enough to resist the applied loads. Capacity reduction happened for specimens SIII8-75, SIII10-75 and TRIAL beam as they were designed with a relatively reduced stirrup cage width in addition to having large concrete covers of 75mm and 50mm (on one side of the trial beam). For specimen SI8-50, SII10-50 and SII10-75, even though an increased side concrete cover of 50mm and 75mm were used the specimens resisted the required amount of load adequately without premature failure.

Varying side concrete cover thickness also had an observable effect on the spalling mechanism of the beams. Specimens with side concrete cover of 25mm and 50mm spalled off piece by piece after reaching the peak load. But for specimens SIII8-75 and SIII10-75 with side concrete cover of 75mm, the cover delaminated in one piece as shown in Figure 4-38. This indicates that side cover thickness has an overall effect on the way side cover delaminates from the core concrete.

Reported results from all tested specimens indicated that indeed out of plane deformations are happening for in plane loaded beams. This is quantified by the out of plane strain measurements obtained. Maximum results were recorded near peak load indicating side cover spalling or complete delamination occurs near ultimate load. Out of plane strain differing from zero (original unloaded state) was recorded for all specimens as loading progressed regardless of the thickness of side cover assigned. Although few of the specimens shared similar trends, specific responses recorded from the out of plane deformation were different among each specimen. Out of plane deformation initiated at the forming of the first flexural crack and progressed after the first shear crack was encountered.

As stated in section 2.3.4 previously done researches that have encountered side cover spalling gave an explanation on how these phenomena came into existence. These literatures stated that delamination starts from the corner edge of the beam as the concrete compressive stresses resisting shear after cracking have to change direction near the corners of the beam creating tensile stresses perpendicular to the directions of these trajectories. Although the main cause of delamination is existence of tensile stresses having a magnitude greater than concrete cracking stress, the explanation is limited to only describing the reason why tensile stresses develop at the edge. However, delamination of side cover is not only limited to the corner of the beam as observed and quantified from the experimental results reported. Tensile stresses created at locations different from the edge are not accounted for or given explanations. This makes the explanations given by the literatures inadequate to explain the entire spalling mechanism.

In an attempt to bridge this gap, instrumentation that could give additional results were defined. From out of plane strain measurements at three zones, it was evidently reported that tensile strains could happen at compression zone, mid-section and tension zone. This indicates that tensile stresses perpendicular to the direction of compressive stresses are happening along the entire depth of the beam where shear failure is set to happen. Although this research was not able to pin point the exact reason as to why out of plane strains were happening, it shed a light on the different values of out of plane strain reported along the depth of the beam. From specimen's whose out of plane instrumentations were mounted on the failure side, it can be said that spalling is initiated from the top compression zone having the maximum tensile out of plane strain as compared to the mid-section and tension zone strain readings. This is well illustrated in Figure 6-16.

After the loose concrete side cover was removed, it was observed that spalling had happened following the plane of stirrups leaving the core concrete confined within the stirrup intact. Stirrups are therefore planes of weaknesses leading to out of plane deformation of side cover. The existence of out of plane tensile strains along the leg of stirrups could be related to the bond stresses induced by the yielding web reinforcement into the surrounding concrete. But in order to quantify this reason further researches should be done inspecting web reinforcement bond behaviors with regard to cover spalling.

From experimental observations two types of spallings were reported. The first is spalling of concrete side cover in both sides of the beam including top and bottom delamination. (Figure 6-28). While the other type was observed in specimen SIII8-75 and SIII10-75, this type follows the diagonal failure crack and delaminated exactly above it on one side of the beam. (Figure 6-29)

Figure 6-28: Spalling on Both Sides of the Beam

Figure 6-29: Spalling on One Side of the Beam Above the Diagonal Crack

7. CONCLUSION AND RECOMMENDATION

7.1. Conclusion

This experimental program sheds a light on the complex mechanism of spalling demonstrating that side cover spalling indeed happens for in-plane loaded shear critical reinforced concrete beams near peak load. It is observed that, out of plane deformation strain initiates at the load at which the first flexural crack happens and progresses with pronounced deformation after the first diagonal shear crack. The evidence, on the spalling of side cover, mechanistically observed in this study entails a question on the adequacy of the shear capacity prediction equations stipulated in the exsisting International codes.

From out of plane strain measurements at three zones, it was evidently reported that tensile strains could happen at compression zone, mid-section and tension zone. Tensile stresses perpendicular to the direction of compressive stresses are happening along the entire depth of the beam where shear failure is set to happen. However, from specimen's whose out of plane instrumentations were mounted on the failure side, it can be concluded that spalling is more likely to be initiated from the top compression zone which had the maximum tensile out of plane strain as compared to the mid-section and tension zone strain readings. Explanations given by previous literatures regarding the possible reasons for side cover spalling of beams subjected to shear were found to be inadequate to explain the entire mechanism of spalling. Delamination initiation is not limited to the corner edge of a beam.

From observations of spalled specimens, stirrups found to be planes of weaknesses in which out of plane deformation of side concrete cover takes place leading to delamination of side cover.

Side cover thickness and stirrup spacing had observable effect on the spalling mechanism of the beams. Varying side cover thickness affected the size of the loose spalled sections delaminating from the core. Specimens with a relatively smaller side concrete cover spalled off piece by piece by following the failure paths created by the multiple diagonal cracks. But for specimens with a large side concrete cover of 75mm, the cover delaminated in one piece. This indicates that side cover thickness has an overall effect on the way side cover delaminates from the core concrete. Varying stirrup spacing had an observable effect on the mechanism of side cover spalling in terms of core concrete roughness in between stirrups. Specimens with tightly spaced stirrups had a relatively smooth surface roughness of concrete between stirrups. While for specimens with lighter stirrup spacing the concrete from the core was spalled along with the side cover causing valleys in between stirrups leading to an irregular rough surface.

The variation of side concrete cover thickness doesn't seem to compromise the load resistance of beams as long as the core concrete is adequate enough to resist the applied loads. Premature failure happened for specimens designed with a relatively reduced stirrup cage width in addition to having large concrete covers.

Specimens with reduced stirrup cage width couldn't resist the expected load and failed prematurely indicating that ultimately after a certain load stage a beam's shear resistance depends on the width of the stirrup cage and not the entire beam width.

Comparisons of vertical surface strain measurements and web reinforcement strain for specimens with smaller side cover thickness, indicated that the core concrete and side cover outside of the stirrup act together and have the same deformation response throughout the loading scheme until failure. However, for specimens with larger covers, the concrete core confined within the stirrups and side cover outside of the stirrup do not have a synced response for the entire load stage. The side cover becomes less effective for load resistance as out of plane deformations leading to spalling starts to happen. This is an additional indication that the entire beam section is not fully effective throughout the entire loading stage in resisting the applied load but rather the core concrete.

The design codes reviewed in section 2.2 all use the entire beam width (bw) for ultimate capacity prediction. The CSA and JSCE design codes were able to predict the peak loads accurately with an average test to prediction ratio of 1.01 and are used as a basis of comparison. For four of the main specimens with a stirrup cage width of 150mm, code gave an accurate ultimate load prediction as compared to the experimental results. However, code prediction gave an overestimated failure load for specimens with reduced cage width. This questions the adequacy and accuracy of design code provisions for the design of beam in shear with regards to the usage of the entire beam width (bw) for capacity prediction.

In addition to design codes, a two-dimensional finite element program, VecTor 2, was used to analyze the specimens. As the software lacks to recognize details in the out of plane direction, it gave overestimated prediction results. The cross-sectional details (side cover and stirrup cage width variations) included in the experimental program couldn't be incorporated in the modelling due to the limitations set by 2D NLFEA programs in general. The software considered the entire beam width defined to be effective for resisting applied loads, neglecting out of plane deformations and their consequences.

Similar to findings in previous experimental researches[9] , for the same web reinforcement ratio but different stirrup spacing, tightly spaced stirrups gave a better load resistance as compared to lightly spaced ones. Spacing and configuration of stirrups has an effect on the shear resistance of beams even when provided with the same web reinforcement ratio.

7.2. Recommendation

Mechanism of side cover spalling is a complex phenomenon with no/little research database that has measurable structural effects on load resisting members. This research, although not adequate enough to fully explain the mechanism of side concrete cover spalling for beams subjected to shear it has shed a light on important areas of interest and affecting variables relevant for spalling. Out of plane strain measurements in different regions gave an idea on its initiation and propagation.

The instrumentations used for measuring out of plane deformations were however disturbed by local stress induced cracks at the surface where aluminum plates were mounted and internal cracks passing through the holes of testing. These disturbances can be minimized by designing a better suited out of plane deformation measuring instruments that aren't prone to being affected by local failurities. Since shear failure path in beams is difficult to predict, out of plane instrumentations should be mounted at both sides of the beam inorder to catch the actual shear failure response whichever way it decides to propagate.

Beam specimens experimented on this research had an a/d ratio of 2.5, to have a complete understanding and refined database of spalling mechanism, beams with different ranges of a/d ratios should be tested (both deep and slender). Additional variables such as the use of smooth reinforcements as stirrups, and concrete grade should also be investigated.

The study reported that roughness differences were observed on concrete sections in between stirrups due to the variation of stirrup spacing. For a better quantified explanation, surface roughness measurements should be included to enumerate the effect of stirrup spacing on spalling mechanism.

Stirrups are labeled as planes of weaknesses leading to out of plane deformation of side cover. The existence of out of plane tensile strains along the leg of stirrups could be related to the bond stresses induced by the yielding web reinforcement into the surrounding concrete. Therefore, further researches should be done inspecting web reinforcement bond behaviors with regard to cover spalling.

Code provisions for shear design should be thoroughly reviewed as inaccurate predictions were encountered for specimens with reduced stirrup cage width. Out of plane deformation for side concrete covers should be accounted for in the design process as it has a significant effect on the structural performance of a beam.

Specimens should be analyzed using three-dimensional nonlinear finite element analysis tools, inorder to measure the adequacy and prediction accuracy of three-dimensional tools in capturing out of plane deformation and its consequences.

In practical aspect, beams are subjected to different types of loading and aren't limited to monotonic loading arrangement. To document realistic loading conditions, mechanism of spalling should be studied under cyclic loading consitions as well.

REFERENCES

[1] A. W. Fisher, E. C. Bentz, and M. P. Collins, “Response of Heavily Reinforced High-Strength Concrete Coupling Beams,” *ACI Struct. J.*, vol. 114, no. 6, pp. 1483–1494, 2017.

[2] K. N. Rahal, “Shear Behavior of Reinforced Concrete Beams with Variable Thickness of Concrete Side Cover,” *ACI Struct. J.*, vol. 103, no. 2, pp. 171–177, 2006.

[3] K. N. Rahal and M. P. Collins, “Effect of Thickness of Concrete Cover on Shear-Torsion Interaction - An Experimental Investigation,” *ACI Struct. J.*, vol. 92, no. 3, pp. 334–342, 1995.

[4] K. Suda and J. Masukawa, “Models for Concrete Cover Spalling and Reinforcement Buckling of Reinforced Concrete,” pp. 1–8.

[5] M. S. Ibrahim, E. Gebreyouhannes, A. Muhdin, and A. Gebre, “Effect of concrete cover on the pure torsional behavior of reinforced concrete beams,” *Eng. Struct.*, vol. 216, p. 110790, Aug. 2020.

[6] C. Republic, “EUROCODE 2. EN Design of Concrete Structures: Part 1-1: General Rules and Rules for Buildings. Brussels: CEN-European Committee for Standardization and,” vol. 1, no. November, 2002.

[7] American Concrete Institute (ACI 318-08), *ACI 318-08: Building Code Requirements for Structural Concrete*, vol. 2007. 1999.

[8] M. Zakaria, T. Ueda, Z. Wu, and L. Meng, “Experimental Investigation on Shear Cracking Behavior in Reinforced Concrete Beams with Shear Reinforcement,” *J. Adv. Concr. Technol.*, vol. 7, no. 1, pp. 79–96, 2009.

[9] M. Taddese, “Effects of Spacing and Configuration of Web Reinforcement on Shear Behavior of Reinforced Concrete Beams,” 2015.

[10] W. Ritter, “Die Bauweise Hennebique,” *Schweizerische Bauzeitung*, vol. 33, no. 7, pp. 49–52, 1899.

[11] V. Broujerdian, H. Karimpour, and S. Alavikia, “Predicting the Shear Behavior of Reinforced Concrete Beams Using Non-linear Fracture Mechanics,” *Int. J. Civ. Eng.*, vol. 17, no. 5, pp. 597–605, 2019.

[12] F. J. Vecchio and M. P. Collins, “Modified Compression-Field Theory for Reinforced Concrete Elements Subjected To Shear.,” *Journal of the American Concrete Institute*, vol. 83, no. 2. pp. 219–231, 1986.

[13] J. K. Wight and J. G. MacGregor, *REINFORCED CONCRETE MECHANICS AND DESIGN 6th Edition*. .

[14] H. Baghi and J. A. O. Barros, “New Approach to Predict Shear Capacity of Reinforced

Concrete Beams Strengthened with Near-Surface-Mounted Technique," no. 114, 2017.

[15] D. Grandić, P. Šćulac, and I. Š. Grandić, "Shear Resistance of Reinforced Concrete Beams In Dependence on Concrete Strength in Compressive Struts," *Teh. Vjesn.*, vol. 22, no. 4, pp. 925–934, 2015.

[16] B. Y. D. Mitchell and M. P. Collins, "Diagonal Compression Field Theory-A Rational Model for Structural Concrete in Pure Torsion," no. 71, pp. 396–408, 1974.

[17] M. P. Collins, "Towards a Rational Theory for Reinforced Concrete Members in Shear," *J. Struct. Div.*, vol. 104, no. 4, pp. 649–666, 1978.

[18] F. J. Vecchio, "Disturbed Stress Field Model for Reinforced Concrete: Implementation," *Journal of Structural Engineering*, vol. 127, no. 1. pp. 12–20, 2001.

[19] E. C. Bentz, F. J. Vecchio, and M. P. Collins, "Simplified Modified Compression Field Theory for Calculating Shear Strength of Reinforced Concrete Elements," no. 103, 2007.

[20] K. H. Reineck, E. Bentz, B. Fitik, D. A. Kuchma, and O. Bayrak, "ACI-DAfStb Databases for Shear Tests on Slender Reinforced Concrete Beams with Stirrups," *ACI Struct. J.*, vol. 111, no. 5, pp. 1147–1156, 2014.

[21] "Eurocode 2: Design of Concrete Structures- Part 1-1: General Rules and Rules for Buildings," vol. 1, no. 2004, 2011.

[22] American Concrete Institute (ACI 318-14). ACI 318-14: Building Code Requirement for Structural Concrete, *ACI 318R-14.pdf*. 2014.

[23] A. W. Fisher, "Shear Performance of Heavily Reinforced High-Strength Concrete Coupling Beams," 2016.

[24] "Simplified Shear Design of Structural Concrete Members: Appendixes," *Simpl. Shear Des. Struct. Concr. Members Append.*, vol. 78, no. July, 2005.

[25] J. S. of C. E. (JSCE), *JSCE GUIDELINES FOR CONCRETE, STANDARD SPECIFICATIONS FOR CONCRETE STRUCTURES 2007 "Design,"* no. 15. 2007.

[26] A. Muhdin, "The Effect of Concrete Cover on Pure Torsional Resistance in Reinforced Concrete Beam- Experimental Investigation," no. June, 2019.

[27] A. Muttoni, F. Moccia, and M. Fern, "Spalling of Concrete Cover Induced by Reinforcement," *Eng. Struct.*, vol. 237, no. April, p. 112188, 2021.

[28] D. Abebe, "Construction Materials - Labratory Manual." 2002.

[29] F. Leonhardt, "Cracks and Crack Control in Concrete Structures," *PCI J.*, vol. 33, no. 4, pp. 124–145, 1988.

APPENDIX

1. Building Code Ultimate Failure Load (Shear Resistance) Prediction Calculation

1.1. Eurocode 2 (EN 1992-1-1: 2004)

$$V_{Rd,c} = \left[0.12k(100\varrho_1 f_{ck})^{1/3} - 0.15\sigma_{cp}\right]b_w d$$

$$k = 1 + \sqrt{\frac{200}{d}} \leq 2$$

$$z = 0.9d$$

$$\varrho_1 = \frac{A_{s1}}{b_w d} \leq 0.02$$

$$V_{Rd,s} = \frac{A_{sw}}{S} z f_{ywd} \cot\theta$$

$$V_{Rd,max} = [\alpha_c \nu_1 f_{cd}/(\cot\theta + \tan\theta)]b_w z$$

$$\nu_1 = 0.6(1 - f_{ck}/250)$$

Where:

- $V_{Rd,c}$- design shear resistance of the member without shear reinforcement
- ϱ_1- Tensile reinforcement ratio
- b_w- the smallest width of the cross-section in the tensile area
- d- effective depth
- z- distance from location of compressive stress resultant to centroid of tension steel
- A_{s1}- area of tensile reinforcement
- $V_{Rd,s}$- design shear capacity with vertical shear reinforcement
- f_{ywd}- yield strength of web reinforcement
- A_{sw}- cross sectional area of shear reinforcement
- $V_{Rd,max}$- maximum shear force sustained by a member limited by crushing of the compression strut
- α_c -a coefficient for the interaction of the stress in the compression chord and any applied axial compressive stress
- θ-the angle between concrete compression strut and main tension chord

1.2. ACI Standard (ACI 318-14)

$$V_n = V_c + V_s$$

$$V_c = \left(\frac{\sqrt{f_c'}}{6}\right) b_w d \ (mm, MPa)$$

$$V_s = \frac{A_V f_{vd}}{S}$$

1.3. Canadian Standard

1.3.1. Simplified Method

$$V_n = V_c + V_s$$

$$V_c = 0.2\sqrt{f_c'}\, b_w d \ \ when\ A_V \geq \frac{0.06\sqrt{f_c'}\, b_w S}{f_y} \ \ or\ d \leq 300mm$$

$$V_c = \frac{260}{1000 + d}\sqrt{f_c'}\, b_w d \geq 0.1\sqrt{f_c'}\, b_w d \ \ when\ A_V < \frac{0.06\sqrt{f_c'}\, b_w S}{f_y} \ \ or\ d > 300mm$$

$$V_s = \frac{A_v f_v d}{S} \ \ where\ V_s \leq 0.8\sqrt{f_c'}\, b_w d$$

1.3.2. General Method

$$V_{rg} = V_{cg} + V_{sg} + V_p \leq 0.25 f_c' b_w d_v + V_p$$

$$d_v = 0.9d$$

$$V_{cg} = \beta\sqrt{f_c'}\, b_w d_v$$

$$V_{sg} = \frac{A_v f_y d_v (\cot\theta + \cot\alpha)\sin\alpha}{S}$$

B and θ are obtained from Table Values

1.3.3. Canadian Standard (CSA A23.3-14)

$$V_{rg} = V_{cg} + V_{sg} + V_p \leq 0.25 f_c' b_w d_v + V_p$$

$$d_v = 0.9d$$

$$V_{cg} = \beta\sqrt{f_c'}\, b_w d_v$$

$$V_{sg} = \frac{A_v f_y d_v (\cot\theta + \cot\alpha)\sin\alpha}{S}$$

$$\beta = \frac{4.8}{(1+1500\varepsilon_x)} \cdot \frac{51}{(39+S_{ze})}, \qquad S_{ze} = \frac{1.38S_z}{0.63+ag}$$

$$\theta = 29 + 7000\varepsilon_x$$

$$\varepsilon_x = \frac{M_f/d_v + 0.5N_f + V_f}{2(E_sA_s)}$$

Where:

- b_w- effective web width
- d_v- lever arm of resisting flexural moment
- β- factor accounting for shear resistance of cracked concrete
- S_{ze}- the equivalent crack spacing parameter
- ag –maximum aggregate size
- A_v- area of shear reinforcement within spacing,
- f_y- specified yield strength of reinforcement
- θ- angle of inclination of diagonal compressive stresses to the longitudinal axis of the member
- α -angle of inclined stirrups to longitudinal axis
- ε_x- longitudinal strain
- M_f- factored moment at section
- V_f- factored shear force at section

1.4. Japanese Code (JSCE Standard, 1986)

$$V_{yd} = V_{cd} + V_{sd} + V_{ped}$$

$$V_{cd} = \beta_d\beta_p\beta_n f_{vcd} b_w d/\gamma_b$$

$$\gamma_b = 1.3$$

$$f_{vcd} = 0.2\sqrt[3]{f_{cd}} \quad f_{vcd} \le 0.72$$

$$\beta_d = \sqrt[4]{1000/d} \; when \; \beta_d > 1.5, \beta_d = 1.5$$

$$\beta_p = \sqrt[3]{100P_v} \; when \; \beta_p > 1.5, \beta_d = 1.5$$

$$P_v = \frac{A_s}{b_w d}$$

$$\beta_n = 1 + \frac{2M_o}{M_{ud}(N_d \ge 0)} \; when \quad \beta_n > 2, \beta_n = 2$$

$$V_{sd} = \left[A_w f_{wyd}(\sin\alpha_s + \cos\alpha_s)/S_s\right] z/\gamma_b \quad where\ \gamma_b = 1.1$$

$$z = \frac{d}{1.15}$$

Where:

- V_{yd}- design shear capacity
- V_{cd}- design Shear Capacity of concrete without shear reinforcing steel
- V_{sd}- design shear capacity of shear reinforcement
- M_{ud}- design flexural moment
- M_o- moment that causes an extreme bottom fiber stress of zero
- S_s- Spacing of shear reinforcement
- αs- angle between shear reinforcement and member axis
- γ_b- factor associated with the design capacity of members

Table 1: Building Codes Ultimate Failure Load Prediction

		Set I		Set II		Set III		TRIAL Beam	
	Specimen	SI8-25	SI8-50	SII10-50	SII10-75	SIII8-75	SIII10-75	TR8-50/75	TR10-50/75
Geometry (mm)	bw (mm)	200	250	250	300	250	250	210	210
	h (mm)	350	350	350	350	350	350	350	350
	d (mm)	309	307	305	305	297	295	317	315
Concrete Strength	fc (MPa)	35.7	35.7	35.7	35.7	35.7	35.7	26.15	26.15
Web Reinforcement Properties	Dia (mm)	8	8	10	10	8	10	8	10
	Asw (mm2)	100.53	100.53	157.08	157.08	100.53	100.53	100.53	157.08
	Spacing (mm)	70	70	110	110	70	110	60	100
	ϱw (%)	0.71	0.57	0.57	0.47	0.57	0.57	0.74	0.74
	fyd/fyt (MPa)	520	520	544	544	520	544	515	534
Longitudinal Reinforcement Properties	ϱl (%)	2.5	2.4	2.4	2	2.4	2.4	3.3	3.3
Eurocode 2 (EN 1992-1-1: 2004)	v	0.51	0.51	0.51	0.51	0.51	0.51	0.54	0.54
	z (mm)	278.1	276.3	274.5	274.5	267.3	265.5	285.3	283.5
	fcd (MPa)	20.23	20.23	20.23	20.23	20.23	20.23	14.82	14.82
	Vrd,max	199.55	247.83	246.21	295.46	239.76	238.14	164.47	163.43
	k	1.8	1.81	1.81	1.81	1.82	1.82	1.79	1.8
	Vrd,c (kN)	59.63	73.15	72.94	82.36	71.3	71.08	63.34	63.03
	Vrd,s (kN)	207.69	206.34	213.24	213.24	199.62	206.25	246.18	237.8
	V (kN)	267.31	279.5	286.18	295.6	270.92	277.33	309.52	300.83
	Failure Load (kN)	**535.9**	**558.2**	**571.5**	**589.5**	**541.1**	**553.9**	**619.1**	**601.66**
ACI Standard (ACI 318-14)	Vc (kN)	61.54	76.43	75.93	91.12	73.94	73.44	56.74	56.38
	Vs (kN)	230.76	229.27	236.93	236.93	221.8	229.16	273.54	264.22
	Vn (kN)	292.3	305.7	312.86	328.05	295.74	302.61	330.27	320.6

	Failure Load (kN)	**586.5**	**610.1**	**624.5**	**653.3**	**590.2**	**603.9**	**660.6**	**641.2**
CSA Simplified Method	Vc (kN)	73.34	91.22	90.77	108.92	88.93	88.47	67.21	66.88
	Vs (kN)	230.76	229.27	236.93	236.93	221.8	229.16	273.54	264.22
	Vn (kN)	304.1	320.49	327.7	345.86	310.73	317.64	340.74	331.11
	Failure Load (kN)	**608.2**	**640.9**	**655.4**	**691.71**	**621.47**	**635.27**	**681.48**	**662.21**
CSA General Method	Vcg (kN)	68.13	84.61	84.06	100.87	81.85	81.3	62.81	62.41
	Vsg (kN)	228.45	226.98	234.56	234.56	219.58	226.87	270.8	261.58
	Vrg (kN)	296.58	311.58	318.62	335.43	301.43	308.17	333.61	323.99
	Failure Load (kN)	**593.16**	**623.17**	**637.24**	**670.86**	**602.87**	**616.35**	**667.22**	**647.99**
Canadian Standard (CSA A23.3-14)	dv (mm)	278.1	276.3	274.5	274.5	267.3	265.5	285.3	283.5
	ϵx	0	0	0	0	0	0	0	0
	Sze	500	500	500	500	500	500	500	500
	β	0.31	0.31	0.31	0.31	0.31	0.31	0.31	0.31
	θ (°)	31.17	31.17	31.17	31.17	31.17	31.17	31.17	31.17
	Vcg (kN)	103.09	128.03	127.19	152.63	123.86	123.02	95.04	94.44
	Vsg (kN)	207.69	206.34	213.24	213.24	199.62	206.25	246.18	237.8
	Vrg (kN)	310.78	334.37	340.43	365.87	323.48	329.27	341.22	332.24
	Failure Load (kN)	**624.8**	**666.6**	**678.7**	**726.9**	**644.9**	**656.5**	**682.5**	**664.48**
Japanese Code (JSCE Standard, 1986)	Fvcd (MPa)	0.66	0.66	0.66	0.66	0.66	0.66	0.59	0.59
	βd	1.34	1.34	1.35	1.35	1.35	1.36	1.33	1.33
	βp	1.35	1.33	1.34	1.26	1.33	1.34	1.49	1.49
	βn	1.5	1.5	1.5	1.5	1.5	1.5	1.5	1.5
	Vcd (kN)	110.79	135.96	135.58	153.1	132.62	132.23	117.62	117.06
	z (mm)	268.7	266.96	265.22	265.22	258.26	256.52	275.65	273.91
	Vsd (kN)	200.66	199.36	206.03	206.03	192.87	199.27	237.86	229.76
	Vyd (kN)	311.46	335.32	341.61	359.13	325.49	331.51	355.47	346.82
	Failure Load (kN)	**625.2**	**669.1**	**681.7**	**715.1**	**649.5**	**661.5**	**710.9**	**693.64**

2. Strain Relationship Equations

$$\epsilon_{1,2} = \frac{\epsilon_x + \epsilon_y}{2} \pm \sqrt{\left(\frac{\epsilon_x - \epsilon_y}{2}\right)^2 + \left(\frac{\gamma_{xy}}{2}\right)^2}$$

$$\tan 2\theta_p = \left(\frac{\gamma_{xy}}{\epsilon_x - \epsilon_y}\right)$$

$$\tan 2\theta_s = -\left(\frac{\epsilon_x - \epsilon_y}{\gamma_{xy}}\right)$$

$$\frac{\gamma_{max}}{2} = \sqrt{\left(\frac{\epsilon_x - \epsilon_y}{2}\right)^2 + \left(\frac{\gamma_{xy}}{2}\right)^2}$$

$$\epsilon_b = \epsilon_x Cos^2\theta_b + \epsilon_y Sin^2\theta_b + \gamma_{xy} Sin\theta_b Cos\theta_b$$

Where:

- $\epsilon_{1,2}$- principal strains
- ϵ_x- strain in the x direction
- ϵ_y- strain in the y direction
- γ_{xy}- shear strain
- θ_p- principal strain angle
- θ_s- inclination at which maximum shear strain occurs
- γ_{max}- maximum in plane shear strain

3. First Flexural cracking load calculation

The first flexural crack is formed when moment at a particular section reaches Mcr, moment of cracking resistance.

$$M_{cr} = \frac{I_c f_{ctm}}{y_t}$$

Where:

- M_{cr}- Moment of cracking resistance
- I_c- Second moment of area
- f_{ctm}- Mean concrete tensile strength
- y_t- the distance from the center of gravity of the beam to the extreme fiber of the tension side

Table 2: First Flexural Cracking Load Calculation

	Specimen	Set I		Set II		Set III		TRIAL Beam	
		SI8-25	SI8-50	SII10-50	SII10-75	SIII8-75	SIII10-75	TR8-50/75	TR10-50/75
Beam Geometry	b (mm)	200	250	250	300	250	250	210	210
	h (mm)	350	350	350	350	350	350	350	350
	d (mm)	309	307	305	305	297	295	317	315
Longitudinal Reinforcement Properties	Bottom Bar No	5	6	6	6	6	6	7	7
	ϕ (mm)	20	20	20	20	20	20	20	20
	As1 (mm^2)	1570.8	1884.96	1884.96	1884.96	1884.96	1884.96	2199.11	2199.11
Modulus of Elasticity	Es (GPa)	200	200	200	200	200	200	200	200
	Ec (GPa)	33	33	33	33	33	33	33	33
	n	6.06	6.06	6.06	6.06	6.06	6.06	6.06	6.06
Concrete Tensile Strength	fctm (Mpa)	2.9	2.9	2.9	2.9	2.9	2.9	2.9	2.9
Area of Section	A1 (mm^2)	70000	87500	87500	105000	87500	87500	73500	73500
	A2 (mm^2)	7948.25	9537.9	9537.9	9537.9	9537.9	9537.9	11127.5	11127.5
Neutral Axis	x1 (mm)	175	175	175	175	175	175	175	175
	x2 (mm)	309	307	305	305	297	295	317	315
	x (mm)	188.66	187.97	187.78	185.83	186.99	186.79	193.67	193.41
Moment of Inertia	I1 (mm^4)	7.1E+08	8.93E+08	8.93E+08	1.07E+09	8.9E+08	8.9E+08	750312500	750312500
	I2 (mm^4)	0	0	0	0	0	0	0	0
	Y1 (mm)	13.66	12.97	12.78	10.83	11.99	11.79	18.67	18.41
	Y2 (mm)	120.34	119.03	117.22	119.17	110.01	108.21	123.33	121.59
	I (mm^4)	8.4E+08	1.04E+09	1.04E+09	1.22E+09	1E+09	1E+09	945184804	939734101
	Yt (mm)	161.34	162.03	162.22	164.17	163.01	163.21	156.33	156.59
Cracking Moment	Mcr (kN.m)	15.15	18.67	18.57	21.54	18.17	18.07	17.53	17.4
Cracking Load	**Pcr (kN)**	**39.1**	**48.18**	**47.92**	**55.59**	**46.89**	**46.63**	**45.24**	**44.9**

4. Load Vs Out of Plane Strain (TRIAL Beam)

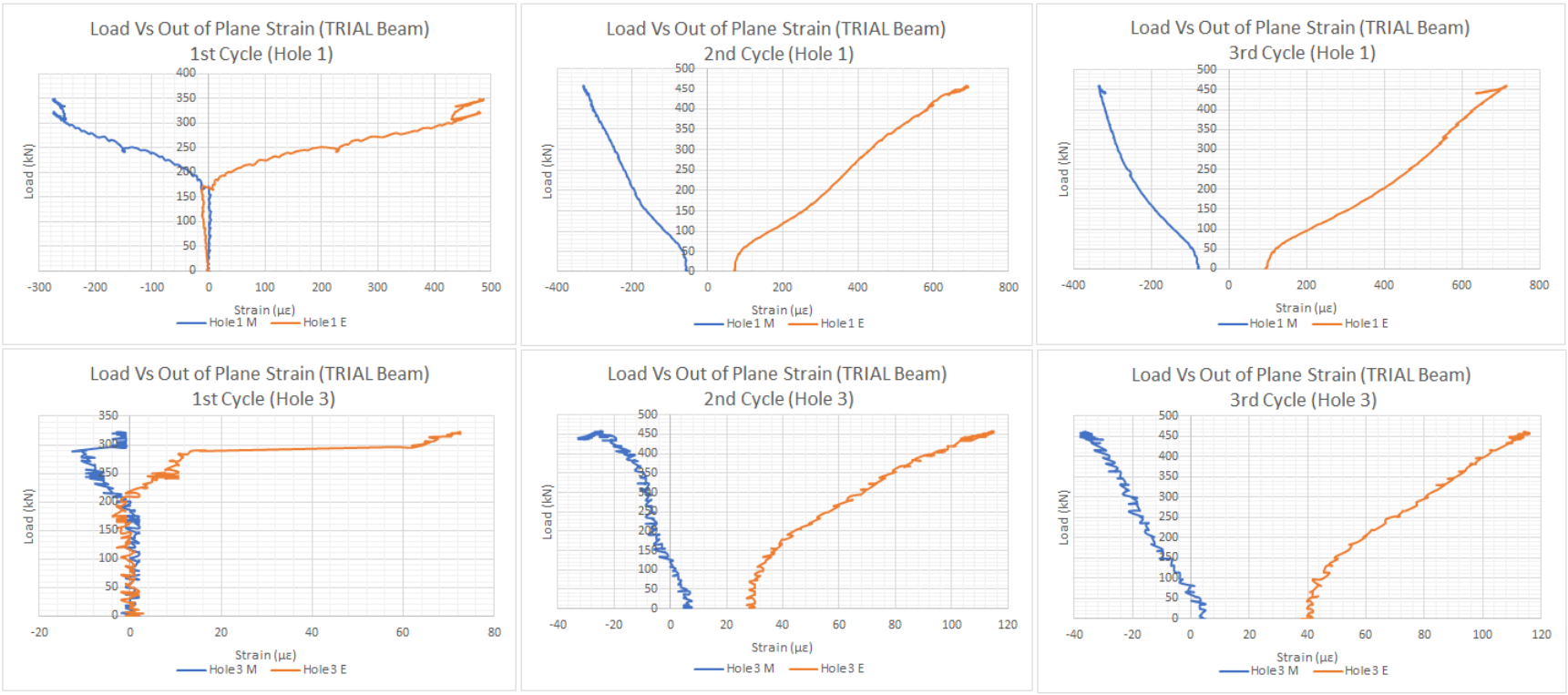

Figure 1: Load Vs Out of Plane Strain (TRIAL Beam 1st -3rd Cycle)

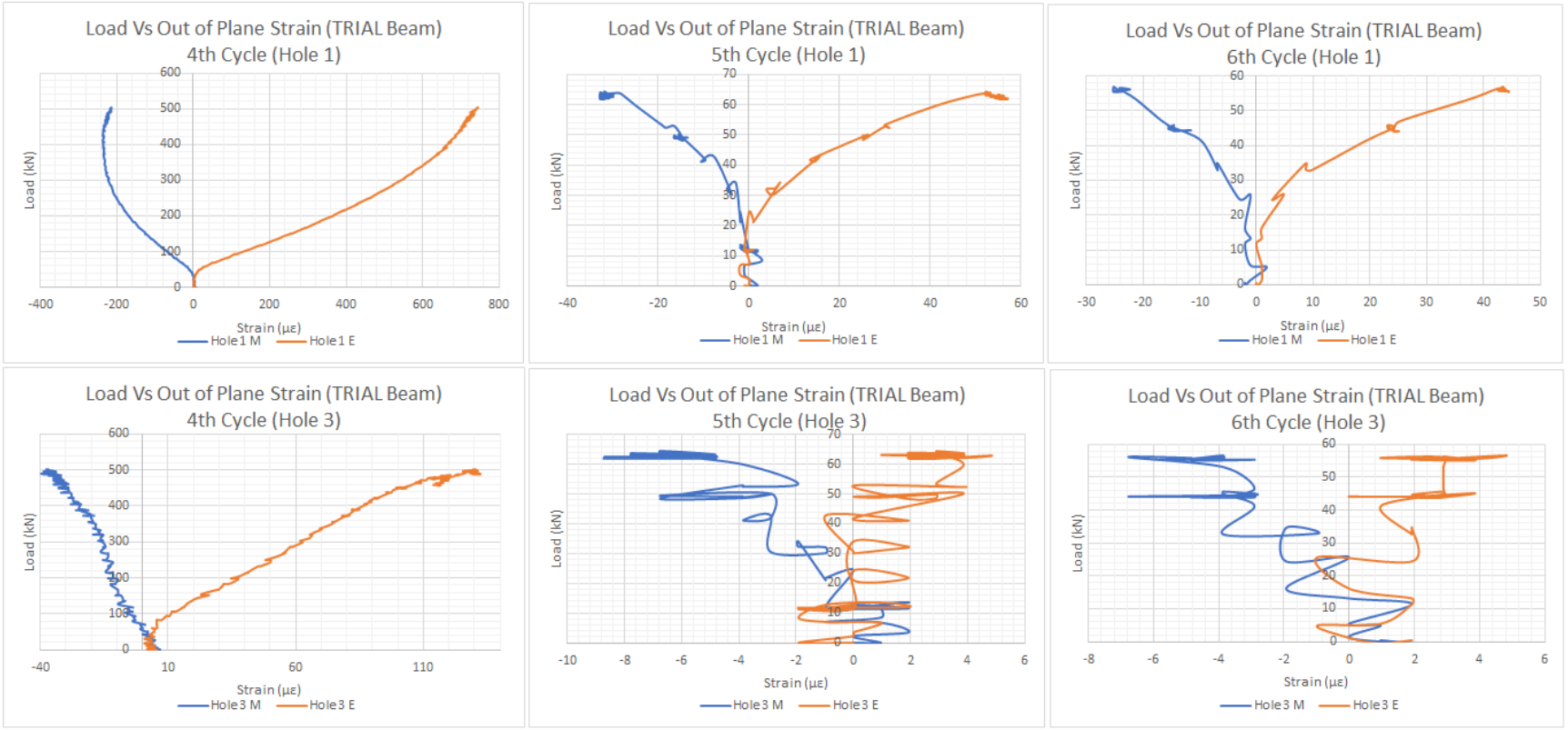

Figure 2: Load Vs Out of Plane Strain (TRIAL Beam 4th -6th Cycle)

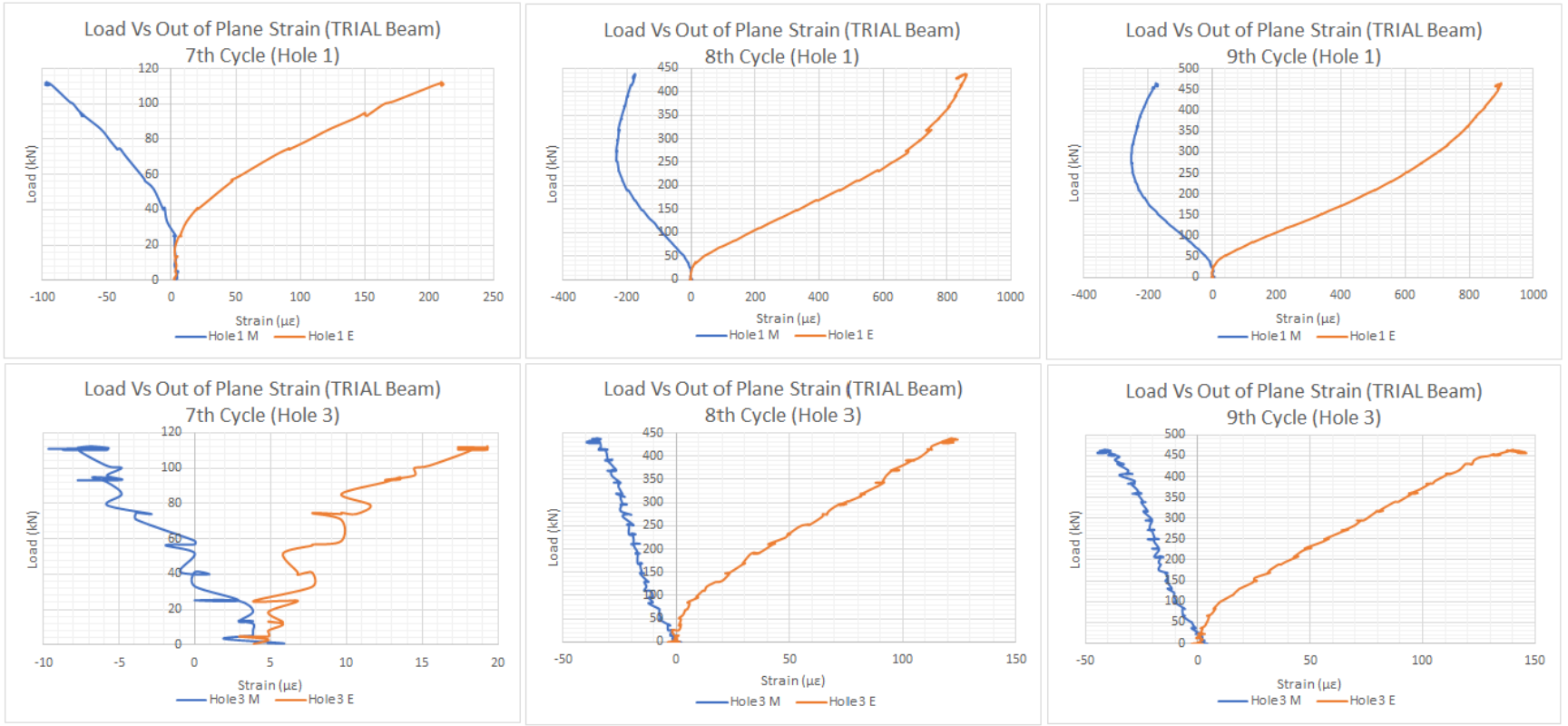

Figure 3: Load Vs Out of Plane Strain (TRIAL Beam 7th -9th Cycle)

5. Load Vs Vertical Strain Plots

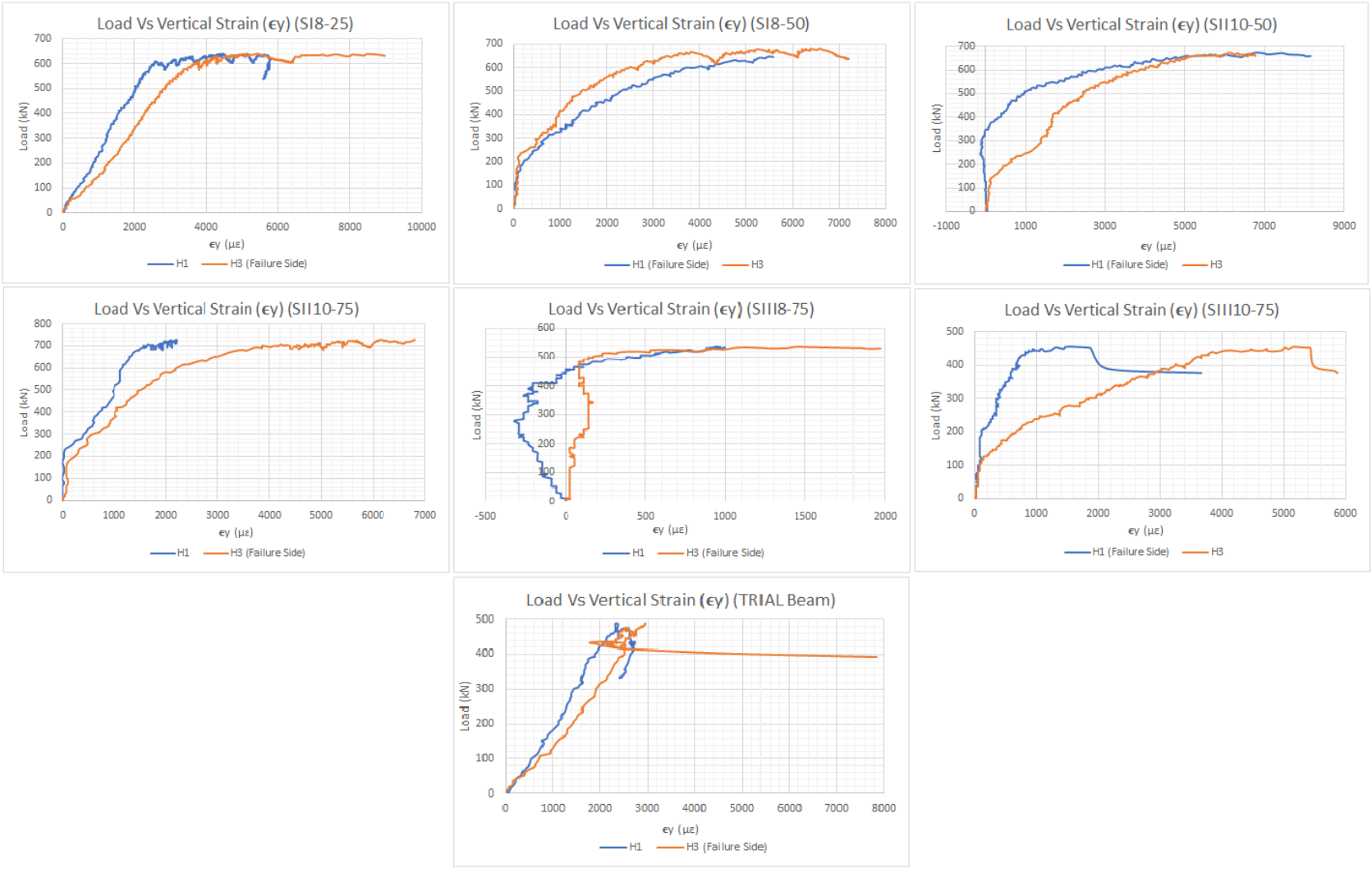

Figure 4: Load Vs Vertical Strain (εy) Plots

6. Load Vs Horizontal Strain Plots

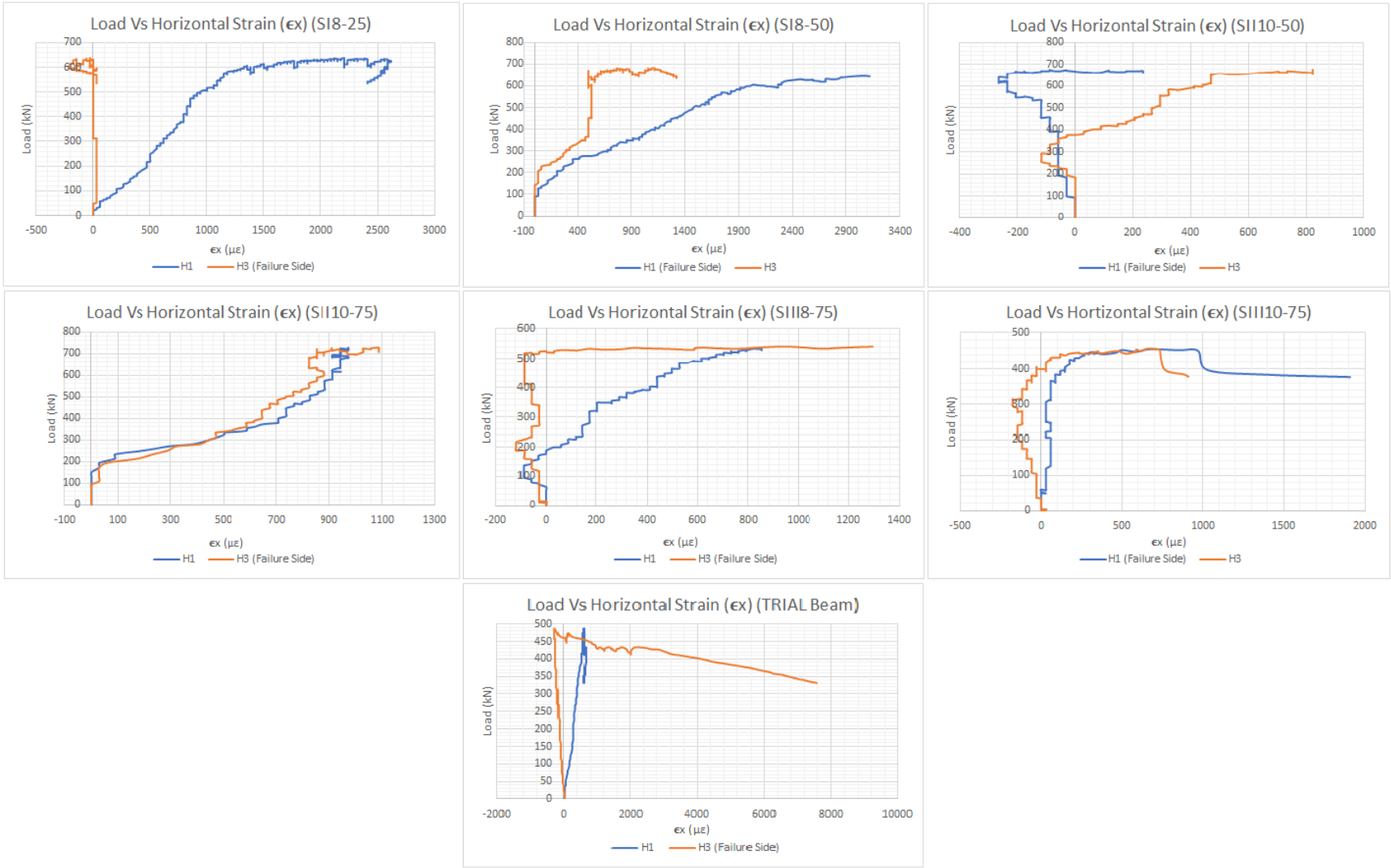

Figure 5: Load Vs Horizontal Strain (εx) Plots

7. Load Vs Maximum Shear Strain Plots

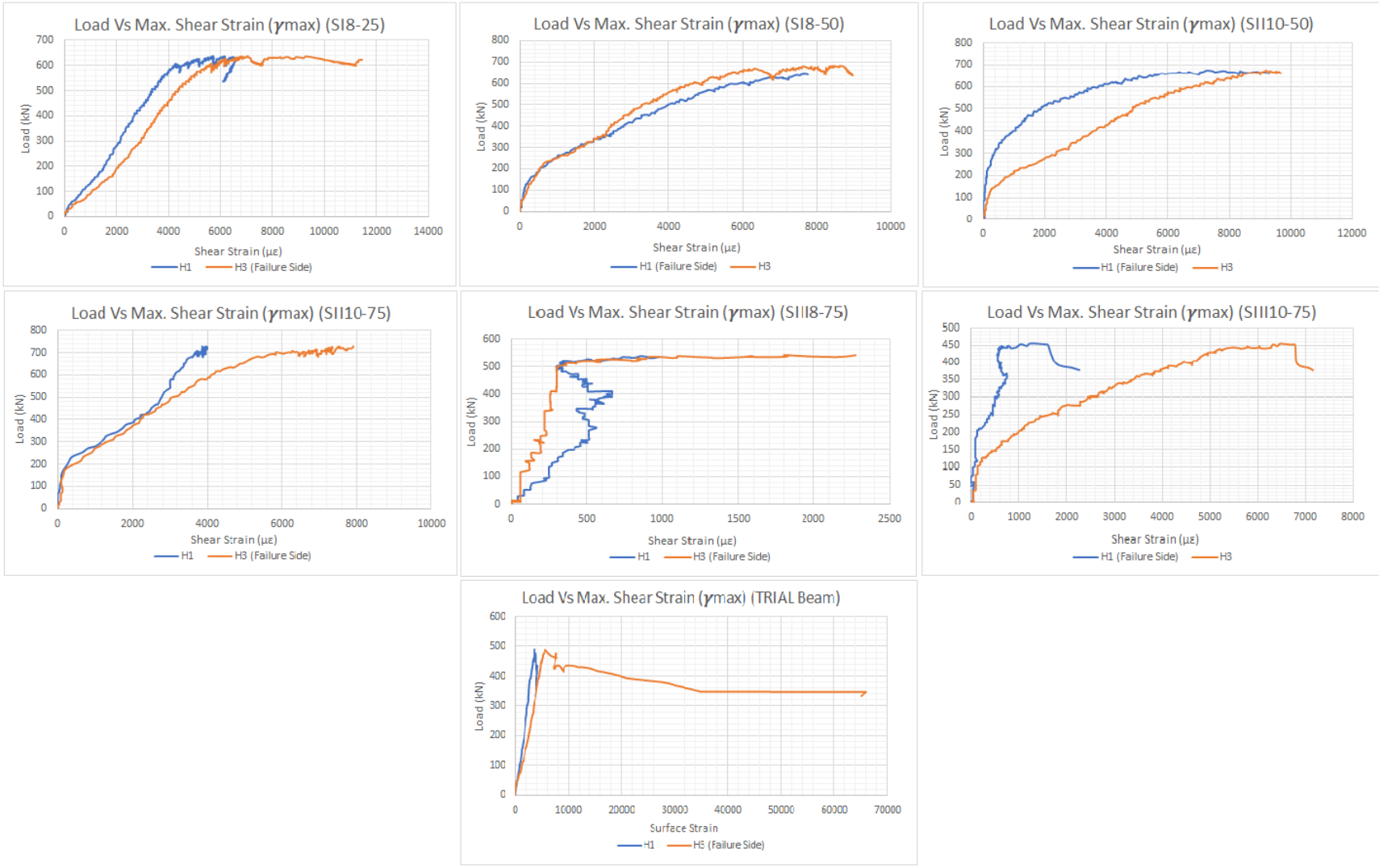

Figure 6: Load Vs Maximum Shear Strain (γmax) Plots

8. Load Vs Principal Strain Plots

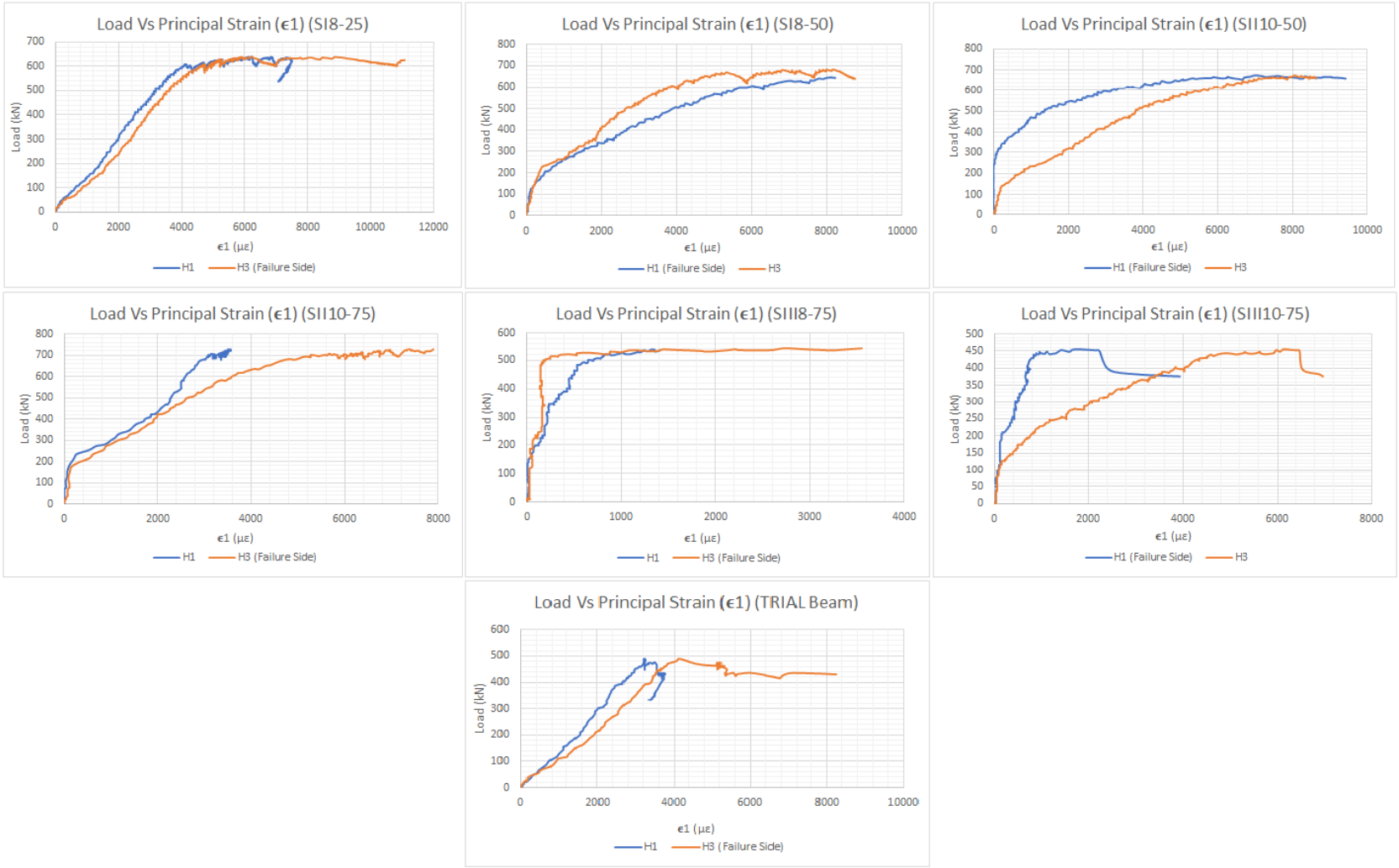

Figure 7: Load Vs Principal Strain (ϵ1) Plots

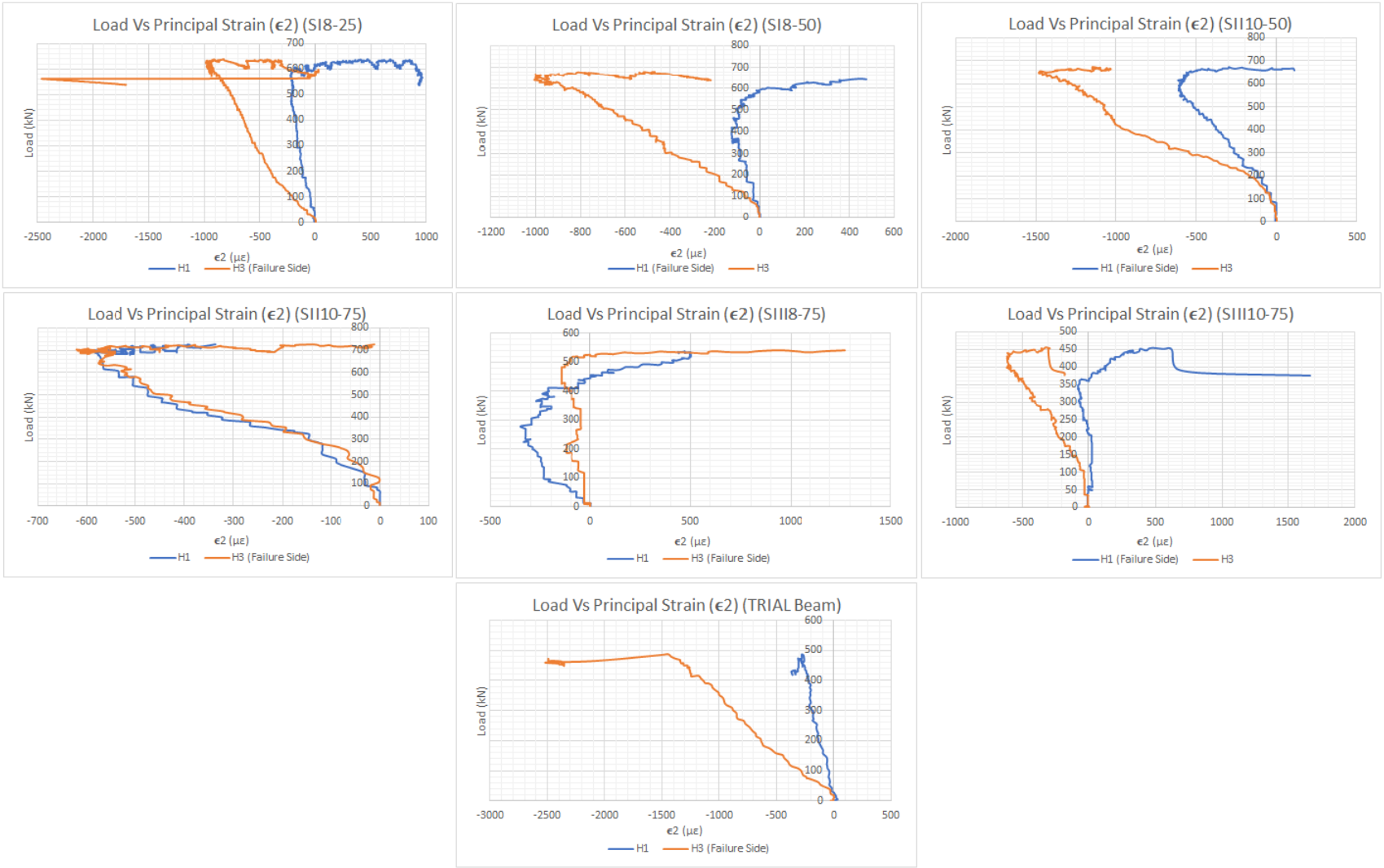

Figure 8: Load Vs Principal Strain (ϵ2) Plots

9. Load Vs Principal Angle (θp)

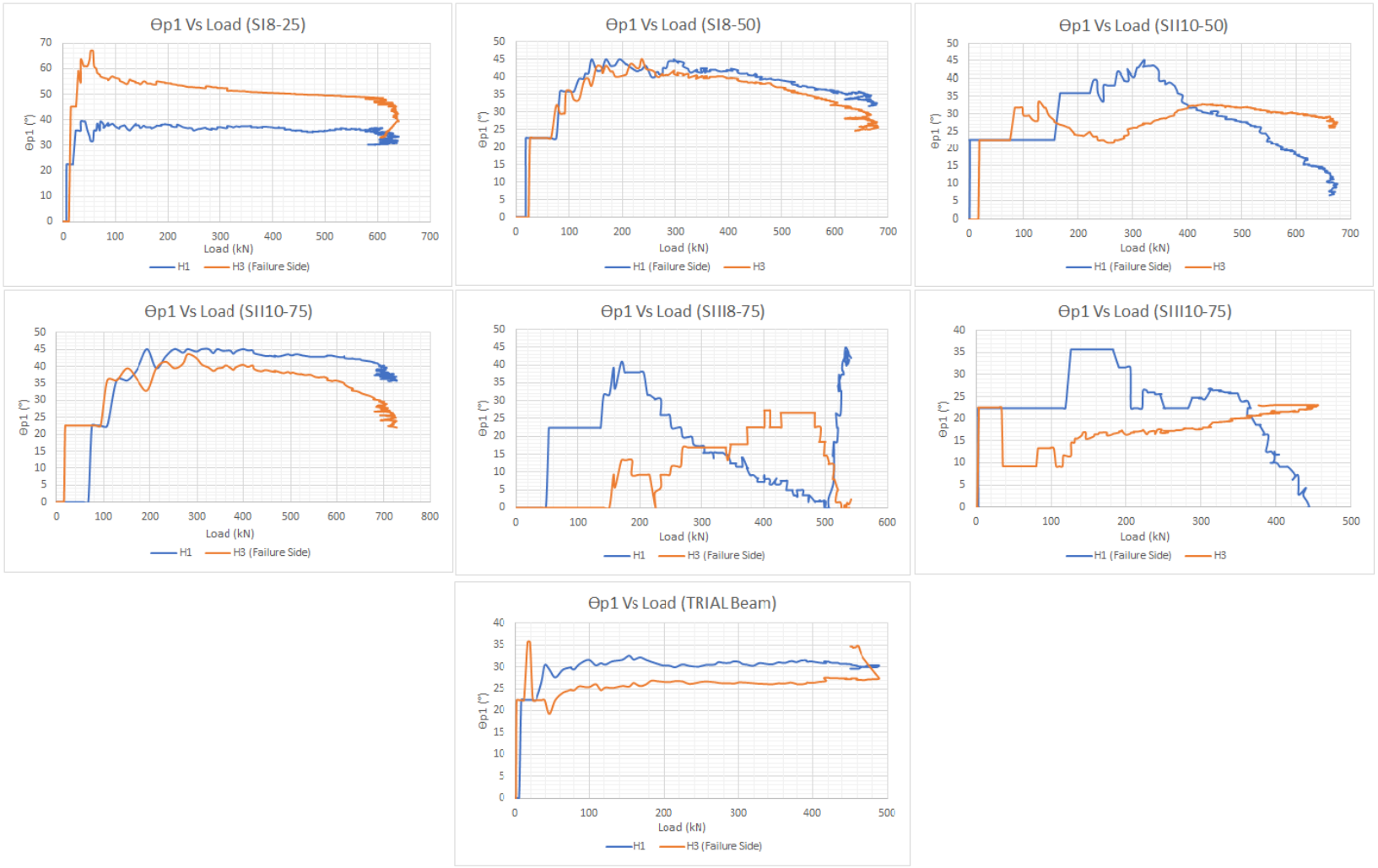

Figure 9: Principal Angle (θp) Vs Load Plots

10. Equivalent Displacement Conversion from Out of Plane Strain

Strain is converted into displacement in mm for the illustration drawings A scale factor of 4000 was used. (bw*Strain*scale factor)

$$Strain = \frac{Change\ in\ Length}{Original\ Length}$$

Table 3: Equivalent Displacement Conversion from Out of Plane Strain

		SI8-25			SI8-50		
		First Flexural Crack	First Diagonal Shear Crack	Peak Load	First Flexural Crack	First Diagonal Shear Crack	Peak Load
	Load (kN)	39	222	639.51	48	272	681.77
Strain (με)	Compression	1	70	200	0	10	-180
	Mid-Section	0	-25	-60	0	20	120
	Tension	0	25	90	0	-70	-120
Displacement (mm)	Compression	0.8	56	160	0	10	-180
	Mid-Section	0	-20	-48	0	20	120
	Tension	0	20	72	0	-70	-120
		SII10-50			SII10-75		
		First Flexural Crack	First Diagonal Shear Crack	Peak Load	First Flexural Crack	First Diagonal Shear Crack	Peak Load
	Load (kN)	48	272	674.77	56	306	727
Strain (με)	Compression	-1	1	200	0	-20	260
	Mid-Section	0	-10	0	0	0	20
	Tension	0	200	450	0	-100	-100
Displacement (mm)	Compression	-1	1	200	0	-24	312
	Mid-Section	0	-10	0	0	0	24
	Tension	0	200	450	0	-120	-120
		SIII8-75			SIII10-75		
		First Flexural Crack	First Diagonal Shear Crack	Peak Load	First Flexural Crack	First Diagonal Shear Crack	Peak Load
	Load (kN)	47	265	541.72	47	265	455.93
Strain (με)	Compression	0	2	250	0	60	275
	Mid-Section	0	-60	120	0	50	250
	Tension	0	-60	50	0	40	120
Displacement (mm)	Compression	0	2	250	0	60	275
	Mid-Section	0	-60	120	0	50	250
	Tension	0	-60	50	0	40	120